UNIVERSITÉ DE MONTRÉAL

A study of K_V channel dynamics using a fluorescent unnatural amino acid

par
Tanja Kalstrup

Département de Pharmacologie et Physiologie

Faculté de Médecine

Thèse présentée en vue de l'obtention du grade de philosophiæ doctor (Ph.D.)
en physiologie
option biophysique et physiologie moléculaires

Octobre, 2017

UNIVERSITÉ DE MONTRÉAL

Faculté de Médecine

Cette thèse intitulée :

A study of K_V channel dynamics characterized by a fluorescent unnatural amino acid

présenté par

Tanja Kalstrup

a été évaluée par un jury composé des personnes suivantes :

Lucie Parent,	Président rapporteur
Rikard Blunck,	Directeur de recherche
Roberto Araya,	Membre du jury
Francisco Bezanilla,	Examinateur externe
Daniel Zenklusen,	Représentant du doyen

Résumé

Les protéines sont les nanomachines moléculaires de la nature et leurs diverses fonctions sont essentielles au fonctionnement de tous les mécanismes cellulaires. Une grande partie de la recherche fondamentale en physiologie se concentre présentement sur l'étude de la structure et de la fonction des protéines. L'objectif général de cette thèse est d'élargir la compréhension des canaux potassiques voltage-dépendants (K_V), un groupe de protéines gouvernant la signalisation "électrique de divers aspects physiologiques, en particulier la propagation de potentiels d'action dans le système nerveux central et dans les cellules musculaires.

Dans le but d'obtenir des indices quant à la dynamique des canaux K_V, la thèse met l´enphase sur l'utilisation d'un acide aminé non naturel et fluorescent (Anap) comme outil moléculaire pour étudier les changements de conformation protéique avec la fluorimétrie en voltage imposé (FVI). L'avantage de la technique Anap-FVI par rapport aux techniques traditionnelles de marquage fluorescent, tient au fait qu'il n'y a pas de restriction sur le site d'intérêt. Ainsi, Anap est incorporé génétiquement dans des régions clés du canal Shaker K_V en utilisant la technique de substitution du "codon-stop amber", en utilisant une paire orthogonale d'ARNt/synthétase avec les ovocytes de *Xenopus laevis* comme modèle d'expression protéique.

Tout d'abord, la comparaison directe des deux extrémités du senseur de voltage (SV) est rendue possible par FVI bicolore dans lequel une cystéine externe est marquée avec TMR (tetramethylrhodamine), tandis que l'acide aminé (Anap) est incorporé du côté intracellulaire. On constate que la partie intracellulaire du SV s'active de façon similaire à la partie externe (chapitre 3). En outre, on constate que les portes S6 intracellulaires s'ouvrent essentiellement en deux étapes.

Ensuite, Anap a été inséré aux deux extrémités de la boucle cytoplasmique S4-S5 afin d'en étudier le mouvement pendant le couplage électromécanique (chapitre 4). Les expériences FVI bicolores démontrent que la partie N-terminale de la boucle se déplace avec le senseur de voltage alors que le mouvement de la partie C-terminale est retardé. Les résultats supportent un modèle de couplage électromécanique dans lequel l'énergie est stockée au centre du de la

jonction S4-S5. En outre, il est à noter que la boucle qui relie S4 et S5 subit des mouvements indépendants et coopératifs - une découverte qui s'aligne avec un rôle central de la boucle dans le transfert d'énergie du senseur de voltage vers le pore.

Dans un troisième projet, Anap a été inséré dans diverses positions de l'extrémité N-terminale cytosolique afin d'en sonder le mouvement pendant l'inactivation de type N (chapitre 5). Les données FVI montrent que la région hydrophile de la balle d'inactivation (BI) subit un mouvement qui est étroitement lié à l'inactivation mais qui ne joue pas un rôle dans l'obstruction finale du pore. Par contre, la pointe hydrophobe de la BI, subit un mouvement supplémentaire qui est sensible à l'état du pore, suggérant qu'il subit un mouvement qui impacte l'obstruction du pore. Les résultats supportent un modèle d'inactivation sous la forme de mécanisme d'étapes séquentielles d'au moins deux transitions.

Enfin, un quatrième projet se distingue de l'objectif général de la thèse. Il est démontré que les canaux avec un codon-stop N-terminal s'expriment malgré l'absence d'Anap (chapitre 6). Cette expression de fuite est causée par la réinitiation de la traduction de l'ARN messager, à des codons d'initiations non-canoniques en aval, et peut être réduite en supprimant ces codons. Les résultats mettent en évidence l'importance des expériences de contrôles lors d'utilisation d'acides aminés non naturels.

Mots-cléfs : Canaux K_V, acides aminés non-naturels, Anap, fluorimétrie en voltage imposé

Abstract

Proteins are the nature's molecular nanomachines and their diverse set of functions are crucial to the workings of all cellular mechanisms. A great part of fundamental research today is therefore focusing on the elucidation of protein structure and function. The general objective of this thesis is to expand the understanding of voltage-gated potassium (K_V) channels, a group of proteins which governs electrical signalling in various physiological aspects, in particular the propagation of action potentials in the central nervous system and in muscle cells.

In the pursuit of obtaining dynamic information of K_V channels, the focus in this thesis has been on exploring the applicability of a fluorescent unnatural amino acid (Anap) as a molecular tool to study protein conformational changes using voltage clamp fluorometry (VCF). The advantage of the Anap-VCF technique over traditional post-translational fluorescence labeling techniques is that there are no restrictions regarding the choice on the site of interest. Anap is genetically incorporated into key regions in the Shaker K_V channel by using the amber stop codon suppression technique using an orthogonal tRNA/synthetase pair, and *Xenopus laevis* oocytes are used as expression system.

The first project involves direct comparison of both ends of the voltage sensor (VS) and is made possible by two-color VCF, in which an external cysteine is labeled with TMR (tetramethylrhodamine) while Anap is incorporated on the intracellular side (chapter 3). We found that the intracellular part of VS activates together with the external part. Moreover, it is found that the intracellular S6 gates open in a sequential two-step transition.

Next, to investigate electromechanical coupling, Anap was inserted into both ends of the S4-S5 linker (S4-S5L, chapter 4). Two-color VCF experiments demonstrates that the N-terminal part of S4-S5L moves with the VS. On the other hand, the movement of the C-terminal part of the linker is delayed with respect to the VS. The findings support a model for electromechanical coupling in which energy is stored in the middle of the S4-S5L, and not in the C- or N-termini. Moreover, it is found that the S4-S5L undergoes both independent and cooperative movements – a finding which agrees with a pivotal role of the S4-S5 linker in energy transfer from the VS to the pore.

In a third project, Anap was inserted into various positions on the flexible and cytosolic N-terminus to probe the movement during N-type inactivation (chapter 5). VCF data show that the hydrophilic chain region of the inactivation particle (IP) undergoes a motion which is closely related to inactivation but is not involved in the final step of pore block. The hydrophobic tip of the IP, on the other hand, undergoes an additional motion which is sensitive to the state of the pore, suggesting that it causes pore block. The findings support a model for inactivation as a sequential step mechanism of at least two transitions.

Finally, a fourth project stands out from the general objective of the thesis. It is demonstrated that channels with N-terminal stop codons still express despite the absence of Anap (chapter 6). This leak expression is caused by translation reinitiation at downstream non-canonical start codons and can be reduced by removing the start codons. The findings highlight the importance of control experiments when using unnatural amino acids.

Keywords: K_V channels, unnatural amino acids, Anap, voltage clamp fluorometry

Table of contents

Table of figures

List of abbreviations

4-AP	4-aminopyridine
aaRS	aminoacyl tRNA synthethase
Anap	3-(6-acetylnaphthalen-2-ylamino)-2-aminopropanoic acid
BCN	bicyclononynes
COVC	cut-open oocyte voltage clamp
E. coli	Escherichia coli
GV	conductance-voltage relationship
FRET	förster resonance energy transfer
fUAA	fluorescent unnatural amino acid
IP	inactivation particle
K_V	voltage-gated potassium channel
LRET	lanthanide resonance energy transfer
Na_V	voltage-gated sodium channel
pAnap	plasmid encoding for Anap-synthetase and tRNA
QV	charge-voltage relationship
QY	quantum yield
S4-S5L	S4-S5 linker
TCO	trans-cyclooctene
TEA	tetraethylammonium
TEVC	two electrode voltage clamp
TMR	tetramethylrhodamine
TMRM	tetramethylrhodamine maleimide
TTX	tetradotoxin
UAA	unnatural amino acid
VCF	voltage clamp fluorometry
VS	voltage sensor
WT	wild type
X. laevis	Xenopus laevis

Thesis acknowledgements

I wish to thank my supervisor Dr. Rikard Blunck for giving me the opportunity to investigate innovative approaches at an early stage, and for believing in my qualifications as a researcher. His confidence and guidance has truly contributed to my development as an independent scientist.

Chapter 1

Introduction

The electrical signalling which governs cell-cell communication in the nervous system, heart and muscle, form the molecular foundation of our heartbeat and how we store memory, perceive, react and move our limbs, among many other physiological aspects. Excitable cells convert chemical or mechanical signals intro electrical signals by means of ion channels which are proteins that selectively conduct potassium, sodium or calcium ions across the cell membrane. The neuronal electrical signaling is generated by action potentials which are millisecond-long signals that propagate along the nerve fiber.

Excitable cells have a negative resting membrane potential of about -70 mV which arises from the activity of molecular pumps which transport sodium ions out of the cell and potassium into the cell. This creates an electrochemical gradient where, at rest, the concentration of potassium is high inside, and the concentration of sodium is high outside. When the membrane potential reaches a threshold above -50 mV, rapid activation of voltage-dependent sodium (Na_V) channels leads to a Na^+ influx which depolarizes the cell membrane. Voltage-dependent potassium (K_V) channels also activate leading to the influx of K^+ which repolarizes the membrane back to rest. These components of an action potential, or the nerve impulse, constitutes the fundamental brain signalling throughout the animal kingdom.

The story of ion channels begins with the famous experiments performed by Alan Hodgkin and Andrew Huxley in 1952. Their discovery of Na^+ and K^+ currents as the fundamental events underlying the nerve impulse, were made possible by the development of the voltage-clamp concept as introduced to them by Kenneth Cole [1]. By insertion of axial wires into a giant squid axon, a feed-back system could maintain the membrane potential and circumvent the unstable character of the action potential [2]. This way, Hodgkin and Huxley identified independent Na^+

and K^+ currents [3], characterized their kinetic properties [4, 5], and developed a model which predicted the action potential from the regulation of conductance by four sets of charged particles [6] - a gating process which today is known to be controlled by the four voltage sensors in Na_V and K_V channels. The pioneering work of Hodgkin and Huxley awarded them the Nobel prize in 1963.

The field of ion channels as we know it today is based on several key discoveries in the following decades. First, the notion that ions would cross the membrane through transmembrane proteins in a channel-like manner was suggested in the 60's by the findings that tetradotoxin (TTX) and tetraethylammonium (TEA) selectively blocked Na^+ and K^+ currents, respectively [7, 8]. Furthermore, the presence of ion-conducting channels was confirmed by the invention of the patch clamp technique which enabled measurements of electrical activity in small areas of membrane giving rise to single channel recordings [9]. The development of this technique by Drs. Neher and Sakmann lead to the Nobel prize in 1991. Then, in the 80's, gene cloning and recombinant manipulation began to be applied in the field of ion channel research. The cloning of voltage-gated ion channels [10, 11] paved the way for emerging molecular biology methods to be used to identify the role of individual amino acids. Site-directed mutagenesis not only allowed for better understanding of how point mutations could alter channel function and result in diseases, but also became a useful method in the elucidation of fundamental workings of ion channels. The 90's highlight a decade during which biophysical properties of the voltage sensor and the pore were established using electrophysiology and mutagenesis (gating currents, cooperativity, ion selectivity) [12-16]. Finally, atomic structures of voltage-dependent bacterial and eukaryotic potassium channels solved by X-ray crystallography [17, 18] made it possible to relate structural data with gating function, and questions on subunit assembly, pore conformation and permeation could now be addressed structurally. Dr Mackinnon was awarded a share of the Nobel Prize in 2003 for the work. The crystal structures also confirmed a number of structural features postulated by Bertil Hille more than 20 years earlier [19]: These ion channels contain a selectivity filter located towards the extracellular end of the pore, with a voltage sensor controlling a cytoplasmic gate.

Although a wealth of functional and structural data has been provided by electrophysiology and X-ray crystallography in the field of ion channels, they are limited when it comes to unfolding the

molecular dynamics which drive the channel from one state to another. Research in dynamics today is characterized by the parallel emerging of two technological areas. First, experimental findings based on advances in fluorescence-based techniques have yielded kinetic information on conformational changes and relative distance changes, such as voltage clamp fluorometry (VCF), förster resonance energy transfer and lanthanide resonance energy transfer. Second, important advances in highly sophisticated computational approaches is continuously expanding, allowing for the elucidation of microscopic factors governing structural dynamics and ion permeation. There is no doubt that as computational power grows, the theoretic prediction of channel behaviour will play a key role in the future. Also, the recent advances in cryo-electron microscopy which resulted in snapshots of various conformational states of a sodium-activated K^+ channel, surely has shed light on cryo-EM as a valuable tool in capturing transitions [20].

1.1 Potassium channels

The importance of understanding the detailed molecular basis of ion channel function is highlighted by their widespread roles in numerous physiological aspects. The group of K^+ channels is, with 78 members, the largest within the ion channel family [21]. The group is divided into 4 subfamilies based on function and homology: Calcium- and sodium-activated K^+ channels (K_{Ca} and K_{Na}), inwardly rectifying K^+ channels (K_{ir}), two P domain K^+ channels (K2P), and voltage-gated K^+ channels (K_V). The majority of the potassium channel subunits consists of 6 transmembrane domains, but K_{ir} and K2P consists of 2 and 4 transmembrane domains, respectively, and some K_{Ca} channels have 7 transmembrane domains. There is one structural feature which all K^+ channels have in common, and that is a GXG signature sequence which is responsible for the selective permeation of K^+ ions over other ions (X is a tyrosine except in some K2P channels where it can also be a phenylalanine).

K_{Ca} channels are present in a large range of both excitable and non-excitable cells, where they are involved in neuronal excitability, transmitter release and Ca^{2+} homeostasis [22]. They are tightly coupled to, and regulate, the amount of intracellular Ca^{2+}. When activated by Ca^{2+}, the channels open and repolarize the membrane, which in turn causes the closing of voltage-gated calcium channels thus limiting the influx of Ca^{2+}.

K_{Na} channels are predominantly expressed in neuronal tissue. They are activated by high concentrations of intracellular Na^{2+}, suggesting that they are coupled to local increase of sodium in connection with opening of voltage-gated sodium channels and/or in restricted compartments like dendritic spines. Single amino acid mutations in some K_{Na} channels result in devastating effects causing epilepsy and intellectual and physical disabilities [23].

K_{ir} channels allow ions to move into the cell rather than out, due to intracellular block by Mg^{2+} or polyamines at positive potentials. Their physiological function is diverse and depend on type and location. When potassium flows at negative potentials it allows the channels to control the resting membrane potential. Some K_{ir} channels are regulated by G protein-coupled receptors and others are ATP-sensitive and are directly involved in regulation of insulin secretion in pancreatic beta cells.

The structure of K2P channels is markedly different from the other potassium channels in that it is a homodimer of two 4 transmembrane subunits. They play several roles in excitable cells where they give rise to leak K^+ currents to stabilize the negative resting membrane potential. They are regulated by voltage-independent factors like pH, stretch and temperature and a range of intracellular signaling pathways.

Finally, K_V channels are found in all excitable cells with channel open probabilities which depend on changes in the membrane potential, and they carry a voltage sensor which is central to their function. The channels generate action potentials where they are responsible for returning the depolarized cell to resting state. With their different voltage-dependencies and inactivation properties, they regulate action potential duration and firing patterns and sets the resting membrane potential.

The molecular diversity of potassium channels is enhanced by the possibility of heteromeric assembly of different subunits within a subfamily. Furthermore, post-translational modifications (splicing, phosphorylation, glycosylation) and regulation by auxiliary subunits also diversifies the channel properties, creating a wide and complex distribution of K^+ channel function. To better understand the function of K_V channels, which are the subject of the thesis, they are described in more detail in the following section.

1.2 Voltage-gated potassium channels

As Hodgkin and Huxley showed in the squid axon, the action potential consists of rapid feedback processes involving voltage-gated ion channels: Na_V^+ channels which first activate by positive voltage causing sodium ions flowing into the cell which depolarizes the membrane. This step is the rising phase of an action potential. Then, activation of K_V^+ channels causes potassium ions to flow out of cell which allows the cell to return to the resting potential. The different current profiles of K_V channels makes them capable of shaping and regulating the action potential (amplitude, duration, frequency) leading to different patterns of action potentials. This way, in neurons, the types of ion channels in the membrane can vary across the cell, which gives the dendrites, axon and cell body their different electrical properties. K_V channels play an active role in action potentials of heart, brain, spinal cord, sensory neurons and muscle, but are also involved in regulation of cell volume, proliferation, apoptosis and migration of a wide range of cell types.

The K_V channel subfamily are encoded by >40 genes in the human genome and make up half of the potassium channel family. K_V channels are divided into 12 molecular subgroups (K_V1-12) which display different voltage-dependent activation and inactivation properties. They open upon membrane depolarisation and selectively conducts potassium ions across the cell membrane according to the electrochemical gradient of potassium. K_V5, K_V6, K_V8 and K_V9 families give rise to homomeric channels that are electrically silent likely due to their retention in the endoplasmic reticulum. Instead, these silent subunits assemble with members of other K_V groups to form heteromeric channels.

1.2.1 Why is it important to understand the function of K_V channels?

K_V channels shape and regulate neuronal and cardiac action potentials [24], and participate in apoptosis [25] and cell differentiation [26] among other functions. Furthermore, K_V channels are necessary for the release of neurotransmitters and hormones [27, 28] and regulate cell volume, proliferation and migration [24]. The critical roles and physiologically diverse implication of K_V channels makes them a major therapeutic target for treatment of many neurological, metabolic and cardiovascular disorders, in which the cause of the disease affects the function of these channels.

Another reason for studying K_V channels is that malfunction due to genetic mutations result in channelopathies such as cardiac arrhythmias (short and long QT syndromes), episodic ataxia, epilepsy, and deafness, and has also been associated with impaired glucose tolerance, insulin insensitivity and atrial fibrillation [29].

Small molecules and peptide toxins have been developed and identified as drugs for targeting K_V channels as a pharmaceutical strategy, and are also being used as research tools to characterize channel structure and function [29]. Peptide toxins can bind to the outer vestibule of the ion conduction path and block K^+ flow (e.g. charybdotoxin) [30], or they can interact with the voltage sensor to favor the closed state of the channel (e.g. hanatoxin) [31]. Most binding sites for small molecules reside in the inner pore region or are located on the intracellular side, where they can act as channel openers (e.g. retigabine) [32] or blockers (e.g. 4-aminopyridine) [33]. The current U.S. Food and Drug Administration (FDA) requires that all drug candidates for human use are evaluated for potential K_V11.1 activity (encoded by the human *Ether-à-go-go* related gene, hERG) to prevent arrhythmia side effects [34]. The broad pharmacological aspect of K_V channels makes them a group of proteins with great therapeutic potential.

Human health has benefited directly from detailed knowledge about ion channel function because channelopathy diseases can now be readily diagnosed. For example, genetic testing of the cystic fibrosis transmembrane conductance regulator, the CFTR ion channel, helps diagnosis of the cystic fibrosis disease which affects about 1 in 3000 new born in Northern Europe, giving the possibility of early treatment. The continued advances in the field of ion channels from researchers in academia and pharmaceutical companies, will extend this benefit to diagnose and prevent diseases, and develop highly selective drugs targeting ion channels.

Overall, the therapeutic importance and social benefit of understanding K_V channel function is evident. From a biophysical point of view, the elucidation of voltage sensing mechanisms and dynamics of conformational changes is first and foremost driven by our scientific curiosity and fascination by nature. As humans we wish to know how nature works to ultimately answer what we are made of and where we come from. The need to understand nature's origin constitutes the main motivation factor in fundamental research. K_V channels are highly evolutionarily

conserved ion channel families playing fundamental roles in all living organisms, making the study of these channels a prerequisite to understand life and its origin in full.

1.2.2 The Drosophila Shaker channel

The first cloned potassium channel was the Drosophila Shaker K_V channel [11], which was discovered based on a leg-shaking phenotype under ether-induced anesthesia [35]. The shaking is caused by neurons which fail to repolarize as quickly as normal neurons (figure 1.1), making them exceptionally excitable, resulting in abnormal muscle contractions. What happens on the molecular level is that in the absence of K_V channels at the axon of the neuromuscular junction, the action potential is prolonged. In turn, voltage-gated calcium channels at the axon terminal which close upon repolarization, remain open for a longer time than normal, thus increasing the time for Ca^{2+} influx. The increase of intracellular Ca^{2+} stimulates the neurotransmitter release from the synaptic vesicles into the synaptic cleft. This way, postsynaptic receptors are excessively triggered, resulting in abnormal action potentials in the muscle fibers.

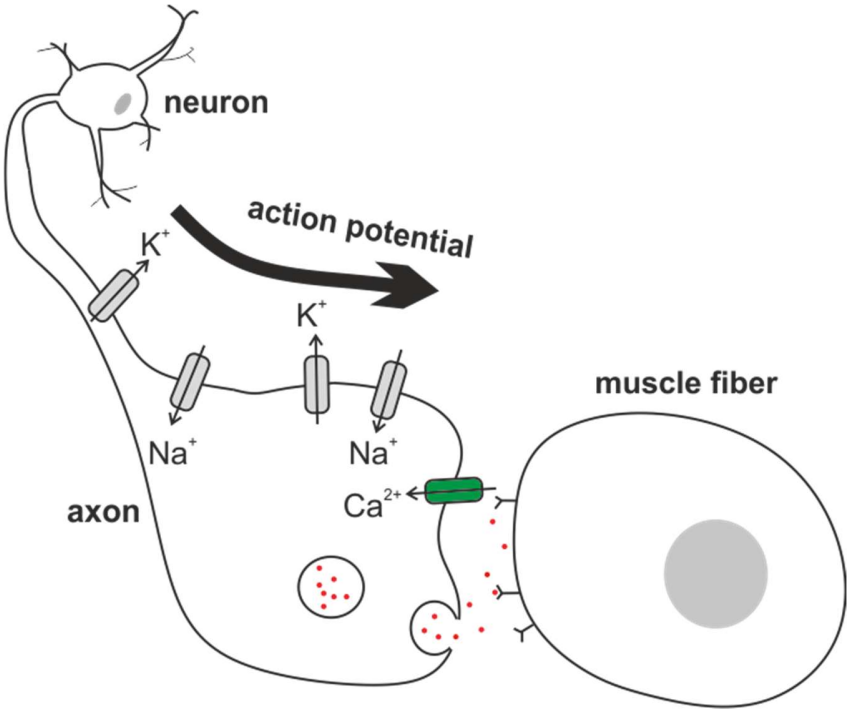

Figure 1.1 Cartoon of neurotransmitter release in the neuromuscular junction
When the neuronal action potential comes down the axon and reaches the axon terminal, it activates Ca_V channels which open upon depolarization. The increase of intracellular Ca^{2+} leads to fusing of the synaptic vesicles with the membrane, so that neurotransmitter molecules diffuse into the synaptic cleft and activate neurotransmitter activated receptors on the target cell, which is muscle fiber cells in the case of the

neuromuscular junction. The voltage-gated potassium channel at the axon are representative of K_V1 channels in human and Shaker channels in Drosophila.

Recently, the Shaker channel has been shown to play a role in controlling Drosophila sleep, in which a point mutation in the first transmembrane helix S1 (a threonine to isoleucine substitution) was identified to cause short-sleeping phenotypes with preserved performance [36]. The molecular link between neuronal firing and sleep in relation to Shaker channels is not known, but it highlights the fundamental and diverse implication of Shaker-related channels in Drosophila, as it also is in mammalians.

1.3 K_V1 channel family

Mammalian K_V1 channels are homologues of the Drosophila Shaker channel and are also called the Shaker-related K_V channels. The group consists of 8 members ($K_V1.1$, $K_V1.2$, $K_V1.3$, $K_V1.4$, $K_V1.5$, K_V 1.6, $K_V1.7$, $K_V1.8$) displaying sustained potassium currents, except $K_V1.4$ which display a transient "A-type" (fast inactivation) current, when heterologously expressed as homomeric tetramers.

$K_V1.1$, $K_V1.2$ and $K_V1.4$ are those which are most abundant in the mammalian brain, localized to axons and nerve terminals where they exist in a complex heterogenous subunit association controlling neuronal action potentials and presynaptic transmitter release [37]. Episodic ataxia 1 is a neurological disorder which leads to myokymia and episodes of spastic contractions of skeletal muscle. 30 genetic mutations in the KCNA1 gene encoding for $K_V1.1$ have been identified to be the underlying cause for episodic ataxia 1 [38]. Most of the mutations lead to altered biophysical properties such as positive shift of activation voltage dependency or slower activation kinetics among others, while some abolish channel activity. Several drugs improve symptoms, but no single medication has proven efficient. How $K_V1.1$ mutations result in episodic ataxia 1 phenotypes are not clearly understood. Patients having the same mutation do not necessarily respond to the same drugs, nor do they necessarily demonstrate the same disease characteristics, which means that there are likely other factors than $K_V1.1$ mutations which are involved. Mutations in $K_V1.1$ and $K_V1.2$ have also been identified in a subset of patients to be involved in certain epileptic disorders with seizures associated to episodic ataxia 1 ($K_V1.1$) and epileptic encephalopathy ($K_V1.2$).

K_V1.6 exist in interneurons in the spinal cord, and also in dendrites together with K_V1.1 and K_V1.2 [37], and K_V1.3 is predominantly expressed in the cerebellum. In the brain, K_V1.5 is restricted to glial and endothelial cells, but is also expressed in vascular smooth muscle cells together with K_V1.2 and K_V1.4 [39]. K_V1.7 and K_V1.8 have not been detected in the brain, but K_V1.7 exist in skeletal muscle and heart, and has also been suggested to play an active role in insulin secretion in pancreatic beta cells [40]. K_V1.3 and K_V1.8 are highly expressed in the kidney where they stabilize the membrane potential in the renal tubule [41].

Finally, in the heart, K_V1.4 and K_V1.5 play critical roles in the cardiac action potential [42]. One loss-of-function mutation in K_V1.5 has been shown to cause atrial fibrillation [43], which is a condition characterized by abnormal electrical activity in the heart, and predisposes the patient to stroke and heart failure .

The expression pattern listed here is not comprehensive but highlights the predominant localization of members in the K_V1 subfamily. It remains a challenging task to make a complete list of K_V channel tissue distribution and to identify the molecular function and cellular role of each localised potassium channel gene.

1.4 K_V1 channel structure

The full amino acid sequence of Shaker is ~70% identical to the K_V1 channels, with no homology in the N- and C-termini, whereas the sequence of the transmembrane regions and the intracellular tetramerization domain (T1) is ~90% identical (figure 1.2). Due to the early cloning of Shaker in 1987 [11] and its high expression efficiency in Xenopus oocytes, the majority of interpreted gating data is based on measurements obtained from Shaker. The first mammalian K_V channel crystal structure, which was determined in 2005, was K_V1.2 from rat in complex with a beta subunit (β2) [18], and was followed by a complete structure determination in 2007 at 2.4 Å of the K_V1.2/2.1 chimera [44]. Finally, a complete structure of the native K_V1.2 channel was obtained by using a refinement method in 2010 [45]. These structures are the only available mammalian K_V structures and have thus often served as models to explain functional data obtained from Shaker. Overall, the K_V channel field has two structures, the bacterial KvAP and the mammalian K_V1.2 channels and both are in the open state. The validity of interpretation of functional measurements from Shaker using the K_V1.2 crystal structures is that both channels are

related closely enough such that correlation of their data is appropriate. The high sequence similarity between Shaker and K_V1 channels (figure 1.2), as well as the correlation between predicted structural features of Shaker and the K_V channel crystal structures, indicate that functional Shaker data can be interpreted with K_V structural data. Shaker and $K_V1.2$ both exhibit high sensitivity to channel block by 4-aminopyridine (4-AP) (Table 1) and voltage clamp fluorometry studies show that the top of the S4 helix correlates with charge movement in both channels [46, 47]. The two channels differ only slightly in gating charge, activation midpoint voltage (V_{50}) and in the time course of C-type inactivation (Table 1). Considering the dissimilarity in the loop regions (figure 1.2) such differences would be anticipated. However, Shaker and $K_V1.2$ differ in sensitivity to tetraethylammonium (TEA) block, which is due to a single amino acid difference in the outer pore region [48].

	Shaker	**$K_V1.2$**
Gating charge	12-14 e_0 [49, 50]	10-13 e_0 [51, 52]
V_{50}	-20 mV [53, 54]	-8 mV [55]
4-AP IC_{50}	<1 mM [56]	<1 mM [57]
TEA IC_{50}	27 mM [58]	>100 mM [48]
C-type inactivation time constant	3.5 s [59]	5.5 s [59]

Table 1 Comparison of selected functional parameters for Shaker and $K_V1.2$

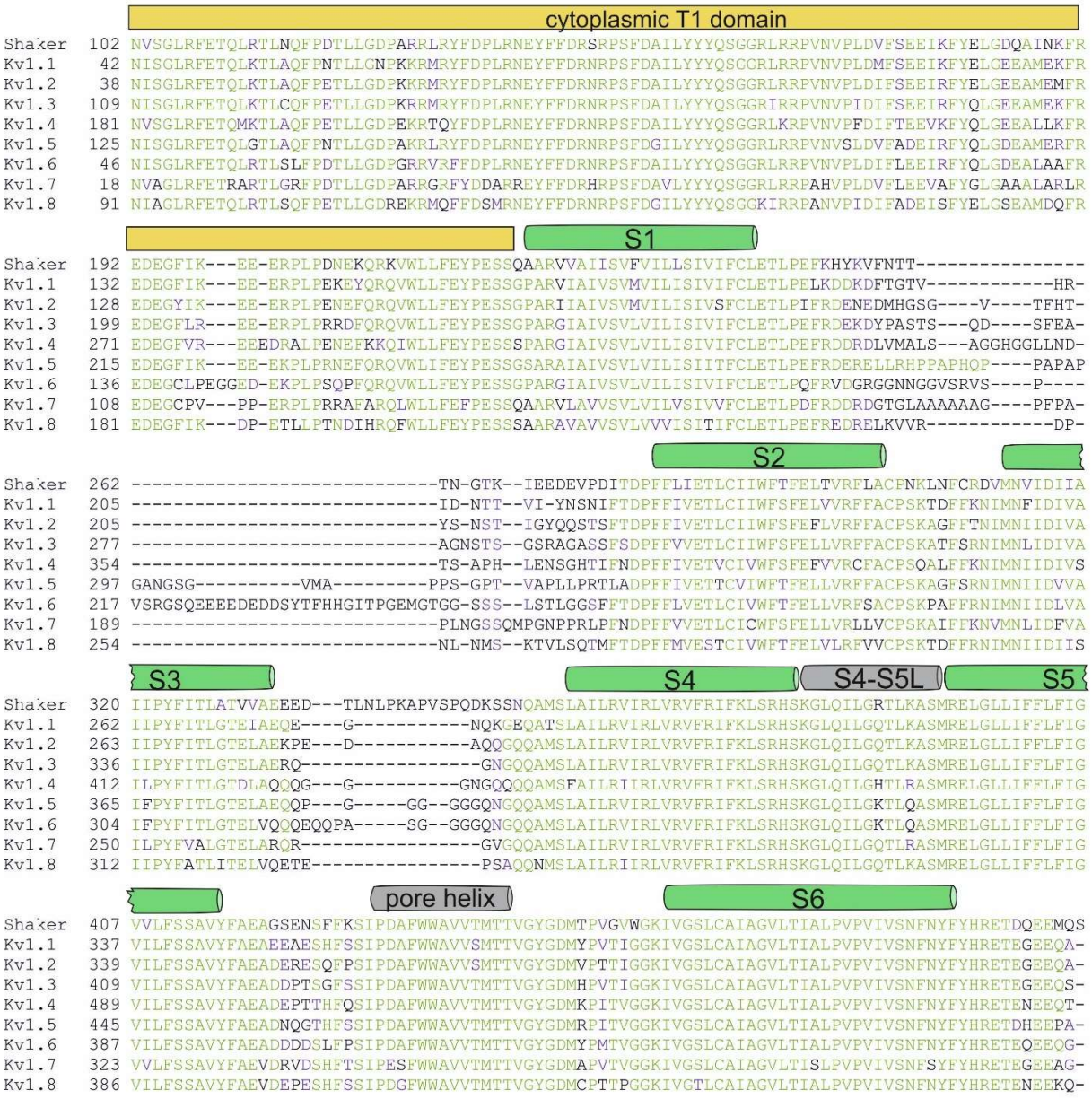

Figure 1.2 Amino acid sequence alignment of Kv channels
Amino acid sequence alignment of Shaker and the human K_V1 subfamily with locations of secondary structures. Green residues are identical and blue residues indicate similarity. The C- and N-termini have been omitted for space-saving purposes. Alignment is generated using T-coffee (http://tcoffee.crg.cat/apps/tcoffee/index.html) with input sequence IDs: Shaker-P08510, Kv1.1-Q09470, Kv1.2-P16389, Kv1.3-P22001, Kv1.4-P22459, Kv1.5-P22460, Kv1.6-P17658, Kv1.7-Q96RP8, Kv1.8-Q16322.

Common to all Shaker-related channels is the structural architecture of tetrameric symmetry. Each monomer consists of six transmembrane helices (S1-S6). A top-view of the channel shows that the first four helices (S1-S4) assemble in the periphery, linked to the pore domain by the intracellular S4-S5 linker that behaves like a protruding arm, and S5 and S6 assemble in the center to form the pore domain (A-B). This organization allows the S1-S4 region to act as independent voltage sensors controlling the ionic pathway. A K_V signature sequence, PXP, is located at the intracellular end of S6 and constitutes the main activation gate which bends open upon pore opening (red residues in figure 1.3C) [18, 60]. A re-entrant loop of the S5-S6 linker forms a narrow selectivity filter which contains the GYG signature sequence [18]. High K^+ selectivity is obtained by the unique ion binding sites which consist of carbonyl oxygens oriented towards the pore (dark blue residues in figure 1.3C). When entering the selectivity filter, the K^+ ion's interaction with water molecules is replaced by interaction with the carbonyl groups [14, 61]. The ions pass through the selectivity filter in a single file diffusion arrangement where each ion binds strongly to the selectivity filter but at the same time is destabilized by repulsion of the neighboring ion [61]. This is how the channel exhibit both high K^+ selectivity and a high K^+ permeation rate. The flexible glycines in the GYG motif allows the selectivity filter to adopt different conformations which prevent ion conduction (C-type inactivation).

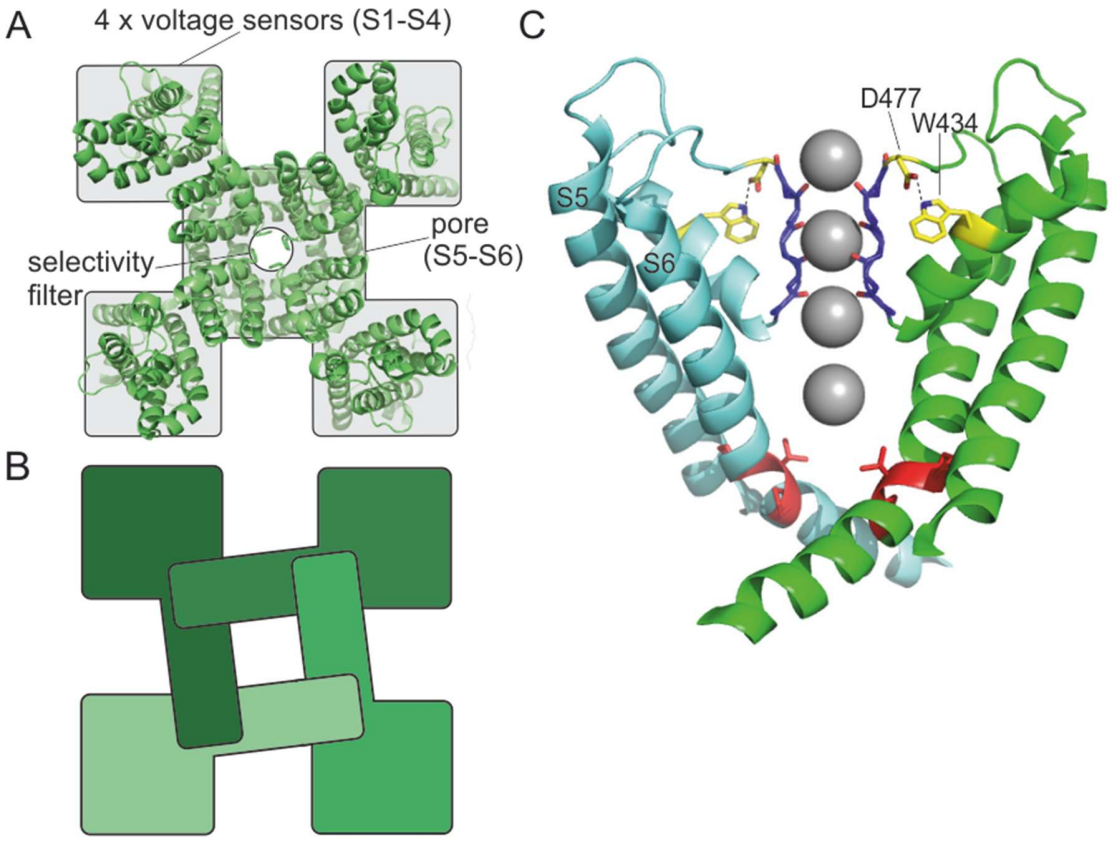

Figure 1.2 Overview of K_V channel structure and function
A) Crystal structure of the tetrameric K_V channel showing the top view (PDB: 2R9R). The four voltage sensors are symmetrically arranged as modules around the central pore which contains the selectivity filter. **B)** Cartoon of the relative rearrangement of the four subunits shows how this organisation allows independent VS movement and cooperative pore movement **C)** K_V1.2 crystal structure showing the S5-S6 helices of two subunits. Potassium ions are shown as grey spheres and the selectivity filter residues are highlighted in dark blue. The PXP motif at the bundlecross is highlighted in red, and in yellow is shown the interaction between Trp434 and Asp477.

There exist four main conformations of the Shaker channel which dictates the flow of K^+ ions (figure 1.4). In resting state or when deactivated, the channel is closed by the bundlecrossing of the four S6 intracellular C-termini. In the open activated state, the bundlecrossing widens and allows K^+ ions to pass. A third state is the N-type inactivated state in which the channel's N-terminus functions as a plug that inserts into the intracellular opening and blocks the pore. Finally, there is the C-type inactivated state in which a gate at the extracellular portion of the pore obstructs the ionic pathway.

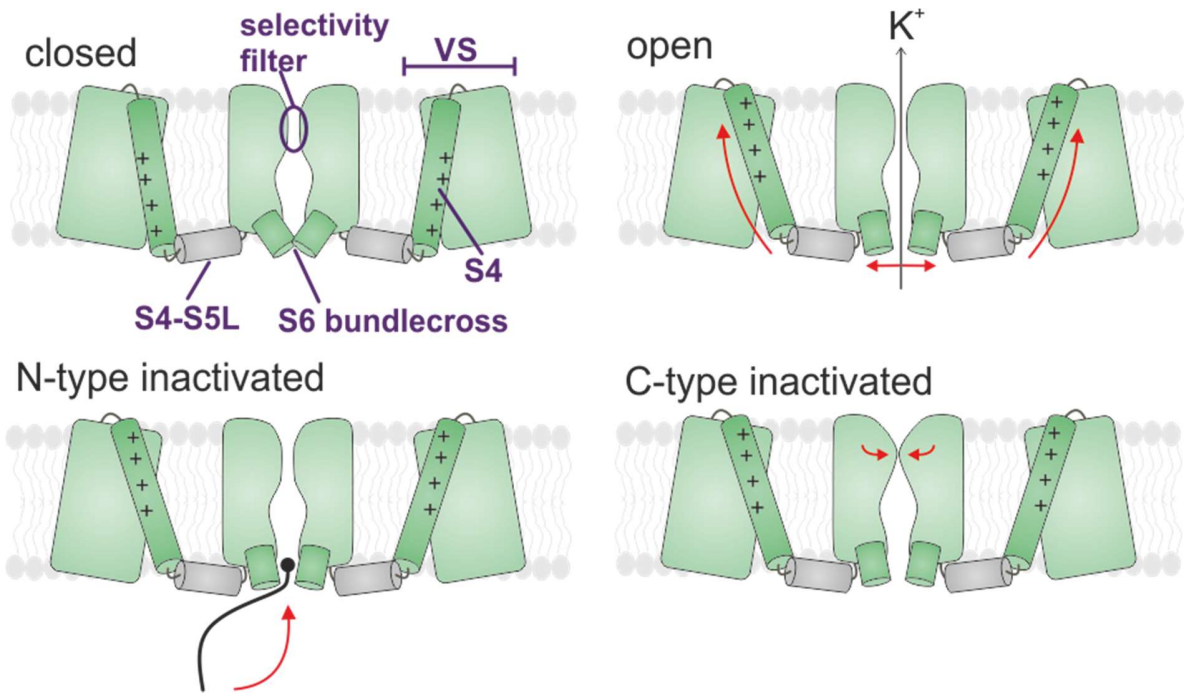

Figure 1.3 Main conformational states of Shaker
Cartoon illustrating the different states which regulate the flow of K^+ ions through the pore. When closed, the voltage sensors are deactivated and the S6 bundlecross blocks the intracellular pathway. In the open state, the voltage sensors are activated and the S6 bundlecross has widened to allow K^+ to flow through. The intracellular N-terminus of either the α subunit (Shaker) or the β subunit (K_V channels) enters the pore and blocks the ionic pathway leading to N-type inactivation. In absence of N-type inactivation, the selectivity filter rearranges which also blocks the ionic pathway and results in C-type inactivation. For clarity, only two subunits are shown.

1.5 Mechanism of K_V channel activation

The process by which K_V channels transition from the deactivated state to the open activated state can be divided into three distinct but tightly coupled mechanisms: Voltage sensing, electromechanical coupling and pore opening. Each mechanism is accomplished by rearrangements in different parts of the channel which are connected structurally and/or energetically. The probability of an open channel is regulated by the voltage sensor which in turn depends on the membrane potential.

The voltage-dependency originates primarily from four arginines in the fourth transmembrane helix, S4. The number of translocated charges per channel has been determined experimentally [49] and theoretically [50] to be 13 elementary charges. Numerous biophysical and computational studies have investigated the resulting motion of the S4 helix, and although they differ in relative distances, a current understanding of the voltage sensor movement has

converged towards a general consensus model [62, 63]. Upon membrane depolarisation, the S4 helix undergoes a 7-10 Å vertical displacement to accommodate the change in the electric field. The electric field has been shown to be highly focused in water-exposed crevices in the VS domain facing the intracellular and extracellular compartments during hyperpolarization and depolarisation, respectively [64]. This explains why the arginines do not need to traverse the bilayer completely to account for the displacement of 13 elementary charges. A second S4 helix movement is accompanied by a tilt and a rotation around its helical axis. The first movement (Q1) occur independently in each VS, applying a force onto the S4-S5 linker. Then, during the second S4 charge movement (Q2), energy is released to the pore domain in a cooperative conformational change which finally results in widening of the bundlecross at the intracellular S6 gates.

The VS movement does not exclusively depend on the rearrangement of charges but requires also a network of stabilizing residues. Substitution studies, performed in Shaker, in the region surrounding the gating charges have identified several hydrophobic residues to play a key role in shaping the steric and energetic landscape as the voltage sensor moves from resting to activated state [65]. These residues are collectively called gating pore residues and are situated close to the membrane center within S1-S3. While one residue (Ser240) allows the passage of arginines, others make up a narrow constriction forming a barrier as a hydrophobic plug (Ile237 and Ile287) [65]. Finally, two phenylalanines form molecular clamps and stabilize the arginines in the activated state via cation-pi interactions (Phe244 and Phe290) [66, 67].

Although complex, the described VS process is relatively well understood. However, when it comes to how the VS governs the state of the pore, the underlying mechanism remains less clear. A fraction of the displaced charges has been shown to be associated with pore opening [67-69] during which the S4 helix also moves [70]. Since pore opening is a transition that requires a cooperative movement of all four subunits, it means that the VS movement is not exclusively independent but also includes a cooperative component. In agreement with this, VS movement has been found to consist of the two major components, Q1 and Q2, which accounts for approximately 80% and 20% of the total displaced charge, respectively [13]. Electromechanical coupling of voltage sensor movement to pore opening is an ongoing subject as the molecular mechanism behind the cooperative motion is not fully understood. The tetrameric organisation

of the channel shown in figure 1.2B, gives an idea of how cooperativity regulates pore opening. The pore region (S5-S6) of each subunit overlaps with that of the adjacent subunit suggesting that intersubunit interactions are required for the pore to open.

Box 1.1 Two-state closed-open channel

When considering the state of the channel pore as a two-state closed-open process in which the voltage sensor either resides in the closed deactivated state or in the open activated state, the transition barrier depends on the relative free energy,

$$\Delta G = \Delta G_C + \Delta G_e, \tag{1.1}$$

where

$$\Delta G_C = \mathrm{RT} \cdot \ln(\mathrm{K}) \tag{1.2}$$

is the voltage-independent chemical energy difference with the equilibrium constant K, and

$$\Delta G_e = \mathrm{zFV} \tag{1.3}$$

is the voltage-dependent electrical work required to activate the voltage sensor, where z is the displaced charge in response to the voltage V, and F is the Faraday constant. The probability of being in the open state P_O, is given by:

$$P_O = \frac{P_O}{P_O + P_C} = \frac{1}{1 + P_O/P_C} = \frac{1}{1 + \exp\left(\frac{\Delta \mathrm{G}}{RT}\right)} = \frac{1}{1 + \exp\left(\frac{RT \cdot \ln(K) + \mathrm{zFV}}{RT}\right)} \tag{1.4}$$

At equilibrium, K can be written as $zFV_{1/2}$, where $V_{1/2}$ is the voltage at which 50% of the voltage sensors have activated (or 50% of the channels are open). Equation 1.2 then rearranges to:

$$P_O = \frac{1}{1 + \exp\left(\frac{V - V_{1/2}}{dV}\right)}, \tag{1.5}$$

where the midpoint value of activation is $V_{1/2,}$ and the steepness of the curve dV=RT/zF which is related to the number of displaced charges, are useful comparative parameters in characterizing effects of mutants on the open probability (P_o). Voltage sensor activation is experimentally measured as gating currents which are caused by movement of charges within the membrane [12]. The voltage dependency of charge displacement is then obtained by plotting the integrated gating currents as a function of voltage (QV curve) which then can be fitted to the Boltzmann function, equation 1.3, to obtain dV and $V_{1/2}$.

1.5.1 Electromechanical coupling

The S4-S5 linker is the covalent link between the VS and the pore region (figure 1.5A). Early indications on its pivotal role in coupling VS movements to pore movements showed that a voltage-dependent channel was functional as long as the S4-S5 linker and the S6 tail were compatible, as in from the same channel [71, 72]. The S4-S5 linker lines the intracellular membrane leaflet in a radial position well situated to translate S4 motions to pore movements (figure 1.5A). A general understanding of the coupling process is that the combined movement of the S4 helix during activation exerts a mechanical force on the S4-S5 linker which in turn acts on the S6 bundlecross. In the K_V crystal structure monomer, the S4-S5 linker is closely situated in parallel to the bundlecross, which could explain how the linker mechanically affects the state of the pore (red subunit, figure 1.5B). Indeed, it has been shown that hydrophobic interactions between residues of each region are critical for coupling VS movement to pore opening (light-pink residues in Figure 1.5B) [73, 74]. However, such intrasubunit interactions are not exclusively responsible for electromechanical coupling and cannot account for cooperativity. In fact, the coupling of movements is more complex than a simple push-and-pull mechanism. Substitution studies show that the ILT triple mutant (V369I, I372L, S376T) situated in the S4 helix, disrupt an energetic coupling between the VS and the pore, such that the final cooperative step is isolated from the early independent VS movements, and is shifted to very positive voltages [68, 70]. Another group of mutations situated on the inner S5 helix also perturb the transition towards the concerted opening [75]. Interestingly, these two groups cluster together in close physical proximity in the K_V channel crystal structure of adjacent subunits (yellow residues in figure 1.5B). Their individual profound effects on coupling of independent VS movements to concerted pore movement, and their possible intersubunit interactions strongly suggest that they play a key role in electromechanical coupling as well as cooperativity. Finally, an intersubunit interaction between the S6 and the corner of the S4-S5 linker and S5 has been shown to be crucial for stabilization of the open state (blue residues in Figure 1.5B) [76]. Taken together, the transfer of movements between VS and pore involves a network of stabilizing molecular interactions, but the exact structural implications and sequence of events of these interactions remain unresolved.

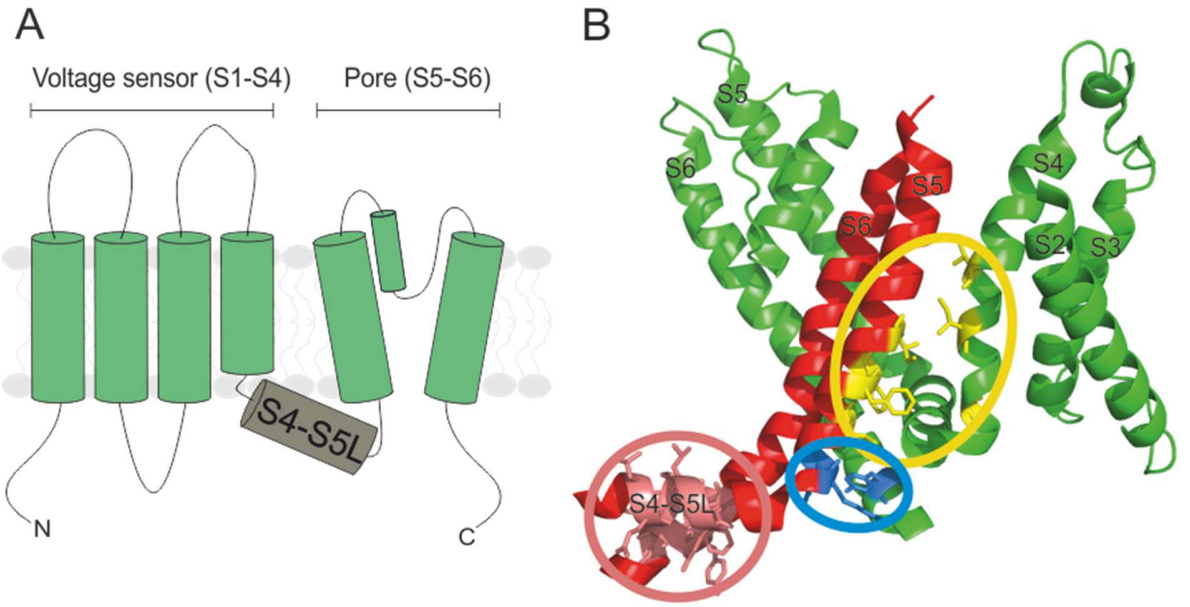

Figure 1.4 Shaker channel topology and gating residues
A) K_V channel topology B) K_V2.1 crystal structure [18] showing parts of two adjacent subunits (red and green) with gating residues and interactions important for electromechanical coupling and pore opening. The group of hydrophobic residues in the S4 helix (ILT: V369, I372, S376) [68] and the inner S5 residues (L398, F401, F402, I405) [75] are shown in yellow. Residues involved in intersubunit interactions between the S6 tail and lower S5 helix are shown in blue [76]. Annealing of the S4-S5L (L382-T388) to the S6 helix (Y481-H486) is shown in light pink [72, 73, 77]. The voltage sensor of the red subunit has been removed for clarity.

1.6 Mechanism of K_V channel inactivation

Voltage-gated ion channels can undergo inactivation, which is a mechanism where the pore becomes non-conducting before the intracellular gates open (closed-state inactivation) or has already opened (open-state inactivation). The various inactivation mechanisms display a wide range of rates (from milliseconds to minutes) and provide functional diversity for cells to shape action potentials and to regulate their physiological roles. K_V and Na_V channels can be inactivated by binding of a cytoplasmic region to the pore which prevents ion flow. For K_V channels, it is the N-terminal region [78, 79] which binds only after pore opening [80] (N-type inactivation), whereas for Na_V channels, it is a cytoplasmic loop [81, 82] which can bind to both a closed and an open pore [83]. A second usually slower inactivation mechanism in Na_V and K_V channels involves global conformational changes surrounding the pore region and the selectivity filter (slow inactivation or C-type inactivation) which in K_V channels result in pore constriction (discussed below) whereas the mechanism is less understood in Na_V channels [84]. U-type inactivation is a different kind of slow inactivation which has been identified in certain K_V channels, including

K_V1.5, K_V2.1, K_V3.1 and Shaker [85-87]. U-type inactivation exhibit different properties than C-type inactivation (e.g. in voltage-dependency, sensitivity to external potassium and blockers) and the molecular determinants are much less understood.

1.6.1 N-type inactivation

N-type inactivation in K_V channels modulates neuronal excitability and signaling by means of shortening the time that current passes through the channel. In N-type inactivation, the long and flexible N-terminus of one of the four subunits enters the side window of the cytosolic tetramerization T1 domain (T1) and physically occludes the open pore to block the ionic pathway in a ball-and-chain mechanism (Figure 1.6A) [78, 79, 88]. Inactivation can be eliminated by removing the N-terminal sequence and be restored by cytoplasmic application of the N-terminal peptide to the channel [78, 79]. Shaker, K_V1.4, K_V3.4 and K_V4.2 channels are intrinsically inactivated by the N-terminus [78, 89-91], while other K_V1 channels are inactivated by the N-terminus of auxiliary β1 or β3 subunits [90, 92] (except K_V1.6 which has an inactivation prevention domain [93]). The other K_V families do not undergo N-type inactivation. Derived peptides of the inactivating N-terminus, or inactivation particle (IP), of Shaker, K_V1.4 and K_V3.4 are capable of blocking K_V1 channels although there is no sequence similarity in the IPs [94-96] (figure 1.6B). Therefore, in contrast to the molecular mechanisms of VS activation and pore opening, the binding of the N-terminus does not seem to require specific amino acid interactions. Instead, the rate of inactivation depends on long-range electrostatic interactions between the chain and putative receptor sites [18, 79, 97, 98], and final pore block depends on general hydrophobic interactions between the tip and pore region [88]. In agreement with this understanding, the first 5-9 amino acids of the IP (inactivation particle) are mainly hydrophobic, while the downstream 20-40 amino acids, which act as the chain, are mainly hydrophilic carrying a net-positive charge (figure 1.6B).

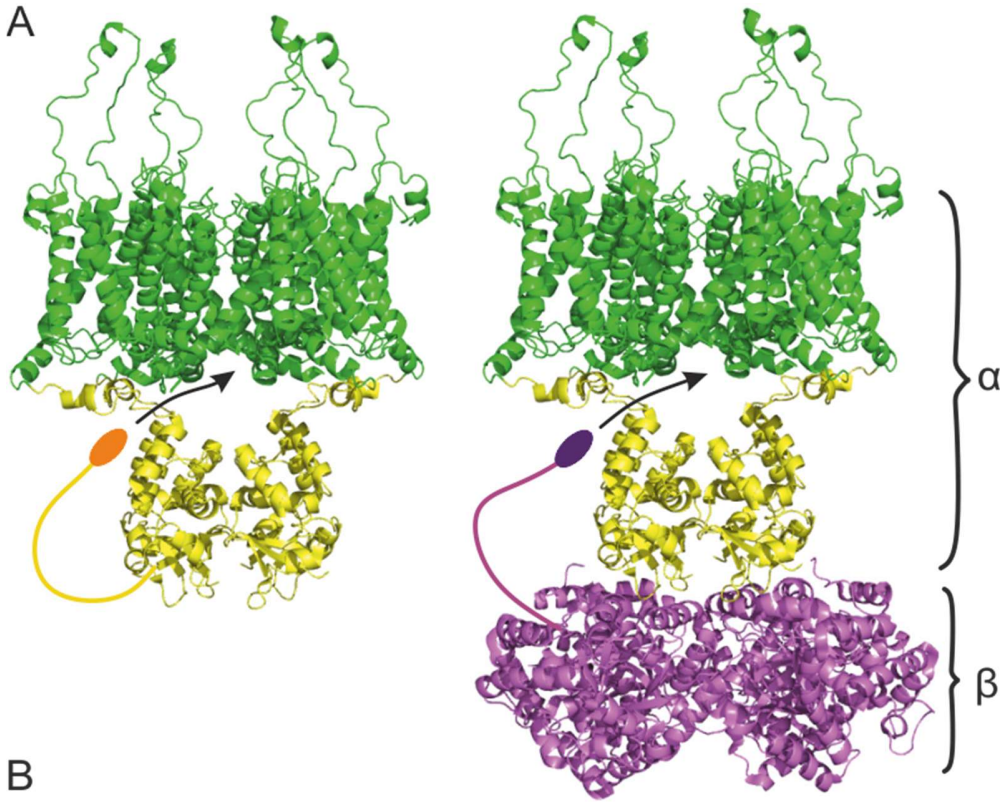

Shaker	MAAVAGLYGLGEDRQHRKKQQQQQQHQKEQLEQKEEQKKIAERKLQLREQQLQRNSL	+2
Kv1.4	MEVAMVSAESSGCNSHMPYGYAAQARARERERLAHSRAAAAAAVAAATAAVEGSGGS	0
Kv3.4	MISSVCVSSYRGRKSGNKPPSKTCLKEEMAKGEASEKIIINVGGTRHETYRSTLRTL	+6
Kvβ3	MQVSIACTEQNLRSRSSEDRLCGPRPGPGGGNGGPAGGGHGNPPGGGGSGPKARAAL	+3
Kvβ1.1	MQVSIACTEHNLKSRNGEDRLLSKQSSTAPNVVNAARAKFRTVAIIARSLGTFTPQH	+5
Kvβ1.2	MHLYKPACADIPSPKLGLPKSSESALKCRWHLAVTKTQPQAACKPVRPSGAAEQKYV	+5
Kvβ1.3	MLAARTGAAGSQISEENTKLRRQSGFSVAGKDKSPKKASENAKDSSLSPSGESQLRA	+4

Figure 1.5 N-type inactivation in K_V channels
A) Structural overview of the ball-and-chain mechanism where the N-terminus of either the alpha (left) or the beta (right) subunit enters the side window of the T1 subunit (in yellow) and binds to the open pore **B)** Comparison of N-termini of Shaker and of human K_V channels and of β subunits (residues 1-60) which are responsible for N-type inactivation. Hydrophobic residues are colored in red and charged residues in blue. To the right is noted the net charge. Sequence Uniprot IDs: Shaker-P08510, Kv1.4-P22459, Kv3.4-Q03721, Kvβ3-O43448, Kvβ1.1-Q14722.2, Kvβ1.2-Q14722.3, Kvβ1.3-Q14722.

It is interesting that different IPs can block the same channels. It suggests that the inactivation pathway is not identical although the receptor site is the same. As an example, the N-terminal glutamates in K_V1.4 (E2 and E9) are of unique importance for efficient inactivation [99], whereas insertion of glutamates in the same region of the Shaker N-terminus has the opposite effect (L7E) [78].

In the $K_V1.2$ crystal structures [18, 45], the channel is in complex with a β subunit which do not cause N-type inactivation (β2), so the position and structure of the IP is not known. NMR studies of IPs indicate different conformations ranging from unstructured (Shaker) to structured ($K_V1.4$ and $K_V3.4$) [100, 101]. These observations suggest that the IP could either always be disordered and available to bind inside the channel after the pore opens, or that binding to early receptor sites trigger a structural unfolding. Interestingly, a recent computational study with Shaker shows that an IP adopting a helical structure spontaneously enters the inner cavity of the pore, and then inserts the tip deeply into the pore when driven by voltage [102].

1.6.2 C-type inactivation

The other inactivation mechanism in Shaker is C-type inactivation and occurs at the selectivity filter. The structural basis of the C-type inactivated state is well understood. First, molecular dynamic simulations of the KcsA channel shows that flexibility provided by the glycines in the GYG motif allows the selectivity filter to adopt several conformations which disturb coordination of the ions, which in turn prevents ion conduction [103]. In agreement with this, X-ray crystallography studies of inactivated KcsA channels show a confirmation in which the selectivity filter is pinched inward at the GYG motif [88, 104]. Also, C-type inactivation is highly sensitive to external K^+ [105, 106], pore blockers [107, 108], cations [109, 110] and mutations in the region surrounding the pore [105, 111, 112], but the mechanism which initially drive the filter to rearrange and cause inactivation is less clear. One hypothesis is that K^+ dissociation from the pore caused by the occasional entry of cations favors the inactivated state [110]. Alternatively, opening of the S6 helical bundlecross has shown to be allosterically coupled to the inactivation gate via a network of steric contacts which in the end cause the filter to collapse [112]. C-type inactivation is a complex process which may involve both mechanisms. Possibly, coupling of the S6 gates to the inactivation gates constitute an intrinsic way for the channel to ensure inactivation, whereas ion vacancy is an extrinsically regulated pathway which accelerates the transition into inactivation further.

An interesting feature of the C-type inactivated state is the presence of water molecules behind the selectivity filter, as demonstrated by molecular dynamic simulations on the KcsA structures [113]. It is shown how recovery of the pinched GYG motif requires release of the water molecules

to the extracellular side. However, the molecular determinants behind the initial entry of the water molecules is not corroborated, yet, and it is not certain whether the water molecules are in fact causing the pinched state. To get a complete understanding of C-type inactivation, it is necessary to find out how and if, activation of the S6 helical bundle and/or K^+ dissociation leads to entry of the inactivating water molecules behind the filter.

Molecular dynamic simulations on $K_V1.2$ [114] support a link between C-type inactivation and water molecules as "gate keepers". A hydrogen bond between Trp434 and Asp477 (yellow residues in figure 1.3C) keeps water away from entering behind the selectivity filter [114]. The W434F mutation is a well known mutant used to abolish ionic currents without affecting the intracellular gate [115] and it has been shown that this mutation results in a constitutively C-type inactivated channel [111]. W434F has therefore been widely used to investigate gating currents. The absence of a hydrogen bond between Trp434 and Asp477 in W434F channels is probably what is accelerating the transition into the C-type inactivated state, by allowing water molecules to enter from the external solution.

1.7 Genetic incorporation of unnatural amino acids

Given the important roles of proteins in biology, it is desirable to be able to manipulate proteins for understanding structure-function relationships and for generating proteins with new properties. Many efforts have been made to incorporate UAAs into proteins to introduce new functional groups different from those found in canonical amino acids. To add a new amino acid to the genetic repertoire, a codon is needed that uniquely specifies that amino acid. The 20 canonical amino acids are encoded by 61 triplet codons, leaving the remaining three stop-codons (TAG, amber; TAA, ochre; and TGA, opal) as candidates for suppression for the incorporation of an UAA. The amber stop codon has been the most used for UAA incorporation as it is the least frequent stop codon in *E.coli* (9%), yeast (24%) and mammalian cells (~18%) [116] thus limiting UAA insertion at endogenous sites.

In 1989, Dr. Schultz reported for the first time the incorporation of UAAs into a protein in a cell-free system via chemical aminoacylation of a suppressor tRNA [117]. In the following decade it was established that the nonsense suppression method could become a general tool in modifying proteins enabling unprecedented structure-function studies. Indeed, in 1995 the approach was

expanded to function in living cells in Xenopus oocytes where the amino-acylated tRNA was injected with the UAA and protein-encoding mRNA [118]. The high expression efficiency of Xenopus oocytes combined with the high sensitivity of electrophysiology made it possible to probe UAA insertion, and once again did Xenopus oocytes play a valuable role in developing a tool for the understanding of ion channels. Today, more than 20 channels and receptors have been expressed with more than 100 different UAAs using the chemical aminoacylation strategy [119]. Although successful, the technique is limiting as the stoichiometry of injected amino-acylated tRNAs still produces relatively small amounts of protein.

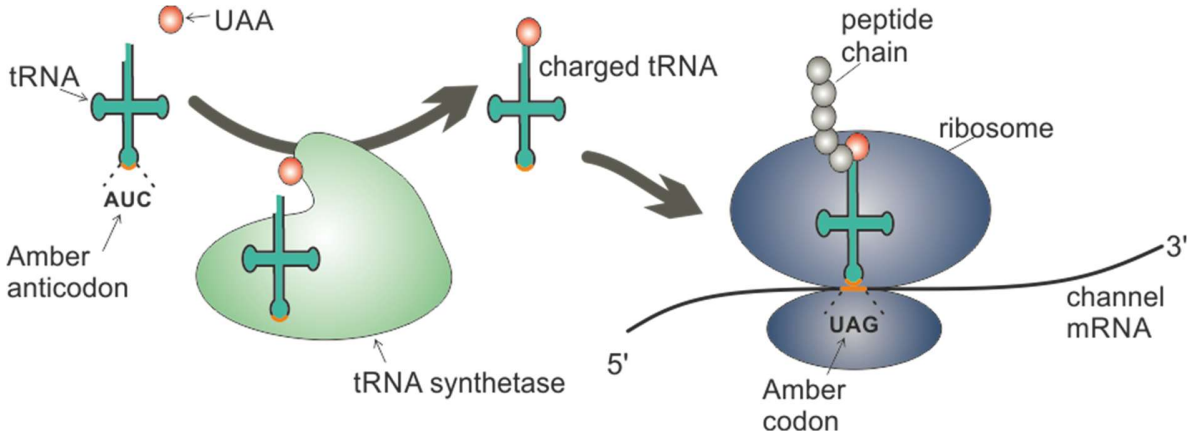

Figure 1.6 Cartoon of genetic incorporation of UAAs via *in vivo* aminoacylation.
The UAA is specifically aminoacylated to the $tRNA^{AUC}$ by the tRNA synthetase. The charged UAA-$tRNA^{CUA}$ is then recognized by the ribosome when translation of the protein mRNA reaches the amber codon, and the UAA is then inserted into the growing peptide chain.

An alternative technique relies on *in vivo* aminoacylation using an engineered aminoacyl tRNA synthetase (aaRS) which specifically charges the tRNA with the UAA without cross-reaction with endogenous tRNAs or amino acids (orthogonality) (figure 1.7). Orthogonality is achieved by identifying aaRS/tRNA pairs from other organisms, which then are altered to specifically recognize an UAA via directive evolution using large libraries of mutant aaRS's. In 2001, the Schultz laboratory generated an orthogonal tRNA/synthetase pair to function in *E. coli* by importing it from the archaea *Methoanoccus jannaschii* whose $tRNA^{Tyr}$ identity elements differ from those in *E.coli* [120]. In the following years, the genetic code expansion advanced rapidly to also include yeast and mammalian cells, in which bacterial aaRS/tRNA pairs are generally orthogonal [121]. So far, three bacterial (tyrosyl, leucyl, tryptophanyl) and one archaea (pyrrolysyl) aaRS/tRNA pair have been used to incorporate distinct UAAs in mammalian cells

[121]. Today, almost 200 different UAAs have been incorporated into proteins in prokaryotic and eukaryotic organisms using the *in vivo* aminoacylation strategy [122].

1.8 Protein translation

While orthogonality between the UAA and the engineered synthetase/tRNA pair is necessary to obtain specificity and high incorporation fidelity, it is not a guarantee. There are other mechanisms of the translational machinery in the cell, which can cause unwanted expression of proteins lacking the UAA.

The process of translation is a step in gene expression during which the single stranded mRNA is translated into protein, according to the genetic code. Each group of three bases in the mRNA molecule codes for an amino acid. Within all eukaryotic cells, translation occurs in a specialized complex called the ribosome, which is located in the cytoplasm, and consists of two large RNA molecules (40S and 60S) and a subset of ribosomal proteins.

When the mature mRNA has left the nucleus, translation begins at the 5'end of the mRNA and ends at the 3'end. An initial complex structure of three initiation factor proteins and the small 40S ribosomal subunit assembles and binds a methionine-charged tRNA. Subsequently, this complex binds to the mRNA 5'end (figure 1.8) and starts to scan the mRNA for the 5'-proximal AUG codon. The large 60S ribosomal subunit binds to the complex and initiation factors are released (figure 1.8). The next step is elongation during which incoming charged tRNAs are recognized by the ribosome according to the mRNA codon, and peptide bonds are formed between the amino acids to create a growing polypeptide chain (figure 1.8). Elongation continues until the ribosome encounters a stop codon, and release factors then binds to facilitate release of the ribosome from the mRNA.

Most mammalian mRNAs follow the straightforward model of linear ribosome scanning, in which initiation occurs exclusively at the 5'-proximal AUG codon, and termination occurs at the downstream stop codon at the end of the open reading frame (ORF). Factors such as sequence context and RNA structure can influence the scanning efficiency and cause alternative translation resulting in different proteins [123]. Both start and stop codons can be "ignored" by the ribosome (readthrough and leaky scanning) resulting in alternative ORFs [123, 124]. Resumption of scanning after termination on the same mRNA is also a mechanism in eukaryotic ribosomes

(reinitiation), adding possibilities to the mRNA coding potential [124]. In this case, the 40S subunit is not released from the mRNA, but stays in a complex with the mRNA. This only happens when the first ORF is short (e.g. 10-20 codons), such that initiation factors are still connected to the ribosome, thus allowing a resumption of scanning for another start codon further downstream.

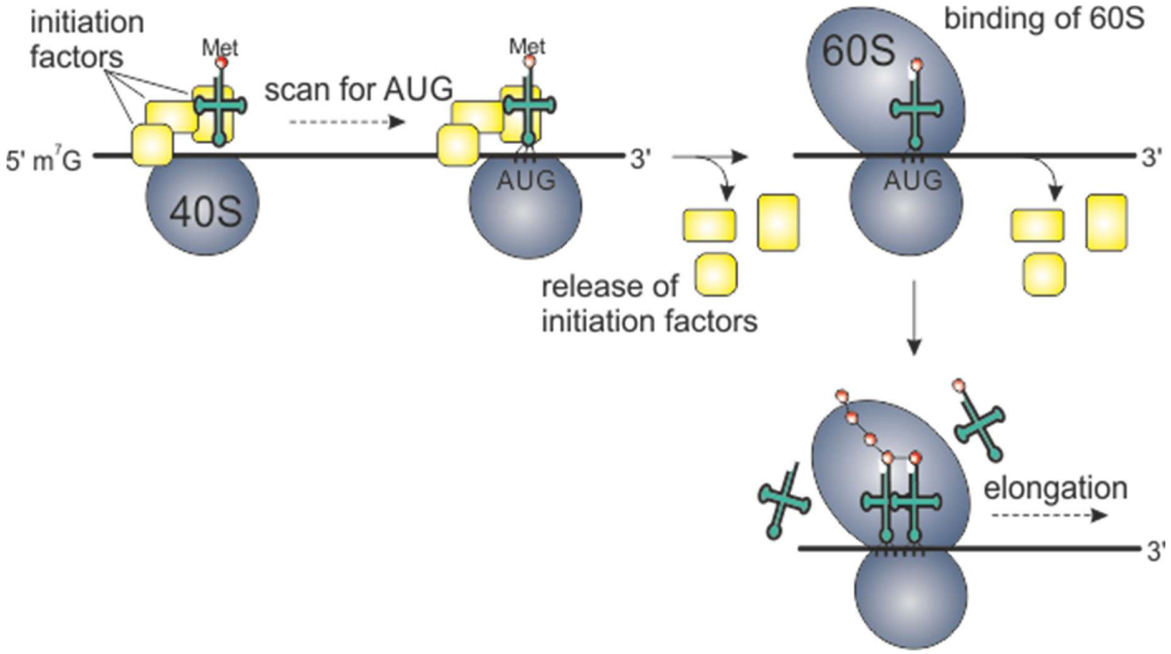

Figure 1.7 Protein translation
Cartoon of the eukaryotic translation machinery. Yellow boxes represent initiation factors which form an initiation complex with a methionine-tRNA, the mRNA and the 40S ribosomal subunit. When scanning for the 5'-proximal AUG start codon, the 60S subunit binds to the complex and initiation factors are released which marks the beginning of the next step, elongation. The ribosome reads the mRNA codons in a base-by-base fashion, binds to the corresponding tRNAs and creates peptide bonds of the incoming amino acids to form a polypeptide chain.

If a stop codon resides near the initiation site (by spontaneous mutation or naturally occurring), there is a possibility that gene expression is compromised. In figure 1.9A is shown an example of an mRNA ORF (blue frame is translated). Then, in figure 1.9B is shown three translation scenarios, in the case where a premature stop codon is mutated in close vicinity to the start site. Linear scanning would result in ribosomal release and give one short ORF. On the other hand, stop-codon readthrough would ignore the stop codon and yield a full length ORF. Since the stop codon is close to the first initiation site, it is also likely that initiation factors are still bound and allows for resumption of initiation at an alternative downstream start codon, thus yielding two ORFs.

When using UAA incorporation with non-available UAA-charged tRNAs, a number of things can happen depending on the position of the stop codon. Ideally, the ribosome stops translation when it encounters the amber stop codon and releases from the mRNA such that no functional protein is translated. This scenario constitutes an intrinsic control for UAA expression, but only if the stop codon is not situated in the C-terminal portion such that a C-terminal truncated and functional protein would be expressed. On the other hand, if the stop codon is situated in the near N-terminal portion, the ribosome may reinitiate translation and result in N-terminal truncated proteins. The latter scenario is demonstrated in chapter 6 where we shed light in important translational factors. Therefore, for each amber stop mutation for any UAA incorporation in any protein, it is important to consider all translational scenarios and measure the amount of leak expression in absence of the UAA to be able to evaluate potential effects of a mixed population during UAA experiments.

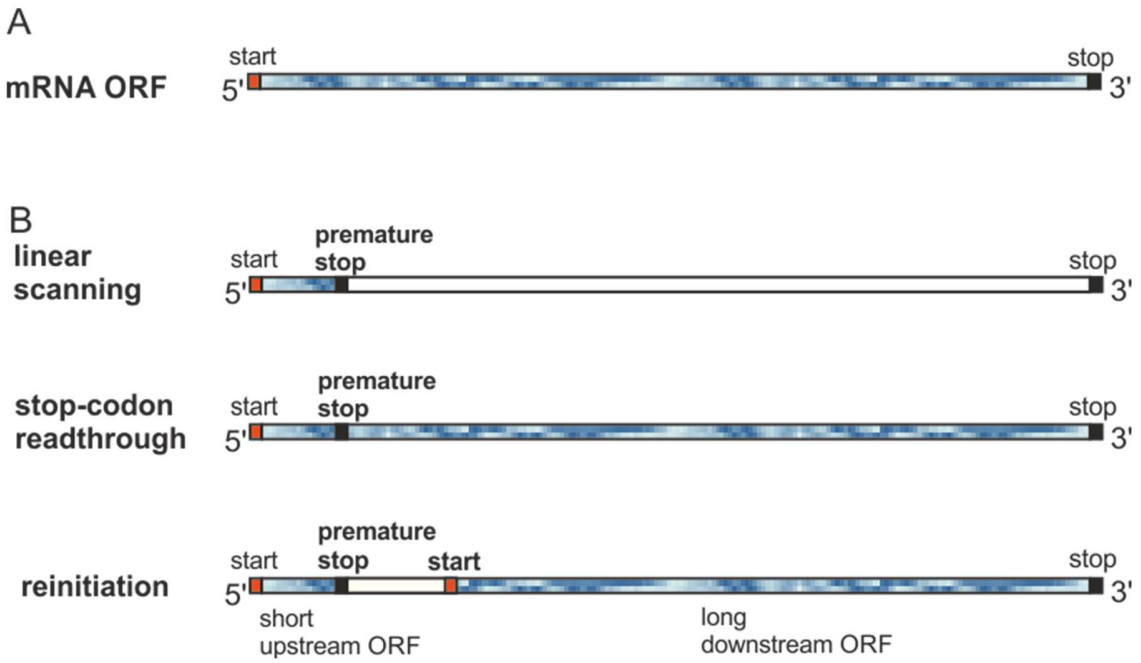

Figure 1.8 mRNA open reading frames and premature stop codons
A) Example of an mRNA ORF where the blue frame indicates translated area. In **B)** are shown three translation scenarios in case of a premature stop codon. Normal linear scanning results in a short ORF, whereas readthrough of the premature stop codon would result in a full length ORF as in A). Reinitiation of translation at a downstream start codon would result in two ORFs.

1.9 Cut-open oocyte voltage clamp

Two-electrode voltage clamp (TEVC) and patch clamp are powerful tools which have characterized numerous functional properties of electrogenic membrane proteins in oocytes. In TEVC, a current-injecting and a voltage-sensing electrode are inserted into the oocyte to control the membrane potential of the whole membrane. In TEVC, the oocyte membrane is large compared to the single points through which current is injected and voltage is sensed, which likely causes a non-homogenous clamp before the whole membrane is fully charged (space clamp). The oocyte membrane is also highly invaginated, adding further to a non-homogenous clamp. It means that the measurement of fast kinetics is compromised by imperfect space clamp, and that recording of fast currents (currents with the same timescale as the time it takes to charge the membrane) do not necessarily originate from a population of channels which is experiencing the same voltage, but is rather a sum of differently clamped channels. In addition to the space clamp issue, the speed with which the membrane potential is changed is not fast enough to resolve fast currents in TEVC (clamp speed). In other words, charging the membrane capacity takes longer time than the kinetics of certain currents of interest.

In order to optimize accurate recordings of fast signals, Drs. Bezanilla and Stefani built the cut-open oocyte voltage clamp (COVC) technique in the 1990's [12, 125-127]. One way to improve the clamp speed, is to limit the access resistance originating from the current-injecting pipette. In COVC, this is done by injecting the current through a "cut-opened" oocyte, giving electrical access to the cytosol. This is obtained by mounting the oocyte onto an apparatus of three electrically isolated compartments (the bottom chamber, guard shield, and top recording chamber) as illustrated in figure 1.10. The concept of separating different parts of the cells via electrical insulations is inspired by the sucrose and vaseline gap methods, which were developed to measure the membrane potential in nerve or muscle fibers [128, 129].

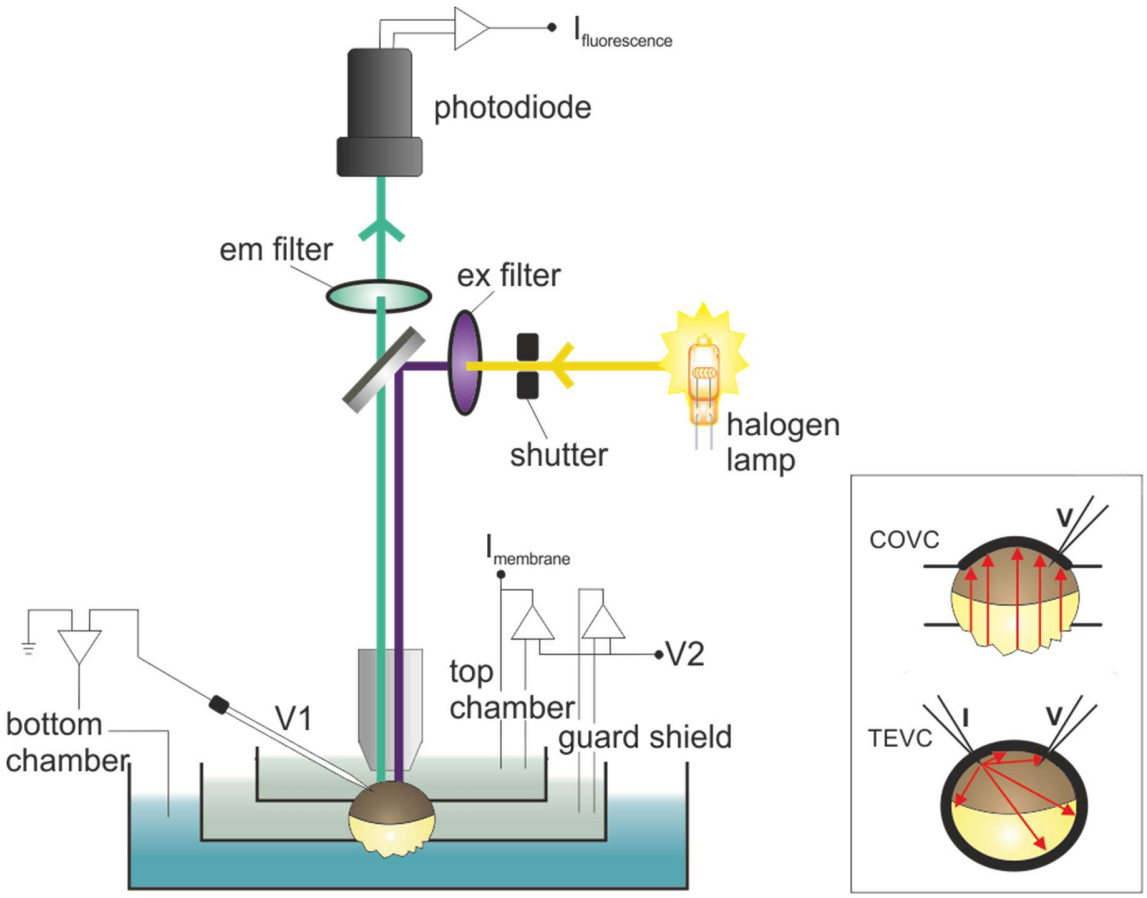

Figure 1.9 Illustration of the COVC and VCF setup
A permeabilized oocyte is mounted on a chamber of three electrically separated compartments. The bottom chamber is clamped to 0 mV (as measured by V1), while the top chamber and guard shield are clamped to the command potential (as measured by V2). V1 senses the voltage under the membrane and current is injected into the oocyte via the bottom chamber. For fluorescence measurements, the excitation light is directed towards the oocyte surface via a dichroic mirror and the emitted light is detected by a photodiode. Inset to the right illustrates the difference between COVC and TEVC. The red lines indicate injected current flow, and the bold part of the membrane highlights the clamped region.

The current is now injected via the solution in the bottom chamber through a saponin-permeabilized part of the oocyte. By eliminating the pipette resistance, the membrane can be charged within less than 1 ms (in optimal conditions, even a 24 µs charging time constant can be achieved [127]). The COVC configuration also improves the space clamp issue as only the upper chamber is clamped, and the geometrical arrangement of the clamped area and the area of current injection are comparable in size (inset, figure 1.9) Finally, the intracellular solution can also be controlled in COVC, allowing application of intracellular blockers or changing the ionic composition.

During COVC recording, the bottom chamber is connected to ground and maintained at 0 mV as measured by the voltage-sensing electrode impaling the oocyte in the top chamber (V1). The top chamber and the guard shield are clamped to the command potential (V2). The purpose of the guard shield is to prevent electrical leakage between the lower and top chamber.

Protein expression in xenopus oocytes is not symmetrically distributed, but is polarized in the animal versus the vegetal pole [130, 131]. Different levels of heterogenous channel expression can yield different current phenotypes (e.g. by external K+ accumulation in the case of high Shaker channel density). Also, asymmetrically distributed endogenous auxiliary subunits may affect open probabilities. It is therefore preferable if the fluorescence in VCF is collected from the same region which is clamped, such that fluorescence and current data originate from the same channels. Since the main purpose of VCF is to compare fluorescence with current signals and relate their kinetics and voltage-dependencies to each other, the COVC configuration is more suitable compared to TEVC, since in TEVC, the whole membrane is clamped, and in COVC, only the upper chamber is clamped. Moreover, due to the non-uniform space clamp during the time it takes to charge the membrane in TEVC, the issue becomes even more important when accurate comparison of fast fluorescence and current signals is needed (< 1ms).

1.10 Voltage clamp fluorometry

While electrophysiology provides functional information about voltage-dependent states of a channel, insights into the underlying conformational changes are lacking. The ability of certain molecules (fluorophores) to emit photons has been used for decades to investigate molecular and cellular mechanisms, and advanced fluorescence-based techniques have become an important tool in biophysical research due to the diverse utilization of fluorophores. Voltage clamp fluorometry (VCF) takes advantage of a fluorophore's sensitivity to the local environment, and thus it's ability to sense certain structural changes within proteins. Before describing VCF, the underlying concepts of fluorescence is introduced first.

1.10.1 Fluorescence basics

Whether a molecule can fluoresce depends on the energy levels of the electrons within the molecule. For the molecule to absorb a photon, the energy of the photon must correspond to the

electronic transition between the ground state (S0) and a higher electronic state (S1) (figure 1.11A). Usually, the absorbed photon contains more energy than is necessary for the S0-S1 transition, which results in excitation to a vibrational level. Following vibrational relaxation to the S1 state, the fluorophore can return to S0 through non-radiative processes or by emitting a photon (figure 1.11A). The probability of a molecule absorbing a photon is described by the extinction coefficient (ε), while the probability of emitting a photon is described by the quantum yield (QY), and the "brightness" of a fluorophore is proportional to both factors.

Box 2.1 Photophysical parameters of fluorescence

The extinction coefficient ε ($L \cdot mol^{-1} \cdot cm^{-1}$) is given by the Lambert-Beer formula:

$$\varepsilon = \frac{log\frac{I}{I_0}}{l \cdot C} = \frac{A}{l \cdot C} \quad (2.1)$$

, where A is the absorbance which depends on the intensity before I_0 and after I absorption, l is the length of the absorbtion path (cm) and C is the molar concentration (mol/L).

The QY is expressed as the number of emitted photons/sec divided by the sum of all pathways to the S0 ground state:

$$QY = \frac{k_f}{k_{nr} + k_f} \quad (2.2)$$

, where k_f is the radiative rate constant leading to fluorescence, and k_{nr} is the non-radiative rate constant.

When the fluorescence intensity during VCF recordings changes due to a protein rearrangement, it is caused by one of two possible mechanisms. Quenching is a mechanism where the fluorophore's ability to emit photons is decreased due to contact with another molecule (a quencher). The effect of quenching can be seen as a decreased excitation spectrum (figure 1.12B). The quenching efficiency is strongly distance-dependent and requires physical contact, i.e. overlap of the van-der-Walls radii (~ 2-3 Å). An efficient quencher which decreases the QY of most fluorophores is molecular oxygen. Other quenchers include aromatic or aliphatic amines and the heavy atom quenchers iodide and bromide. A relevant group of quenchers regarding VCF is amino acids within the protein itself. While tryptophan and tyrosine quenches fluorescein

[132], Alexa fluorophores are also quenched by histidine and methionine [133]. Tryptophan itself, a fluorescent amino acid, is quenched by lysine, tyrosine, glutamine, asparagine, glutamic and aspartic acid and most efficiently by cysteine and histidine side chains [134].

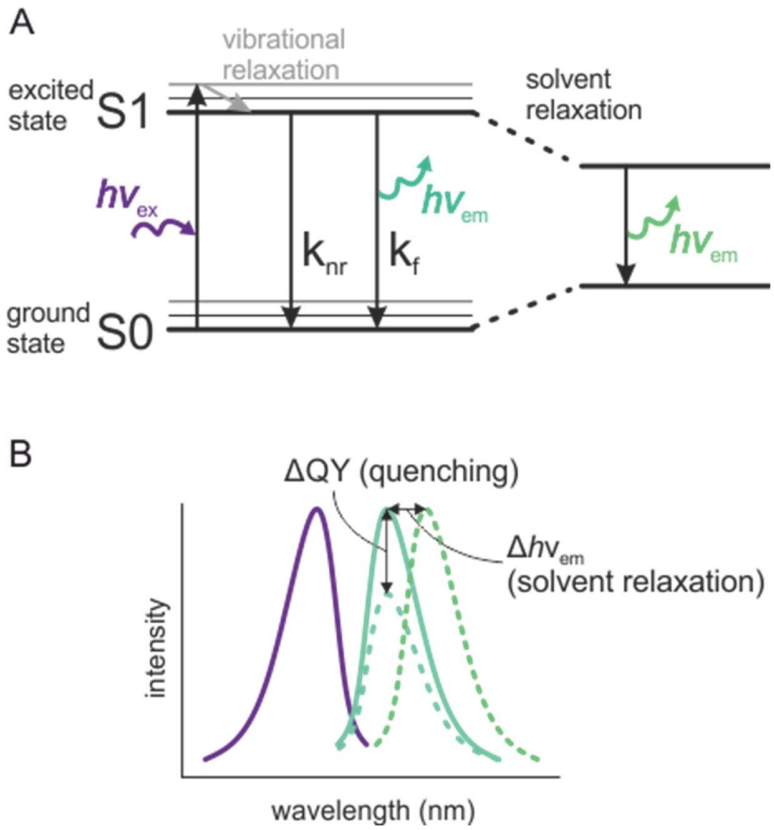

Figure 1.10 Fluorescence parameters
A) Jablonski diagram illustrating excitation of a molecule from the S0 ground state to a vibrational level of the S1 excited state. The molecule returns to ground state either via a non-radiative pathway (k_{nr}) or by emitting a photon (k_f). The energy of the emitted photon depends on the solvent hydrophobicity. **B)** Example of absorption (purple) and excitation (turquoise) spectra, with the effects of fluorescence modulation by either quenching or solvent relaxation.

While quenching is observed as a reduction of the fluorescence intensity, the energy of the emitted photons is also a valuable parameter, which brings us to the second factor that modulates fluorescence in VCF. When the fluorophore's intrinsic dipole moment changes during excitation, while surrounded by dipoles such as water molecules, the energy difference between S0 and S1 decreases due to two reasons. In the ground state, the surrounding dipoles will have aligned with the S0 dipole moment. Upon excitation, the (now) S1 dipole moment is no longer in alignment with the surrounding dipoles, leading to a higher energy state. This difference defines the wavelength of excitation. The surrounding dipoles will now align to the new S1 dipole

moment, effectively lowering the energy of the excited state (figure 1.11A). When the electron returns to the ground state, the (now again) S0 dipole moment is no longer aligned with the surroundings, increasing the energy level of the S0 state upon emission (figure 1.11A). For this reason, the shift between excitation and emission is increased, leading to a shift of the emission to longer wavelengths (figure 1.11B). This is called solvent relaxation and is the reason why the spectrum shifts towards higher wavelengths when the environment becomes more hydrophilic.

The high sensitivity of the fluorophore to the surrounding microenvironment reflects the useful application of fluorescence in studying local protein rearrangements. Whether the rearrangements are associated with changes in the surrounding solvent hydrophobicity or with quenching by nearby amino acids, the fluorophore is capable of probing relative conformational changes within the immediate vicinity. Moreover, typical fluorophore lifetimes are in the picosecond to nanosecond range which, in principle, permits detection of protein conformational changes with high temporal resolution. In practice, the detection is limited by the temporal resolution of stimulation initiating the protein movement (voltage/clamp speed, ligand application, light activation) and of the detection system.

1.10.2 How conformational changes are detected with VCF

Voltage clamp fluorometry was developed shortly after the COVC technique in the Drs Bezanilla and Isacoff laboratories [46, 135]. The approach for fluorophore labelling is based on scanning cysteine accessibility mutagenesis, where exposed residues are identified via agents which specifically react with accessible cysteines [136]. The protocol includes insertion of a cysteine at the site of interest which needs to be extracellular and accessible. Also, removal of intrinsic cysteines that could be accessible, is important to prevent unspecific labelling. Following injection and oocyte incubation, the oocytes are incubated with a maleimide dye for 20 minutes which, via thiol chemistry, becomes covalently linked to the available cysteines on the oocyte surface (including endogenous cysteines).

The VCF setup used for the experiments in the thesis is based on the one described by Drs Cha and Bezanilla (1998) [137]. An upright fluorescence microscope with a photodiode detection system installed at the optical exit port on the microscope is used and a 100 W-12 V halogen lamp is used as excitation source. The wavelength of the incoming light is selected by passing

through an excitation filter. The light directed towards the oocyte surface via a dichroic mirror and through a water-immersed 40X objective (figure 1.10). After excitation of the fluorophores present at the oocyte membrane, the emitted fluorescence is collected by the objective and passes through an appropriate emission filter (to exclude scattered emission) and is detected by the photodiode which is connected to a signal processor to digitize the data. An electrical shutter between the light source and the excitation filter is inserted to synchronize the light with the applied voltage protocol.

In summary, the current and fluorescence in VCF is detected simultaneously in real time from the same region of the oocyte, allowing direct comparison of gating current or channel opening kinetics with associated conformational changes as experienced by the fluorophore. The use of VCF is not limited to COVC or TEVC, but has also been successfully combined with patch clamp and total internal reflection fluorescence microscopy [138-142]. Moreover, instead of environment changes, the technique can be used to measure distance changes using fluorophore pairs for Förster- and lanthanide-based resonance energy transfer (FRET and LRET) techniques [143, 144].

The use of VCF with Shaker in Drs Bezanilla and Isacoff laboratories was a success [46, 135, 137, 145]. Extracellular voltage sensor domains had been TMRM-labeled and conformational changes of the S4 corresponded to charge movements both kinetically and voltage-dependently, confirming the role of S4 movement in channel activation. It rapidly led to application of the technique in other research groups. As a result, key findings of several ion channel dynamics followed, including voltage-dependent sodium and calcium channels [146, 147], ether-a-go-go K+ channels (EAG) [148], HCN and CNG channels [142, 149] as well as a voltage-dependent phosphatase (*Ci*-VSP) [150]. In all the studies, the VS was TMRM-labeled and characterized and compared to VS activation, pore opening or inactivation. Since sodium and calcium channels consist of one large polypeptide chain, VCF allowed the study of individual VS movements. The channels consist of 4 domains of same topology (6 transmembrane segments) but each domain differ in primary structure and thus also contribute differently to channel function. In sodium channels it was found that domain III and IV rearrange during inactivation. In calcium channels it was found that domain II and III moved during channel opening. The findings underline the difference with respect to potassium channels, which consist of four identical subunits with equal

contribution to the activation process. The S4 helix in EAG channels rearranged during gating, but also at more hyperpolarized potentials where no electrical measurements show channel activity. In HCN channels, S4 movements were identified during mode shift, and the S4 movement in CNG channels unraveled a role in the cooperative opening mechanism. Together, the VCF experiments confirm the role of voltage sensor movement during charge movement in ion channels, but also demonstrate that the voltage sensor is involved in other mechanisms. The VCF study of Ci-VSP is interesting because the protein exists as an isolated monomeric voltage sensor of S1-S4 while also lacking a pore. Probing the S4 movements showed that the protein would still undergo multiple rearrangements despite the absence of pore opening, indicating that the VS is structurally stable on its own and undergoes several rearrangements as an independent module.

1.11 Thesis objectives

Because of their widespread physiological implications, ion channels are often involved in mechanisms which are affected by the cause of diseases leading to a range of disorders and symptoms complicating disease treatment, and further reduce life quality and life expectancy. Therefore, in-depth studies of ion channel structure and function are not only necessary to understand and diagnose channelopathies, but also contribute to the development of therapeutic treatments for a range of many other diseases. Many antiarrhythmic drugs approved by the FDA act on several types of ion channels due to their non-specific mode of action resulting in various side effects and limiting their clinical use. A detailed atomic understanding of how ion channels work would contribute to the development of drugs targeting a specific subset of channels. High-throughput screening of ion channel drugs are useful techniques to identify drugs, but without knowledge of why and how they affect channel function, development of highly effective therapeutic treatments remains suboptimal.

The broader scientific issue is that we do not have the full picture, yet, of exactly how these crucial proteins work on a detailed molecular and atomic level. What makes them change between conformational states and what are the consequences? Ion channels are nanomachines which are responsible for communication between cells, keeping our body and mind working. They are a fundamental force in biology and if we understand a given role of each amino acid which is involved in fundamental workings of ion channels, we have the opportunity to

understand how single mutations can cause drastic changes to function and cause disease, allowing early diagnosis and efficient therapeutic treatment. We can target the channels, we can copy them, we can enhance them, and we can control them, allowing the development of highly sophisticated drugs. Such opportunities not only concern channelopathies, but all diseases in which ion homeostasis plays a role directly or indirectly, which to the best of my knowledge comprehend the totality of diseases.

Researchers have used a combination of electrophysiology, mutagenesis, X-ray crystallography, molecular dynamics and optical methods to obtain a detailed biophysical characterization of voltage-gated ion channels. Those techniques have provided most of what we know about the structure and function of ion channels. Today we have an in-depth insight of three main mechanisms of the K_V1 channels: ion conduction, voltage sensor activation and pore opening. We also know the structure of the open activated state and we have a good understanding of the C-type inactivated state of the selectivity filter. However, exact mechanisms explaining electromechanical coupling between voltage sensor and pore, subunit cooperativity, the molecular mechanism leading to C-type inactivation, and finally, the molecular pathway of the IP during N-type inactivation, are incomplete. None of these mechanisms are limited to the extracellular portion of the channel but develop within the transmembrane segments and/or in the intracellular portion. Crystal structures of closed and inactivated states would provide valuable structural information, but independent dynamic information is necessary to get a full picture of the ion channel workings.

The introduction of fluorescent probes into proteins provides a powerful tool to study protein dynamics. One method is the genetical fusing of fluorescent proteins (e.g. GFP) but due to the large size >50 Å and the typical requirement for C- or N- terminal fusing, the usage for local probing is limited. A more useful method is based on the post-translational site-specific labeling of fluorophores (e.g. TMRM) via thiol-reactive linkers and has indeed been successfully used to probe conformational changes with voltage clamp fluorometry (VCF, described in section 2.3.2). However, sites for fluorophore labeling must be accessible from solution (extracellular) and cannot be within the lipid bilayer or buried deep within the protein. In addition, to avoid unspecific labeling, cysteine-less constructs are needed which may modify the function of the protein. These requirements limit the choice of sites and proteins to be studied considerably.

The voltage clamp fluorometry (VCF) technique gives simultaneous functional and structural information in an extremely high temporal resolution in a living cell. Much of what is known about voltage-dependent channel movements facing the extracellular side in K_V1 channels has been provided by this approach. If such dynamic information could be obtained from any location within the protein, and not just from sites which are accessible from the extracellular side, it would have great potential in expanding our knowledge about the missing information of K_V1 function and that of other voltage-gated ion channels.

With the recent advances in genetic incorporation of unnatural amino acids and the availability of an orthogonal tRNA/synthetase pair capable of incorporating a small and environmentally sensitive fluorophore (Anap) into eukaryotes [151, 152], we saw an opportunity to overcome the limits of traditional VCF. By using Anap as a fluorescent probe, it would be possible to address unanswered questions regarding rearrangements of intramembranous and intracellular regions in K_V1 channels. In my thesis the objectives consist of one technical issue concerning the implementation of the Anap-VCF technique, and four main structure-function related issues concerning K_V1 channels:

1. The technical issue was to assess if incorporation of an fUAA using the in vivo amber suppression method would be efficient enough for VCF. The initial challenge was to find out whether high expression levels with Anap incorporation in Xenopus oocytes was possible. Next, we would test if Anap even would be capable of emitting high enough fluorescence intensity changes when probing protein rearrangements, by inserting it at a site where fluorescence changes have already been reported with conventional VCF. Furthermore, since use of the Anap tRNA/synthetase pair had not been described in Xenopus oocytes before, we wanted to characterize the amount and origin of leak expression, if any, and determine success of incorporation in general.
2. The scientific issues which we wanted to address using the Anap-VCF technique was first to obtain information about the intracellular portion of the voltage sensor movement. This would contribute to a complete understanding of the activation mechanism. The consensus model of gating describes the charge displacement during activation to consist of at least two charge components (Q1 and Q2), and of at least two main conformational changes in the form of vertical displacement followed by twist and tilt [63]. Does the whole voltage sensor

undergo the same movements? Or do different parts undergo different movements and if yes, do they happen simultaneously or consecutively? We also wanted to investigate the possibility that the bottom of the voltage sensor rearranges during pore opening since it is bound to the S4-S5 linker which plays an important role in electromechanical coupling. By comparing externally TMRM-labeled voltage sensor movement with internally Anap-labeled voltage sensor movement in the same mutant, we would be able to answer these fundamental questions about K_V1 channel activation.

3. Despite being independent modules, the voltage sensors are also intimately coupled to the pore region via numerous interactions. The S6 bundlecross is known to widen during pore opening as controlled by the voltage sensors, but there exists no direct physical measure of the S6 bundlecross dynamics. Does pore opening really occur in one concerted step? Or are there initial voltage sensor movements which translocate to the pore, even before pore opening? Does the pore region also rearrange after pore opening?
4. Activation of the voltage sensors give rise to gating currents originating from the displacement of charged amino acids within the transmembrane segments and widening of the S6 bundlecross give rise to ionic currents originating from the passing K^+ ions. The electrogeneric behavior of these regions is directly related to conformational changes which is why these mechanisms are well characterized. However, dynamic information about the S4-S5 linker movement is less understood because it is not intrinsically electrogenic and it is not accessible for fluorophore labeling either. How does the linker move in relation to S4 and in relation to pore opening? Is it just a passive mechanical arm, or is it directly implicated in electromechanical coupling? Does it move as one rigid helix or as a dynamic and flexible unit? Does it rearrange principally with the independent or with the concerted steps during activation?
5. The last structural issue concerns N-type inactivation. When K_V1 channels undergo this rapid inactivation (A-type currents), it shapes the length of the repolarization phase of an action potential. The faster the channel inactivates, less channels are open and less current runs, resulting in a longer period of repolarization, and vice versa. Moreover, when channels inactivate, there is a refractory period during which the inactivated channels need to recover from inactivation, determining the number of channels available for the next action potential

(the IP needs to leave the binding site, for the voltage sensors to deactivate). K_V1.1 and 1.2 channels are often coexpressed with the auxiliary β subunit which is responsible for rapid inactivation, and N-type inactivation is therefore a crucial mechanism in neuronal excitability. Structural information about this mechanism is limited due, in part, to the flexible and dynamic nature of the process. This is why voltage clamp fluorometry is a suitable technique to investigate the dynamics of N-type inactivation. Electrophysiological, structural and mutational studies of Shaker, K_V1.4, and K_V1 channels coexpressed with auxiliary β subunits, all suggest that the IP first enters the openings of T1 side windows followed by binding to the open pore [78, 88, 153, 154] but any direct dynamic measurements about the process is missing. The two main questions which we wanted to address was: How does the IP rearrange to enter the pore binding site and where does the IP reside at rest?

1.12 References

1. Cole, K.S., *Dynamic electrical characteristics of the squid axon membrane.* Arch. Sci. Physiol., 1949. **3**: p. 253-258.
2. Hodgkin, A.L., A.F. Huxley, and B. Katz, *Measurement of current-voltage relations in the membrane of the giant axon of Loligo.* J Physiol, 1952. **116**(4): p. 424-48.
3. Hodgkin, A.L. and A.F. Huxley, *Currents carried by sodium and potassium ions through the membrane of the giant axon of Loligo.* J Physiol, 1952. **116**(4): p. 449-72.
4. Hodgkin, A.L. and A.F. Huxley, *The components of membrane conductance in the giant axon of Loligo.* J Physiol, 1952. **116**(4): p. 473-96.
5. Hodgkin, A.L. and A.F. Huxley, *The dual effect of membrane potential on sodium conductance in the giant axon of Loligo.* J Physiol, 1952. **116**(4): p. 497-506.
6. Hodgkin, A.L. and A.F. Huxley, *A quantitative description of membrane current and its application to conduction and excitation in nerve.* J Physiol, 1952. **117**(4): p. 500-44.
7. Narahashi, T., J.W. Moore, and W.R. Scott, *Tetrodotoxin Blockage of Sodium Conductance Increase in Lobster Giant Axons.* J Gen Physiol, 1964. **47**: p. 965-74.
8. Hille, B., *The selective inhibition of delayed potassium currents in nerve by tetraethylammonium ion.* J Gen Physiol, 1967. **50**(5): p. 1287-302.
9. Neher, E. and B. Sakmann, *Single-channel currents recorded from membrane of denervated frog muscle fibres.* Nature, 1976. **260**(5554): p. 799-802.
10. Noda, M., et al., *Primary structure of Electrophorus electricus sodium channel deduced from cDNA sequence.* Nature, 1984. **312**(5990): p. 121-7.
11. Papazian, D.M., T.L. Schwarz, B.L. Tempel, Y.N. Jan, and L.Y. Jan, *Cloning of genomic and complementary DNA from Shaker, a putative potassium channel gene from Drosophila.* Science, 1987. **237**(4816): p. 749-53.
12. Stefani, E., L. Toro, E. Perozo, and F. Bezanilla, *Gating of Shaker K+ channels: I. Ionic and gating currents.* Biophys J, 1994. **66**(4): p. 996-1010.

13. Bezanilla, F., E. Perozo, and E. Stefani, *Gating of Shaker K+ channels: II. The components of gating currents and a model of channel activation.* Biophys J, 1994. **66**(4): p. 1011-21.
14. Doyle, D.A., et al., *The structure of the potassium channel: molecular basis of K+ conduction and selectivity.* Science, 1998. **280**(5360): p. 69-77.
15. Yellen, G., M.E. Jurman, T. Abramson, and R. MacKinnon, *Mutations affecting internal TEA blockade identify the probable pore-forming region of a K+ channel.* Science, 1991. **251**(4996): p. 939-42.
16. Yool, A.J. and T.L. Schwarz, *Alteration of ionic selectivity of a K+ channel by mutation of the H5 region.* Nature, 1991. **349**(6311): p. 700-4.
17. Jiang, Y., A. Lee, J. Chen, V. Ruta, M. Cadene, B.T. Chait, and R. MacKinnon, *X-ray structure of a voltage-dependent K+ channel.* Nature, 2003. **423**(6935): p. 33-41.
18. Long, S.B., E.B. Campbell, and R. Mackinnon, *Crystal structure of a mammalian voltage-dependent Shaker family K+ channel.* Science, 2005. **309**(5736): p. 897-903.
19. Hille, B., *Ionic channels of nerve: questions for theoretical chemists.* Biosystems, 1977. **8**(4): p. 195-9.
20. Hite, R.K. and R. MacKinnon, *Structural Titration of Slo2.2, a Na+-Dependent K+ Channel.* Cell, 2017. **168**(3): p. 390-399 e11.
21. Harmar, A.J., et al., *IUPHAR-DB: the IUPHAR database of G protein-coupled receptors and ion channels.* Nucleic Acids Res, 2009. **37**(Database issue): p. D680-5.
22. Faber, E.S. and P. Sah, *Calcium-activated potassium channels: multiple contributions to neuronal function.* Neuroscientist, 2003. **9**(3): p. 181-94.
23. Kaczmarek, L.K., *Slack, Slick and Sodium-Activated Potassium Channels.* ISRN Neurosci, 2013. **2013**(2013).
24. Hille, B., *Ion channels of excitable membranes*. 2001: Sinauer Associates, Inc.
25. Pal, S.K., K. Takimoto, E. Aizenman, and E.S. Levitan, *Apoptotic surface delivery of K+ channels.* Cell Death Differ, 2006. **13**(4): p. 661-7.
26. Deutsch, C. and L.Q. Chen, *Heterologous expression of specific K+ channels in T lymphocytes: functional consequences for volume regulation.* Proc Natl Acad Sci U S A, 1993. **90**(21): p. 10036-40.
27. Singer-Lahat, D., et al., *K+ channel facilitation of exocytosis by dynamic interaction with syntaxin.* J Neurosci, 2007. **27**(7): p. 1651-8.
28. MacDonald, P.E., et al., *Inhibition of Kv2.1 voltage-dependent K+ channels in pancreatic beta-cells enhances glucose-dependent insulin secretion.* J Biol Chem, 2002. **277**(47): p. 44938-45.
29. Wulff, H., N.A. Castle, and L.A. Pardo, *Voltage-gated potassium channels as therapeutic targets.* Nat Rev Drug Discov, 2009. **8**(12): p. 982-1001.
30. MacKinnon, R. and C. Miller, *Mutant potassium channels with altered binding of charybdotoxin, a pore-blocking peptide inhibitor.* Science, 1989. **245**(4924): p. 1382-5.
31. Swartz, K.J. and R. MacKinnon, *Hanatoxin modifies the gating of a voltage-dependent K+ channel through multiple binding sites.* Neuron, 1997. **18**(4): p. 665-73.
32. Wuttke, T.V., G. Seebohm, S. Bail, S. Maljevic, and H. Lerche, *The new anticonvulsant retigabine favors voltage-dependent opening of the Kv7.2 (KCNQ2) channel by binding to its activation gate.* Mol Pharmacol, 2005. **67**(4): p. 1009-17.
33. Smith, K.J., P.A. Felts, and G.R. John, *Effects of 4-aminopyridine on demyelinated axons, synapses and muscle tension.* Brain, 2000. **123 (Pt 1)**: p. 171-84.
34. *U.S. Food and Drug Administration* www.fda.gov/downloads/Drugs/GuidanceComplianceRegulatoryInformation/Guidances/ucm074963.pdf.

35. Kaplan, W.D. and W.E. Trout, 3rd, *The behavior of four neurological mutants of Drosophila.* Genetics, 1969. **61**(2): p. 399-409.
36. Cirelli, C., D. Bushey, S. Hill, R. Huber, R. Kreber, B. Ganetzky, and G. Tononi, *Reduced sleep in Drosophila Shaker mutants.* Nature, 2005. **434**(7037): p. 1087-92.
37. Vacher, H., D.P. Mohapatra, and J.S. Trimmer, *Localization and targeting of voltage-dependent ion channels in mammalian central neurons.* Physiol Rev, 2008. **88**(4): p. 1407-47.
38. D'Adamo, M.C., S. Hasan, L. Guglielmi, I. Servettini, M. Cenciarini, L. Catacuzzeno, and F. Franciolini, *New insights into the pathogenesis and therapeutics of episodic ataxia type 1.* Front Cell Neurosci, 2015. **9**: p. 317.
39. Cox, R.H., *Molecular determinants of voltage-gated potassium currents in vascular smooth muscle.* Cell Biochem Biophys, 2005. **42**(2): p. 167-95.
40. Finol-Urdaneta, R.K., et al., *Block of Kv1.7 potassium currents increases glucose-stimulated insulin secretion.* EMBO Mol Med, 2012. **4**(5): p. 424-34.
41. Wang, W., *Renal potassium channels: recent developments.* Curr Opin Nephrol Hypertens, 2004. **13**(5): p. 549-55.
42. Grandi, E., et al., *Potassium channels in the heart: structure, function and regulation.* J Physiol, 2017. **595**(7): p. 2209-2228.
43. Olson, T.M., et al., *Kv1.5 channelopathy due to KCNA5 loss-of-function mutation causes human atrial fibrillation.* Hum Mol Genet, 2006. **15**(14): p. 2185-91.
44. Long, S.B., X. Tao, E.B. Campbell, and R. MacKinnon, *Atomic structure of a voltage-dependent K+ channel in a lipid membrane-like environment.* Nature, 2007. **450**(7168): p. 376-82.
45. Chen, X., Q. Wang, F. Ni, and J. Ma, *Structure of the full-length Shaker potassium channel Kv1.2 by normal-mode-based X-ray crystallographic refinement.* Proc Natl Acad Sci U S A, 2010. **107**(25): p. 11352-7.
46. Cha, A. and F. Bezanilla, *Characterizing voltage-dependent conformational changes in the Shaker K+ channel with fluorescence.* Neuron, 1997. **19**(5): p. 1127-40.
47. Horne, A.J., C.J. Peters, T.W. Claydon, and D. Fedida, *Fast and slow voltage sensor rearrangements during activation gating in Kv1.2 channels detected using tetramethylrhodamine fluorescence.* J Gen Physiol, 2010. **136**(1): p. 83-99.
48. Al-Sabi, A., S.K. Kaza, J.O. Dolly, and J. Wang, *Pharmacological characteristics of Kv1.1- and Kv1.2-containing channels are influenced by the stoichiometry and positioning of their alpha subunits.* Biochem J, 2013. **454**(1): p. 101-8.
49. Schoppa, N.E., K. McCormack, M.A. Tanouye, and F.J. Sigworth, *The size of gating charge in wild-type and mutant Shaker potassium channels.* Science, 1992. **255**(5052): p. 1712-5.
50. Seoh, S.A., D. Sigg, D.M. Papazian, and F. Bezanilla, *Voltage-sensing residues in the S2 and S4 segments of the Shaker K+ channel.* Neuron, 1996. **16**(6): p. 1159-67.
51. Khalili-Araghi, F., V. Jogini, V. Yarov-Yarovoy, E. Tajkhorshid, B. Roux, and K. Schulten, *Calculation of the gating charge for the Kv1.2 voltage-activated potassium channel.* Biophys J, 2010. **98**(10): p. 2189-98.
52. Ishida, I.G., G.E. Rangel-Yescas, J. Carrasco-Zanini, and L.D. Islas, *Voltage-dependent gating and gating charge measurements in the Kv1.2 potassium channel.* J Gen Physiol, 2015. **145**(4): p. 345-58.
53. Kalstrup, T. and R. Blunck, *Reinitiation at non-canonical start codons leads to leak expression when incorporating unnatural amino acids.* Sci Rep, 2015. **5**: p. 11866.
54. Tiwari-Woodruff, S.K., M.A. Lin, C.T. Schulteis, and D.M. Papazian, *Voltage-dependent structural interactions in the Shaker K(+) channel.* J Gen Physiol, 2000. **115**(2): p. 123-38.

55. Elinder, F., M. Madeja, H. Zeberg, and P. Arhem, *Extracellular Linkers Completely Transplant the Voltage Dependence from Kv1.2 Ion Channels to Kv2.1.* Biophys J, 2016. **111**(8): p. 1679-1691.
56. Martinez-Morales, E., D.J. Snyders, and A.J. Labro, *Mutations in the S6 gate isolate a late step in the activation pathway and reduce 4-AP sensitivity in shaker K(v) channel.* Biophys J, 2014. **106**(1): p. 134-44.
57. Smith, C., S. Kongsamut, H. Wang, J. Ji, J. Kang, and D. Rampe, *In Vitro electrophysiological activity of nerispirdine, a novel 4-aminopyridine derivative.* Clin Exp Pharmacol Physiol, 2009. **36**(11): p. 1104-9.
58. Hadley, J.K., M. Noda, A.A. Selyanko, I.C. Wood, F.C. Abogadie, and D.A. Brown, *Differential tetraethylammonium sensitivity of KCNQ1-4 potassium channels.* Br J Pharmacol, 2000. **129**(3): p. 413-5.
59. Labro, A.J., J.J. Lacroix, C.A. Villalba-Galea, D.J. Snyders, and F. Bezanilla, *Molecular mechanism for depolarization-induced modulation of Kv channel closure.* J Gen Physiol, 2012. **140**(5): p. 481-93.
60. Webster, S.M., D. Del Camino, J.P. Dekker, and G. Yellen, *Intracellular gate opening in Shaker K+ channels defined by high-affinity metal bridges.* Nature, 2004. **428**(6985): p. 864-8.
61. Berneche, S. and B. Roux, *Energetics of ion conduction through the K+ channel.* Nature, 2001. **414**(6859): p. 73-7.
62. Vargas, E., F. Bezanilla, and B. Roux, *In search of a consensus model of the resting state of a voltage-sensing domain.* Neuron, 2011. **72**(5): p. 713-20.
63. Blunck, R. and Z. Batulan, *Mechanism of electromechanical coupling in voltage-gated potassium channels.* Front Pharmacol, 2012. **3**: p. 166.
64. Starace, D.M. and F. Bezanilla, *A proton pore in a potassium channel voltage sensor reveals a focused electric field.* Nature, 2004. **427**(6974): p. 548-53.
65. Lacroix, J.J., H.C. Hyde, F.V. Campos, and F. Bezanilla, *Moving gating charges through the gating pore in a Kv channel voltage sensor.* Proc Natl Acad Sci U S A, 2014. **111**(19): p. E1950-9.
66. Tao, X., A. Lee, W. Limapichat, D.A. Dougherty, and R. MacKinnon, *A gating charge transfer center in voltage sensors.* Science, 2010. **328**(5974): p. 67-73.
67. Lacroix, J.J. and F. Bezanilla, *Control of a final gating charge transition by a hydrophobic residue in the S2 segment of a K+ channel voltage sensor.* Proc Natl Acad Sci U S A, 2011. **108**(16): p. 6444-9.
68. Ledwell, J.L. and R.W. Aldrich, *Mutations in the S4 region isolate the final voltage-dependent cooperative step in potassium channel activation.* J Gen Physiol, 1999. **113**(3): p. 389-414.
69. Loboda, A. and C.M. Armstrong, *Resolving the gating charge movement associated with late transitions in K channel activation.* Biophys J, 2001. **81**(2): p. 905-16.
70. Pathak, M., L. Kurtz, F. Tombola, and E. Isacoff, *The cooperative voltage sensor motion that gates a potassium channel.* J Gen Physiol, 2005. **125**(1): p. 57-69.
71. Lu, Z., A.M. Klem, and Y. Ramu, *Ion conduction pore is conserved among potassium channels.* Nature, 2001. **413**(6858): p. 809-13.
72. Lu, Z., A.M. Klem, and Y. Ramu, *Coupling between voltage sensors and activation gate in voltage-gated K+ channels.* J Gen Physiol, 2002. **120**(5): p. 663-76.
73. Haddad, G.A. and R. Blunck, *Mode shift of the voltage sensors in Shaker K+ channels is caused by energetic coupling to the pore domain.* J Gen Physiol, 2011. **137**(5): p. 455-72.
74. Schoppa, N.E. and F.J. Sigworth, *Activation of Shaker potassium channels. II. Kinetics of the V2 mutant channel.* J Gen Physiol, 1998. **111**(2): p. 295-311.

75. Soler-Llavina, G.J., T.H. Chang, and K.J. Swartz, *Functional interactions at the interface between voltage-sensing and pore domains in the Shaker K(v) channel.* Neuron, 2006. **52**(4): p. 623-34.
76. Batulan, Z., G.A. Haddad, and R. Blunck, *An intersubunit interaction between S4-S5 linker and S6 is responsible for the slow off-gating component in Shaker K+ channels.* J Biol Chem, 2010. **285**(18): p. 14005-19.
77. McCormack, K., et al., *A role for hydrophobic residues in the voltage-dependent gating of Shaker K+ channels.* Proc Natl Acad Sci U S A, 1991. **88**(7): p. 2931-5.
78. Hoshi, T., W.N. Zagotta, and R.W. Aldrich, *Biophysical and molecular mechanisms of Shaker potassium channel inactivation.* Science, 1990. **250**(4980): p. 533-8.
79. Zagotta, W.N., T. Hoshi, and R.W. Aldrich, *Restoration of inactivation in mutants of Shaker potassium channels by a peptide derived from ShB.* Science, 1990. **250**(4980): p. 568-71.
80. Demo, S.D. and G. Yellen, *The inactivation gate of the Shaker K+ channel behaves like an open-channel blocker.* Neuron, 1991. **7**(5): p. 743-53.
81. West, J.W., D.E. Patton, T. Scheuer, Y. Wang, A.L. Goldin, and W.A. Catterall, *A cluster of hydrophobic amino acid residues required for fast Na(+)-channel inactivation.* Proc Natl Acad Sci U S A, 1992. **89**(22): p. 10910-4.
82. Eaholtz, G., T. Scheuer, and W.A. Catterall, *Restoration of inactivation and block of open sodium channels by an inactivation gate peptide.* Neuron, 1994. **12**(5): p. 1041-8.
83. Armstrong, C.M., *Na channel inactivation from open and closed states.* Proc Natl Acad Sci U S A, 2006. **103**(47): p. 17991-6.
84. Goldin, A.L., *Mechanisms of sodium channel inactivation.* Curr Opin Neurobiol, 2003. **13**(3): p. 284-90.
85. Cheng, Y.M., et al., *Molecular determinants of U-type inactivation in Kv2.1 channels.* Biophys J, 2011. **101**(3): p. 651-61.
86. Klemic, K.G., G.E. Kirsch, and S.W. Jones, *U-type inactivation of Kv3.1 and Shaker potassium channels.* Biophys J, 2001. **81**(2): p. 814-26.
87. Kurata, H.T., K.W. Doerksen, J.R. Eldstrom, S. Rezazadeh, and D. Fedida, *Separation of P/C- and U-type inactivation pathways in Kv1.5 potassium channels.* J Physiol, 2005. **568**(Pt 1): p. 31-46.
88. Zhou, M., J.H. Morais-Cabral, S. Mann, and R. MacKinnon, *Potassium channel receptor site for the inactivation gate and quaternary amine inhibitors.* Nature, 2001. **411**(6838): p. 657-61.
89. Covarrubias, M., A. Wei, L. Salkoff, and T.B. Vyas, *Elimination of rapid potassium channel inactivation by phosphorylation of the inactivation gate.* Neuron, 1994. **13**(6): p. 1403-12.
90. Sewing, S., J. Roeper, and O. Pongs, *Kv beta 1 subunit binding specific for shaker-related potassium channel alpha subunits.* Neuron, 1996. **16**(2): p. 455-63.
91. Gebauer, M., D. Isbrandt, K. Sauter, B. Callsen, A. Nolting, O. Pongs, and R. Bahring, *N-type inactivation features of Kv4.2 channel gating.* Biophys J, 2004. **86**(1 Pt 1): p. 210-23.
92. Leicher, T., R. Bahring, D. Isbrandt, and O. Pongs, *Coexpression of the KCNA3B gene product with Kv1.5 leads to a novel A-type potassium channel.* J Biol Chem, 1998. **273**(52): p. 35095-101.
93. Roeper, J., S. Sewing, Y. Zhang, T. Sommer, S.G. Wanner, and O. Pongs, *NIP domain prevents N-type inactivation in voltage-gated potassium channels.* Nature, 1998. **391**(6665): p. 390-3.
94. Robertson, B. and D.G. Owen, *Pharmacology of a cloned potassium channel from mouse brain (MK-1) expressed in CHO cells: effects of blockers and an 'inactivation peptide'.* Br J Pharmacol, 1993. **109**(3): p. 725-35.

95. Stephens, G.J. and B. Robertson, *Inactivation of the cloned potassium channel mouse Kv1.1 by the human Kv3.4 'ball' peptide and its chemical modification.* J Physiol, 1995. **484 (Pt 1)**: p. 1-13.
96. Antz, C. and B. Fakler, *Fast Inactivation of Voltage-Gated K(+) Channels: From Cartoon to Structure.* News Physiol Sci, 1998. **13**: p. 177-182.
97. Murrell-Lagnado, R.D. and R.W. Aldrich, *Interactions of amino terminal domains of Shaker K channels with a pore blocking site studied with synthetic peptides.* J Gen Physiol, 1993. **102**(6): p. 949-75.
98. Prince-Carter, A. and P.J. Pfaffinger, *Multiple intermediate states precede pore block during N-type inactivation of a voltage-gated potassium channel.* J Gen Physiol, 2009. **134**(1): p. 15-34.
99. Prince, A. and P.J. Pfaffinger, *Conserved N-terminal negative charges support optimally efficient N-type inactivation of Kv1 channels.* PLoS One, 2013. **8**(4): p. e62695.
100. Antz, C., et al., *NMR structure of inactivation gates from mammalian voltage-dependent potassium channels.* Nature, 1997. **385**(6613): p. 272-5.
101. Schott, M.K., C. Antz, R. Frank, J.P. Ruppersberg, and H.R. Kalbitzer, *Structure of the inactivating gate from the Shaker voltage gated K+ channel analyzed by NMR spectroscopy.* Eur Biophys J, 1998. **27**(2): p. 99-104.
102. Vergara-Jaque, A., F. Palma-Cerda, H. Poblete, A. Lowet, A. Sukharev, J. Comer, and M. Holmgren, *A Structural Model of the Inactivation Gate of Voltage Activated Potassium Channels.* Biophysical Journal, 2017. **112**(3): p. 247a.
103. Berneche, S. and B. Roux, *A gate in the selectivity filter of potassium channels.* Structure, 2005. **13**(4): p. 591-600.
104. Cuello, L.G., V. Jogini, D.M. Cortes, and E. Perozo, *Structural mechanism of C-type inactivation in K(+) channels.* Nature, 2010. **466**(7303): p. 203-8.
105. Lopez-Barneo, J., T. Hoshi, S.H. Heinemann, and R.W. Aldrich, *Effects of external cations and mutations in the pore region on C-type inactivation of Shaker potassium channels.* Receptors Channels, 1993. **1**(1): p. 61-71.
106. Baukrowitz, T. and G. Yellen, *Modulation of K+ current by frequency and external [K+]: a tale of two inactivation mechanisms.* Neuron, 1995. **15**(4): p. 951-60.
107. Claydon, T.W., M. Vaid, S. Rezazadeh, S.J. Kehl, and D. Fedida, *4-aminopyridine prevents the conformational changes associated with p/c-type inactivation in shaker channels.* J Pharmacol Exp Ther, 2007. **320**(1): p. 162-72.
108. Choi, K.L., R.W. Aldrich, and G. Yellen, *Tetraethylammonium blockade distinguishes two inactivation mechanisms in voltage-activated K+ channels.* Proc Natl Acad Sci U S A, 1991. **88**(12): p. 5092-5.
109. Baukrowitz, T. and G. Yellen, *Use-dependent blockers and exit rate of the last ion from the multi-ion pore of a K+ channel.* Science, 1996. **271**(5249): p. 653-6.
110. Thomson, A.S., F.T. Heer, F.J. Smith, E. Hendron, S. Berneche, and B.S. Rothberg, *Initial steps of inactivation at the K+ channel selectivity filter.* Proc Natl Acad Sci U S A, 2014. **111**(17): p. E1713-22.
111. Yang, Y., Y. Yan, and F.J. Sigworth, *How does the W434F mutation block current in Shaker potassium channels?* J Gen Physiol, 1997. **109**(6): p. 779-89.
112. Cuello, L.G., et al., *Structural basis for the coupling between activation and inactivation gates in K(+) channels.* Nature, 2010. **466**(7303): p. 272-5.
113. Ostmeyer, J., S. Chakrapani, A.C. Pan, E. Perozo, and B. Roux, *Recovery from slow inactivation in K+ channels is controlled by water molecules.* Nature, 2013. **501**(7465): p. 121-4.

114. Lueck, J.D., A.L. Mackey, D.T. Infield, J.D. Galpin, J. Li, B. Roux, and C.A. Ahern, *Atomic mutagenesis in ion channels with engineered stoichiometry.* Elife, 2016. **5**.
115. Perozo, E., R. MacKinnon, F. Bezanilla, and E. Stefani, *Gating currents from a nonconducting mutant reveal open-closed conformations in Shaker K+ channels.* Neuron, 1993. **11**(2): p. 353-8.
116. *http://www.genscript.com/tools/codon-frequency-table.*
117. Noren, C.J., S.J. Anthony-Cahill, M.C. Griffith, and P.G. Schultz, *A general method for site-specific incorporation of unnatural amino acids into proteins.* Science, 1989. **244**(4901): p. 182-8.
118. Nowak, M.W., et al., *Nicotinic receptor binding site probed with unnatural amino acid incorporation in intact cells.* Science, 1995. **268**(5209): p. 439-42.
119. Dougherty, D.A. and E.B. Van Arnam, *In vivo incorporation of non-canonical amino acids by using the chemical aminoacylation strategy: a broadly applicable mechanistic tool.* Chembiochem, 2014. **15**(12): p. 1710-20.
120. Wang, L., A. Brock, B. Herberich, and P.G. Schultz, *Expanding the genetic code of Escherichia coli.* Science, 2001. **292**(5516): p. 498-500.
121. Liu, C.C. and P.G. Schultz, *Adding new chemistries to the genetic code.* Annu Rev Biochem, 2010. **79**: p. 413-44.
122. Xiao, H. and P.G. Schultz, *At the Interface of Chemical and Biological Synthesis: An Expanded Genetic Code.* Cold Spring Harb Perspect Biol, 2016. **8**(9).
123. Shabalina, S.A., N.A. Spiridonov, and A. Kashina, *Sounds of silence: synonymous nucleotides as a key to biological regulation and complexity.* Nucleic Acids Res, 2013. **41**(4): p. 2073-94.
124. Kochetov, A.V., S. Ahmad, V. Ivanisenko, O.A. Volkova, N.A. Kolchanov, and A. Sarai, *uORFs, reinitiation and alternative translation start sites in human mRNAs.* FEBS Lett, 2008. **582**(9): p. 1293-7.
125. Bezanilla, F., E. Perozo, D.M. Papazian, and E. Stefani, *Molecular basis of gating charge immobilization in Shaker potassium channels.* Science, 1991. **254**(5032): p. 679-83.
126. Taglialatela, M., L. Toro, and E. Stefani, *Novel voltage clamp to record small, fast currents from ion channels expressed in Xenopus oocytes.* Biophys J, 1992. **61**(1): p. 78-82.
127. Stefani, E. and F. Bezanilla, *Cut-open oocyte voltage-clamp technique.* Methods Enzymol, 1998. **293**: p. 300-18.
128. Stampfli, R., *A new method for measuring membrane potentials with external electrodes.* Experientia, 1954. **10**(12): p. 508-9.
129. Hille, B. and D.T. Campbell, *An improved vaseline gap voltage clamp for skeletal muscle fibers.* J Gen Physiol, 1976. **67**(3): p. 265-93.
130. Callamaras, N., X.P. Sun, I. Ivorra, and I. Parker, *Hemispheric asymmetry of macroscopic and elementary calcium signals mediated by InsP3 in Xenopus oocytes.* J Physiol, 1998. **511 (Pt 2)**: p. 395-405.
131. Peter, A.B., J.C. Schittny, V. Niggli, H. Reuter, and E. Sigel, *The polarized distribution of poly(A+)-mRNA-induced functional ion channels in the Xenopus oocyte plasma membrane is prevented by anticytoskeletal drugs.* J Cell Biol, 1991. **114**(3): p. 455-64.
132. Gotz, M., S. Hess, G. Beste, A. Skerra, and M.E. Michel-Beyerle, *Ultrafast electron transfer in the complex between fluorescein and a cognate engineered lipocalin protein, a so-called anticalin.* Biochemistry, 2002. **41**(12): p. 4156-64.
133. Chen, H., S.S. Ahsan, M.B. Santiago-Berrios, H.D. Abruna, and W.W. Webb, *Mechanisms of quenching of Alexa fluorophores by natural amino acids.* J Am Chem Soc, 2010. **132**(21): p. 7244-5.

134. Chen, Y. and M.D. Barkley, *Toward understanding tryptophan fluorescence in proteins.* Biochemistry, 1998. **37**(28): p. 9976-82.
135. Mannuzzu, L.M., M.M. Moronne, and E.Y. Isacoff, *Direct physical measure of conformational rearrangement underlying potassium channel gating.* Science, 1996. **271**(5246): p. 213-6.
136. Akabas, M.H., D.A. Stauffer, M. Xu, and A. Karlin, *Acetylcholine receptor channel structure probed in cysteine-substitution mutants.* Science, 1992. **258**(5080): p. 307-10.
137. Cha, A. and F. Bezanilla, *Structural implications of fluorescence quenching in the Shaker K+ channel.* J Gen Physiol, 1998. **112**(4): p. 391-408.
138. Taraska, J.W. and W.N. Zagotta, *Fluorescence applications in molecular neurobiology.* Neuron, 2010. **66**(2): p. 170-89.
139. Sonnleitner, A., L.M. Mannuzzu, S. Terakawa, and E.Y. Isacoff, *Structural rearrangements in single ion channels detected optically in living cells.* Proc Natl Acad Sci U S A, 2002. **99**(20): p. 12759-64.
140. Blunck, R., D.M. Starace, A.M. Correa, and F. Bezanilla, *Detecting rearrangements of shaker and NaChBac in real-time with fluorescence spectroscopy in patch-clamped mammalian cells.* Biophys J, 2004. **86**(6): p. 3966-80.
141. Zheng, J. and W.N. Zagotta, *Gating rearrangements in cyclic nucleotide-gated channels revealed by patch-clamp fluorometry.* Neuron, 2000. **28**(2): p. 369-74.
142. Biskup, C., et al., *Relating ligand binding to activation gating in CNGA2 channels.* Nature, 2007. **446**(7134): p. 440-3.
143. Cha, A., G.E. Snyder, P.R. Selvin, and F. Bezanilla, *Atomic scale movement of the voltage-sensing region in a potassium channel measured via spectroscopy.* Nature, 1999. **402**(6763): p. 809-13.
144. Glauner, K.S., L.M. Mannuzzu, C.S. Gandhi, and E.Y. Isacoff, *Spectroscopic mapping of voltage sensor movement in the Shaker potassium channel.* Nature, 1999. **402**(6763): p. 813-7.
145. Baker, O.S., H.P. Larsson, L.M. Mannuzzu, and E.Y. Isacoff, *Three transmembrane conformations and sequence-dependent displacement of the S4 domain in shaker K+ channel gating.* Neuron, 1998. **20**(6): p. 1283-94.
146. Cha, A., P.C. Ruben, A.L. George, Jr., E. Fujimoto, and F. Bezanilla, *Voltage sensors in domains III and IV, but not I and II, are immobilized by Na+ channel fast inactivation.* Neuron, 1999. **22**(1): p. 73-87.
147. Pantazis, A., N. Savalli, D. Sigg, A. Neely, and R. Olcese, *Functional heterogeneity of the four voltage sensors of a human L-type calcium channel.* Proc Natl Acad Sci U S A, 2014. **111**(51): p. 18381-6.
148. Bannister, J.P., B. Chanda, F. Bezanilla, and D.M. Papazian, *Optical detection of rate-determining ion-modulated conformational changes of the ether-a-go-go K+ channel voltage sensor.* Proc Natl Acad Sci U S A, 2005. **102**(51): p. 18718-23.
149. Bruening-Wright, A. and H.P. Larsson, *Slow conformational changes of the voltage sensor during the mode shift in hyperpolarization-activated cyclic-nucleotide-gated channels.* J Neurosci, 2007. **27**(2): p. 270-8.
150. Kohout, S.C., M.H. Ulbrich, S.C. Bell, and E.Y. Isacoff, *Subunit organization and functional transitions in Ci-VSP.* Nat Struct Mol Biol, 2008. **15**(1): p. 106-8.
151. Lee, H.S., J. Guo, E.A. Lemke, R.D. Dimla, and P.G. Schultz, *Genetic incorporation of a small, environmentally sensitive, fluorescent probe into proteins in Saccharomyces cerevisiae.* J Am Chem Soc, 2009. **131**(36): p. 12921-3.
152. Chatterjee, A., J. Guo, H.S. Lee, and P.G. Schultz, *A genetically encoded fluorescent probe in mammalian cells.* J Am Chem Soc, 2013. **135**(34): p. 12540-3.

153. Gulbis, J.M., M. Zhou, S. Mann, and R. MacKinnon, *Structure of the cytoplasmic beta subunit-T1 assembly of voltage-dependent K+ channels.* Science, 2000. **289**(5476): p. 123-7.
154. Fan, Z., X. Ji, M. Fu, W. Zhang, D. Zhang, and Z. Xiao, *Electrostatic interaction between inactivation ball and T1-S1 linker region of Kv1.4 channel.* Biochim Biophys Acta, 2012. **1818**(1): p. 55-63.

Chapter 2

Methodology

2.1 Oocyte handling and injection

Oocytes from the South African clawed frog *Xenopus laevis* have become a widely used expression system for heterologous proteins since the discovery of their ability to express proteins when injected with foreign mRNA in 1971 [1]. Due to their large size (1 mm), easy handling and relatively limited number of endogenous membrane proteins [2], the oocytes are especially well suited for investigating membrane transport mechanisms on a cellular level using electrophysiology. Finally, RNA or DNA is easily introduced into oocytes for heterologous expression using simple injection apparatus, and the oocytes can be cultured up to several days. To give an example of the expression efficiency in oocytes, the channel density for heterogeneously expressed WT Shaker channels can reach up to 5000/μm^2 [1], whereas the endogenous population of proteins is approximately 250/μm^2 [3].

The procedure for oocyte isolation is based on Goldin 1992 [4] with minor modifications. Mature oocytes of stage V or VI are obtained upon surgical removal of ovary nodes of a *X. laevis* female which is anesthetized with 3-aminobenzoic acid ethyl ester. The nodes are carefully opened using two forceps and transferred into a sterile 50 mL tube containing 1 mg/ml collagenase in SOS solution[2] (three nodes/tube). The collagenase digests the extracellular structure of the ovarian follicular layer by breaking the collagen peptide bonds. The tube is agitated for 20-30 min on a horizontal shaker and oocytes are then washed three times with SOS solution. Spherical oocytes of 1 mm in diameter with a distinct black animal pole and a bright vegetal pole are individually

[1] Calculated from 30 nC of charge movement by using 13.2 *e*/channel and the formula for the area of a spherical cap (the clamped area in COVC). The invaginations were approximated by doubling the area.
[2] SOS solution in mM: 102 NaCl, 2 KCl, 1 $MgCl_2$, 5 Hepes; pH 7.2

selected and incubated in Barth's solution at 18°C. Often, oocytes are injected one day later to screen for damaged oocytes and to avoid contamination from dead oocytes. Also, the collagenase treatment has been shown to affect the metabolic state of the oocytes at least 8 hours after treatment [5], possibly because the requirement of a calcium-free medium severely affects protein synthesis [6].

2.2 Incorporation of Anap into Shaker expressed in Xenopus oocytes

In the years following the successful implementation of VCF, it had come to a point where many of the external sites in ion channels and transporters had been investigated, whereas numerous questions remained unanswered for dynamics of non-accessible regions (intramembrane and intracellular). Three fUAAs had already been incorporated into proteins expressed in oocytes by injecting chemically aminoacylated tRNAs (figure 2.1). First, NBD-Dap (3-N-(7-nitrobenz-2-oxa-1,3-diazol-4-yl)-2,3-diaminopropionic acid) reported on relative distance changes in isolated membranes expressing neurokin-2 receptors [7]. Then, Aladan (an alanine derivative of prodan, N,N-Dimethyl-6-propionyl-2-naphthylamine) was incorporated into Shaker and Kir channels to show that the fUAA expression was compatible with the translation machinery by assessing the ionic currents [8]. Finally, lys(BODIPYFL) was incorporated into muscle nicotinic acetylcholine receptors for single-molecule detection using total internal reflection fluorescence microscopy [9]. This was the first time a fUAA was probing conformational changes in a living Xenopus oocyte. Although the chemical aminoacylation strategy was useful for fluorescence steady-state measurements and single-molecule detection studies, the technique did not allow VCF studies of protein conformational changes due to limited expression efficiency. A way to circumvent the limited expression could be to use the amber suppression method to incorporate a fUAA. Among other fUAAs, a tRNA/synthetase pair for Anap had been successfully incorporated into proteins in yeast by the Schultz laboratory, which led us to try and express Anap in Xenopus oocytes in Shaker. Surprisingly, we were able to produce robust expression levels which were sufficient to capture fluorescence changes for the purpose of VCF. The implementation of this method forms the technical foundation of this thesis.

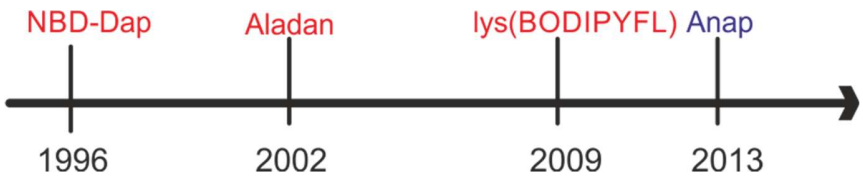

Figure 11.1 fUAA timeline for expression in Xenopus oocytes
Timeline for fUAAs incorporated into proteins expressed in Xenopus oocytes. fUAAs marked in red were incorporated with the chemical aminoacylation technique and marked in blue is Anap which was incorporated via a tRNA/synthetase pair.

2.3 Experimental procedure

2.3.1 Molecular biology

1. Mutagenic primers of 20-40 bases in length are designed such that they contain the desired mutation in the center and terminate with a G or a C.
2. Point mutations are generated using site-directed mutagenesis (QuikChange; Agilent Technologies)
3. 1 µl DpnI restriction enzyme is added to digest template DNA
4. Heat pulse transformation into XL1-Blue supercompetent cells is followed by adding 300 µl of SOC medium. Sample is put to 1 hour incubation with shaking at 250 rpm at 37 °C
5. 200 µl are plated on LB-ampicilin agar plates and incubated overnight at 37 °C
6. Single colonies are selected and are incubated in 5 ml LB medium and 100 µg/mL ampicillin, with shaking at 250 rpm at 37 °C overnight
7. A Spin Miniprep Kit (Qiagen) is used to obtain isolated 200 ng/µl DNA in 50 µl
8. Sequences are verified in an in-house sequencing facility
9. DNA is amplified with a second round of transformation into XL1-Blue supercompetent cells. 10 µl is plated on LB-ampicilin agar plates and incubated overnight at 37 °C
10. Single colonies are selected and are incubated in 250 ml LB medium and 100 µg/mL ampicillin, with shaking at 250 rpm at 37 °C overnight
11. A Midiprep Kit (Qiagen) is used to obtain isolated 1.5 ug/µl DNA in 20 µl
12. The DNA is linearized with NotI restriction enzyme and used for RNA *in vitro* transcription with the mMESSAGE mMACHINE® T7 Ultra Kit (ThermoFisher)

13. RNA is extracted with phenol/chloroform and precipitated with ethanol to obtain a pellet which is resuspended in 20 µl nuclease-free water. Typically, 2 µg/µl of pure RNA is obtained and is ready for injection into oocytes. RNA is stored at -80 °C.

2.3.2 Expression

The pAnap plasmid, a pCDNA3.1^{+} vector (Addgene #48696), encodes for an E.coli leucyl synthethase and 8 copies of E.coli tRNA$^{Leu(CUA)}$.

The injection protocol used for all the projects presented in my thesis is the same and has also been visualized [10]. That is, 4.6-9.2 nl of 0.1 µg/µl of pAnap is injected into the oocyte nucleus, 6-24 hours prior to co-injection of 2-40 ng of mRNA and 23 nl of 1 mM Anap, in a total volume of 46 nl. The 1 mM Anap stock solution is diluted in nuclease-free water with 1% 1N NaOH and is stored at -20˚C. The oocytes are then incubated at 18˚C in Barth's solution[3] supplemented with 5% horse serum for 1-3 days after which they are ready for VCF recordings. The amount of DNA and RNA, and the incubation time depends on individual mutant expression efficiency and expression level needed.

Principally, both injections could be done concurrently, but to ensure high yield and to limit leak expression of channels lacking Anap, it is preferable to allow tRNA and synthetase expression before injection of channel mRNA. That way, there will be immediately Anap-charged tRNAs available for insertion when the ribosome encounters the amber stop codon during translation.

The success rate for robust expression varies within the mutants and within batches of oocytes. When the most efficient mutants express, they show robust currents in 75% of the injected oocytes. The least efficient mutants generally exhibited a success rate of 25%. Regardless of the expression efficiency, it would occasionally happen that a batch of oocytes or injections exhibit no currents at all.

2.4 Data analysis

Current and fluorescence are recorded and registered using the GPatch acquisition software and data is analyzed with Analysis software (Department of Anesthesiology, University of California,

[3] Barth's solution in mM: 90 NaCl, 3 KCl, 0.82 $MgSO_4$, 0.41 $CaCl_2$, 0.33 $Ca(NO_3)_2$, 5 HEPES, 100U/mL penicilin, 100µg/L streptomycin, 10mg/100mL kanamycin

Los Angeles, CA). Currents and fluorescence changes are elicited by a typical voltage 10 mV step protocol ranging from -120 mV to +50/150 mV from a holding potential of -90 mV.

2.4.1 Ionic currents

Steady state ionic current amplitudes from conducting mutants are analyzed at the end of the voltage step (orange line in figure 2.2) from which the conductance G, is calculated using $G = \frac{I}{V-V_0}$, where I is the current amplitude, V is the voltage and V_0 is the reversal potential. The GV curve is obtained by plotting the normalized conductance as a function of voltage (figure 2.2).

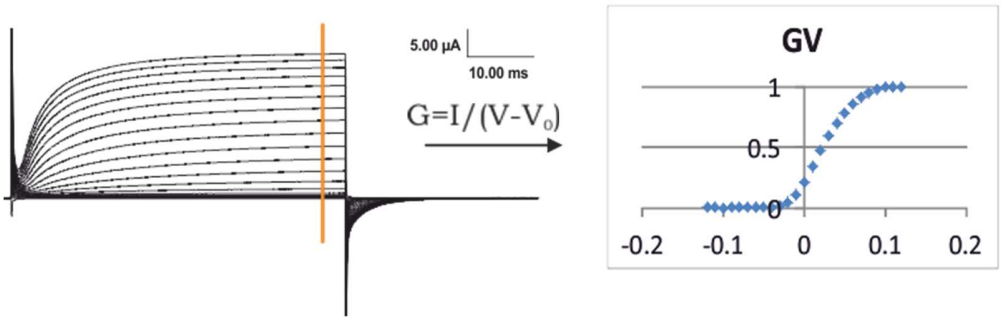

Figure 2.212 Ionic currents and GV
Example of raw data from a Shaker L382Anap expressing oocyte eliciting outward ionic currents in response to a voltage step protocol. The current amplitudes denoted at the orange line are converted to conductance G and plotted as a function of voltage (GV)

2.4.2 Gating currents

Gating currents from W434F mutants are obtained by subtracting the capacitive currents using the P/4 procedure [11]. After each voltage step, a pulse in the region of no charge movement and of the same magnitude as the applied voltage step, is added or subtracted online, depending on the direction of the subtraction step (figure X.X). To prevent membrane breakdown at large voltage steps, the subtraction step is divided into 4 equal steps. The equivalent gating charge of the elicited gating currents, is the integral of the gating current that flows when the ion channel moves within the electric field. The QV curve is then obtained by plotting the calculated charge at the end of the voltage step (orange line in figure 2.3) as a function of voltage and normalize.

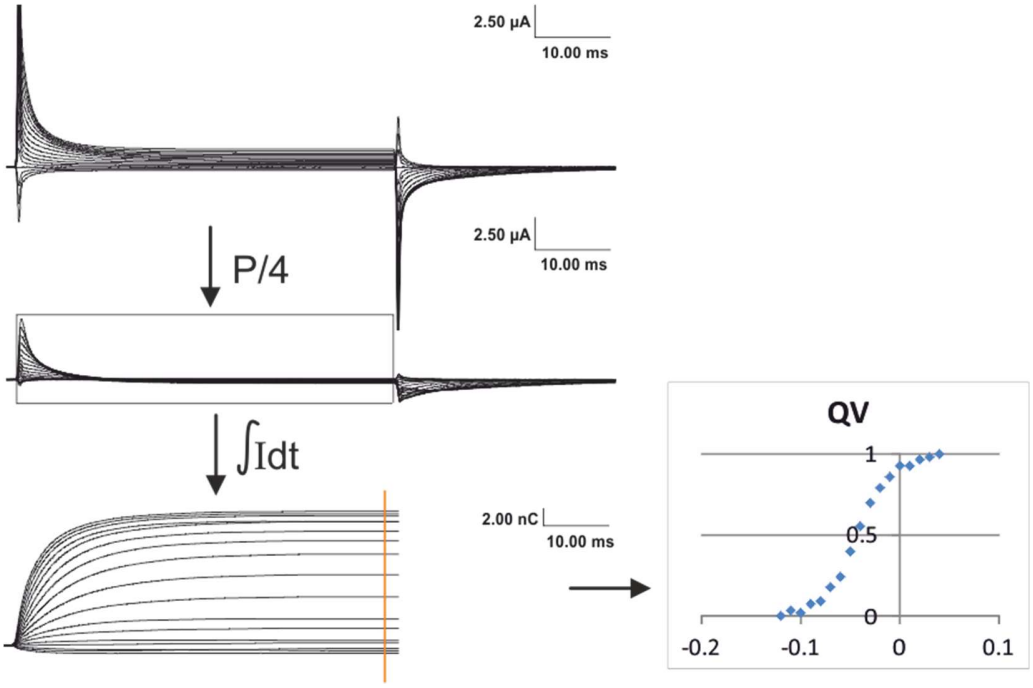

Figure 2.3 Gating currents and QV
Example of a Shaker L382Anap-W434F expressing oocyte eliciting transient gating currents in response to the same voltage step protocol as in figure 2.2. Gating currents are isolated from the capacitance current via the P/4 procedure. Next, the gating charge is calculated by integration, and values are plotted at the orange line as a function of voltage (QV).

2.4.3 Fluorescence changes

The fluorescence intensities are detected simultaneously with the currents. Because of fluorophore bleaching between the voltage steps, the intensity of each trace decreases over time. The bleaching effect is corrected for by baselining each trace to the same value before the voltage step (small arrows in Figure 2.4). The fluorescence intensity amplitudes at the end of the voltage step (orange line in figure 2.4) are then normalized and plotted as a function of voltage, giving the FV curve.

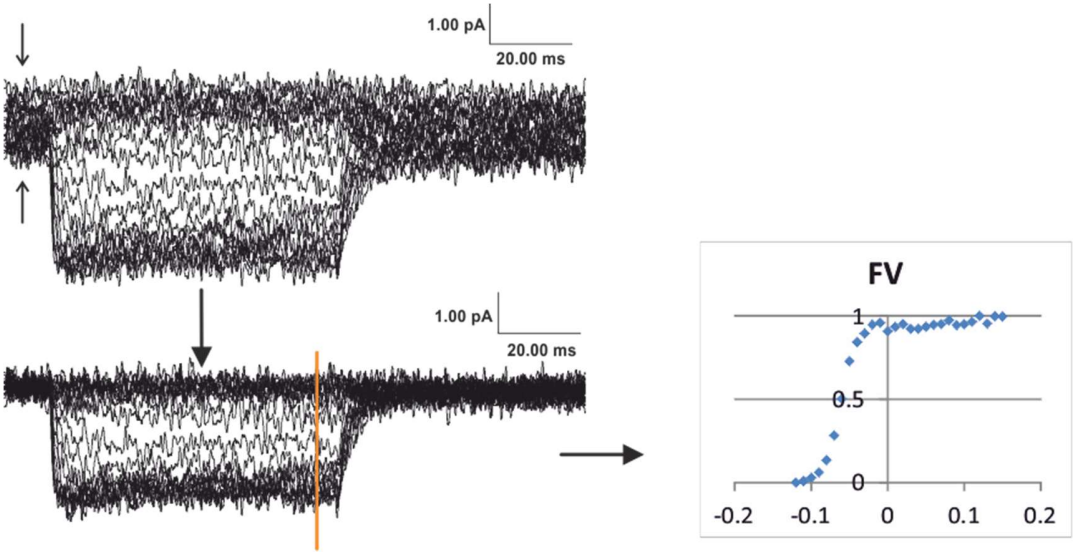

Figure 2.413 Fluorescence intensity and FV
Example of fluorescence data from the same oocyte as in figure 2.3. Bleaching effects are accounted for by baselining each trace before the voltage step. The fluorescence intensities are then plotted at the orange line as a function of voltage (FV).

2.4.4 Fitting the data

To demonstrate the validity of GV, QV and FV curves, data is obtained from 4-10 oocytes from at least two different batches of oocytes. The normalized average is plotted as a function of voltage with mean standard deviation error bars calculated as

$$mean\ SD = \sqrt{\frac{\sum(x-\bar{x})^2}{n}},$$

where x is the sample value, $\bar{x}$ is the mean of all the values and n is the sample size.

Next, the Boltzmann distribution function is used to fit the sigmoidal GV, QV and FV curves as we assume that the channel can be in either of two energy levels e.g. open/closed for the pore (GV), deactivated/activated for the voltage sensor (QV) and either of two conformational states (FV) (see box 1.1 section 1.2).

Finally, kinetic information is obtained by fitting the time course traces to an exponential function (figure 2.5), or the sum of two or three when necessary,

$$y = A \cdot \exp\left({}^{t}/_{T}\right) + B,$$

where A is the amplitude, t is time, T is the time constant and B is the baseline. The time constant is a useful fitting parameter to characterize the dynamics of a process.

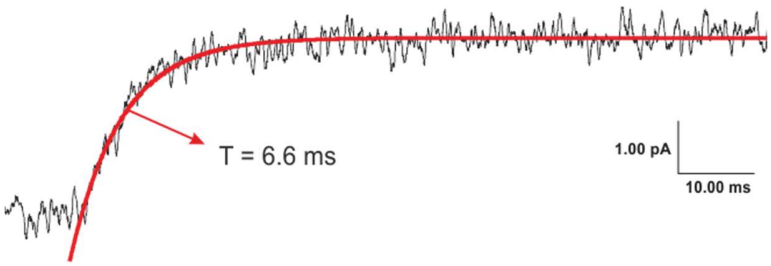

Figure 2.5 Exponential fit of a fluorescence time course
Example of a fluorescence time course fit to one exponential component (red) yielding a time constant of 6.6 ms

2.5 References

1. Gurdon, J.B., C.D. Lane, H.R. Woodland, and G. Marbaix, *Use of frog eggs and oocytes for the study of messenger RNA and its translation in living cells.* Nature, 1971. **233**(5316): p. 177-82.
2. Weber, W., *Ion currents of Xenopus laevis oocytes: state of the art.* Biochim Biophys Acta, 1999. **1421**(2): p. 213-33.
3. Zampighi, G.A., et al., *A method for determining the unitary functional capacity of cloned channels and transporters expressed in Xenopus laevis oocytes.* J Membr Biol, 1995. **148**(1): p. 65-78.
4. Goldin, A.L., *Maintenance of Xenopus laevis and oocyte injection.* Methods Enzymol, 1992. **207**: p. 266-79.
5. Smith, L.D., W.L. Xu, and R.L. Varnold, *Oogenesis and oocyte isolation.* Methods Cell Biol, 1991. **36**: p. 45-60.
6. Wallace, R.A., D.W. Jared, J.N. Dumont, and M.W. Sega, *Protein incorporation by isolated amphibian oocytes. 3. Optimum incubation conditions.* J Exp Zool, 1973. **184**(3): p. 321-33.
7. Turcatti, G., et al., *Probing the structure and function of the tachykinin neurokinin-2 receptor through biosynthetic incorporation of fluorescent amino acids at specific sites.* J Biol Chem, 1996. **271**(33): p. 19991-8.
8. Cohen, B.E., T.B. McAnaney, E.S. Park, Y.N. Jan, S.G. Boxer, and L.Y. Jan, *Probing protein electrostatics with a synthetic fluorescent amino acid.* Science, 2002. **296**(5573): p. 1700-3.
9. Pantoja, R., E.A. Rodriguez, M.I. Dibas, D.A. Dougherty, and H.A. Lester, *Single-molecule imaging of a fluorescent unnatural amino acid incorporated into nicotinic receptors.* Biophys J, 2009. **96**(1): p. 226-37.
10. Kalstrup, T. and R. Blunck, *Voltage-clamp Fluorometry in Xenopus Oocytes Using Fluorescent Unnatural Amino Acids.* J Vis Exp, 2017(123).
11. Armstrong, C.M. and F. Bezanilla, *Inactivation of the sodium channel. II. Gating current experiments.* J Gen Physiol, 1977. **70**(5): p. 567-90.

Chapter 3

Dynamics of internal pore opening in K(V) channels probed by a fluorescent unnatural amino acid

Tanja Kalstrup[1] and Rikard Blunck[1,2]

[1]Department of Physiology and Pharmacology, and [2]Department of Physics, Montreal University, Montreal, Quebec, Canada

Accepted April 8, 2013 (received for review November 22, 2012).

Proc Natl Acad Sci USA, vol. 110, no. 20, p. 8272-8277, May 14, 2013

Author contributions: R.B. designed research; T.K. performed experiments; T.K. and R.B. analyzed data; and T.K. and R.B. wrote the paper.

3.1 Abstract

Atomic-scale models on the gating mechanism of voltage-gated potassium channels (Kv) are based on linear interpolations between static structures of their initial and final state derived from crystallography and molecular dynamics simulations, and, thus, lack dynamic structural information. The lack of information on dynamics and intermediate states makes it difficult to associate the structural with the dynamic functional data obtained with electrophysiology. Although voltage-clamp fluorometry fills this gap, it is limited to sites extracellularly accessible, when the key region for gating is located at the cytosolic side of the channels. Here, we solved this problem by performing voltage-clamp fluorometry with a fluorescent unnatural amino acid. By using an orthogonal tRNA-synthetase pair, the fluorescent unnatural amino acid was incorporated in the Shaker voltage-gated potassium channel at key regions that were previously inaccessible. Thus, we defined which parts act independently and which parts act cooperatively and found pore opening to occur in two sequential transitions.

3.2 Introduction

Voltage-gated potassium channels (K_V) are essential for generating action potentials in the central nervous system and, when defective, are linked to severe familial diseases including cardiac arrhythmias and epilepsy. The voltage-sensing domains (VSD) of K_V channels (transmembrane helices S1–S4; figure 3.1A) undergo a major conformational change upon membrane depolarization driven by the positive charges in the S4, which finally leads to opening of the pore domain (transmembrane helices S5–S6). Based on the consensus on the closed (initial) and open (final) state structures [1-6], the gating movement has been predicted; the S4 helix is projected to slide upward and tilt with respect to the membrane normal, and this movement pushes the S4–S5 linker and the S6 helix inward and closes the ion-conducting pore. However, this projection relies on linear interpolations between the closed and open state and lacks any information on dynamics or intermediate states.

As a result, the projected movement does not suffice to explain fundamental characteristics of voltage sensor and pore domain kinetics, detected as “gating” and “ionic” currents, respectively. Such functional electrophysiology measurements revealed that, first, at least one intermediate state has to exist during voltage sensor movement [7] and that, second, voltage sensor

movement and pore opening do not occur simultaneously. Each channel consists of four voltage sensors controlling a single central pore. It is thought that the four voltage sensors activate independently, and only after all four have activated, the central pore opens cooperatively [8, 9]. This mechanism implies that the energy generated by the movement of the first three voltage sensors has to be "conserved" in the system and has to be released to the pore during opening [10]. The linear interpolations between closed and open structures leave the basis of both cooperativity and energy conservation unknown.

The most effective way to link dynamic functional and structural information of electrogenic membrane proteins is voltage-clamp fluorometry (VCF) [11, 12] - simultaneous electrophysiology and site-directed fluorescence spectroscopy monitoring local rearrangements. By labeling a specific position in the protein, rearrangements of this position can be monitored in real time and can be correlated with the functional data recorded simultaneously. VCF has been successfully used to follow movements in a variety of membrane transport proteins including ion channels [12-19], transporters [20-23], and receptors [24].

Despite its power, VCF has been restricted to rearrangements on the external surface of the transport proteins due – mainly - to the thiol-reactive chemistry used for labeling. Labeling in the cytosol has proven very difficult owing to the large number of cysteines present there. Similarly, residues buried in the protein or in the membrane were not accessible. Here, we overcame these limitations by using intrinsically fluorescent unnatural amino acids (fUAAs), which are incorporated into the protein during synthesis and, thus, do not underlie the above limitations.

Previously, unnatural amino acids with various properties have been incorporated into ion channels by injecting chemically aminoacylated tRNAs into *Xenopus* oocytes [25-27] including a fUAA [28]. Here, we used a fUAA to successfully carry out VCF experiments. We achieved higher expression levels by using an orthogonal $tRNA_{CUA}^{Anap}$/tRNA-synthetase pair to introduce the fUAA 3-(6-acetylnaphthalen-2-ylamino)-2-aminopropionic acid (Anap) [29] into the protein (figure 1*B*). Because it is genetically encoded by an *amber* nonsense codon (TAG), no limitations are set on the site of labeling. Anap has properties similar to an organic dye, although it is only slightly more voluminous than tryptophan (figure 3.1*C*). Anap was incorporated at strategic locations in the Shaker potassium channel to follow the dynamics of their movements (*i*) on "top" of the S4,

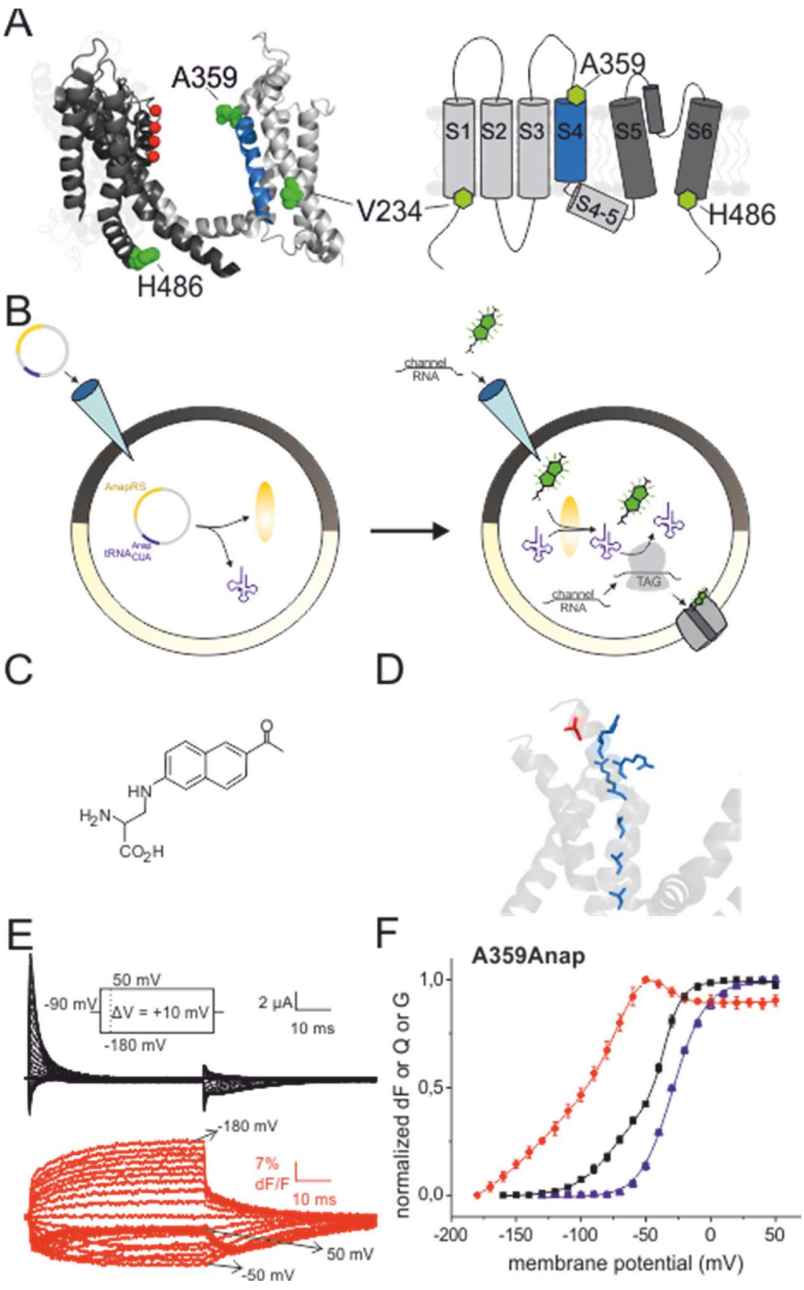

Figure 3.1
A) Structure of $K_V1.2/2.1$ chimera (PDB ID code 2R9R, two subunits) and topology (transmembrane segments S1–S6). The position of the mutations V234, A359, and H486 are displayed in green, and the potassium ions in the selectivity filter in red. **B)** Principle of expression of fUAA. First, the plasmid to express the AnapRS and the corresponding tRNA is injected. On the subsequent day, fUAA and channel mRNA are injected, which leads to incorporation of the fUAA into the channel. **C)** Structure of Anap. **D)** Position of A359 (red) with respect to the arginines in the S4 (blue; PDB ID code 2A79). **E)** Fluorescence response and gating currents of A359Anap in response to pulses from −90 mV to potentials between −180 and 50 mV. **F)** Fluorescence voltage (FV, red circles), gating charge voltage (QV, black squares), and conductance voltage (GV, blue triangles) relations of A359Anap. The GV was fitted to a Boltzmann relation (V1/2 = −29.1 mV, dV = 12.6 mV). The QV and FV were fitted to a sum of two ($V_{1/2,1}$ = −66.3 mV, dV_1 = 19.1 mV, $V_{1/2,2}$ = −35.2 mV, dV_2 = 5.4 mV) and three Boltzmann relations ($V_{1/2,1}$ = −134.6 mV, dV_1 = 32.8 mV, $V_{1/2,2}$ = −62.2mV, dV_2 =15.1 mV, $V_{1/2,3}$ = −41.6 mV, dV_3 = 11.6 mV), respectively.

the gating segment, (*ii*) in the bottom of S1 proximal to the transition from the S4 to the S4–S5 linker and (*iii*) at the C-terminal S6 close to the cytosolic gate and the S4–S5 linker C terminus (figure 3.1*A*) (top and bottom refer to the extracellular and cytosolic surface, respectively).

3.3 Results

The gating process is initiated by the positively charged S4 moving in response to depolarization of the membrane potential. To follow the movement of the outer S4, we introduced Anap on top of S4 at position A359Anap (figure 3.1*A*). The fluorescence voltage relation (FV) featured three components, two of which coincided with the major charge movements (QV; figure 3.1 *E* and *F*), i.e., with the upward translation and tilt of the S4 moving the positive charges through the electric field. Our results not only suggested that the top of S4 rearranges during the major charge movements [11, 12, 30], but also that this rearrangement occurs in two distinct movements of S4 as evidenced by the opposite direction of the two fluorescence components (figure 3.1 *E* and *F* and figure S3.1*A*). An alternative interpretation of the fluorescence change would be that the surrounding residues changed their position; however, in other biphasic FV relations found by labeling positions proximal to A359 at the top of S4 (S352 and M356) [11, 31, 32], also the two components coincided with the two major charge movements, and accessibility and VCF studies showed that the S4 itself is altering its position with respect to its surrounding during each movement [31].

Anap labeling, in contrast to organic dye labeling, enabled us to detect movements that occurred at strongly hyperpolarized potentials ($V_{1/2}$ = −134.6 mV) beyond the detectable charge movements. Cole and Moore [33] postulated, based on a delayed onset of the ionic current, a number of closed-state transitions in this voltage range occurring before the two major gating charge-carrying transitions. The fluorescence changes of A359Anap indicate that these early closed-state transitions induce structural changes in the N-terminal S4. In this voltage range, gating currents with time constants faster than 20 µs have been detected when measuring with very high bandwith [34]. These gating currents might thus be related to the rearrangements we observed. Although the structural origin of these fast gating events remains unclear, charge movements in this time range have been observed to be related to an outward shift of the basic side chains in the S4 in molecular dynamics simulations [35]. Such side chain “flips” were

suggested earlier to occur during gating [3]. This mechanism would explain why these arrangements are sensed by Anap and not by organic labels, because Anap is located right above the first arginine, whereas an organic label, covalently linked to the –SH group of a cysteine, would be further away from the backbone (figure 3.1*D*). However, this interpretation remains highly speculative as long as in long-term simulations no separation between fast and slow events is observed [5] or until similar rearrangements are observed in simulations at lower potentials where no major charge movement occurs.

3.3.1 Rearrangements in the C-Terminal S4 Region.

Next, we tested the dynamics of the lower S4, because no information about its movements is available yet. To this end, we introduced Anap in the lower S1 (V234Anap) in close proximity to the C terminus of the S4 helix (figure 3.1*A*). Remarkably, mutation of V234 in the N terminus of the S1 helix led to partial uncoupling of the S4 movement from pore opening, similar to different mutants in the lower S4 and S4–S5 linker [30, 36] (figure 3.2*B*). As in other uncoupled mutants, charge movement (QV) and pore opening (GV) were separated. Our finding that a mutation in the lower S1 led to uncoupling indicated that the VSD surrounding the S4 helix (S1–S3) does not merely form a passive cocoon but contributes to the gating movement. In addition, the separation between QV and GV had the advantage that it allowed us to better associate the structural rearrangements with the electrophysiological signals.

The fluorescence traces of V234Anap displayed two opposite fluorescence changes, indicating that two transitions occur in the lower S4 region (figure.3. 2 *A* and *B*). The first coincided directly with the charge movement (figure 3.2*B*); the dynamics of gating charge movement superposed with the fluorescence changes of the first component (figure 3.2*C*). Considering that the upper S4 (A359Anap) also followed gating charge movement, the question arises as to whether both ends of the S4 move as one entity or whether the movement is initiated by either the upper or lower part, pulling the other one in a second transition into its final position. Comparison of the kinetics would let us gain insight into this question, however, the V234Anap mutant is partly uncoupled and, thus, kinetics intrinsically differ from the A359Anap mutant. We therefore decided to monitor the movement of both ends of the S4 in the V234Anap-W434F mutant simultaneously. To this end, we introduced the mutation A359C and chemically linked a tetramethylrhodamine

(TMR) via a maleimide linker to this position. As excitation and emission spectra of Anap and TMR are well separated, we were able to obtain the kinetics of the upper S4 and of the lower S4 from the same oocyte by monitoring TMR and Anap fluorescence, respectively.

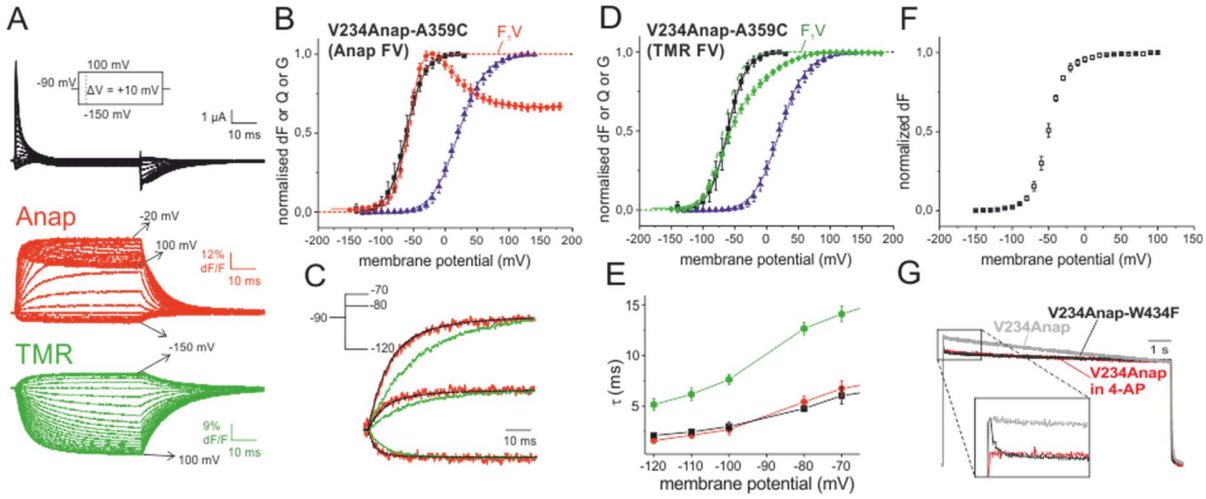

Figure 3.2 Two-colour VCF results of V234Anap-A359C
A) Gating currents and fluorescence responses of a TMR-labeled oocyte expressing V234Anap-A359C in response to pulses from −90 mV to potentials between −150 and 100 mV. **B)** Anap fluorescence voltage (FV, red circles), gating charge voltage (QV, black squares) and conductance voltage (GV, blue triangles) relations of V234Anap-A359C. The GV and QV were each fitted to Boltzmann relations (GV: $V_{1/2}$ = 20.3 mV, dV = 20.6 mV; QV: $V_{1/2}$ = −61.4 mV, dV = 14.5 mV). The FV was fitted to a sum of two Boltzmann relations ($V_{1/2,1}$ = −56.7 mV, dV_1 = 11.8 mV, $V_{1/2,2}$ = −1.0 mV, dV_2 = 25.4 mV). F_1V refers to the first component of the FV. **C)** Comparison of time dependence between charge movement (black) and fluorescence changes of V234Anap-A359C (red, Anap; green, TMR) for depolarizing pulses to voltages indicated in Inset. **D)** TMR fluorescence voltage (FV, green diamonds) relation of V234Anap-A359C and the QV and GV with colors coded as in B. The FV was fitted to a sum of two Boltzmann relations ($V_{1/2,1}$ = −68.7 mV, dV_1 = 14.3 mV, $V_{1/2,2}$ = 0 mV, dV_2 = 23.0 mV). **E)** Comparison among time constants of charge movement (black), Anap (red), and TMR (green) fluorescence of V234Anap-A359C. (F) Anap fluorescence voltage relation of the conducting mutant V234Anap. **G)** Superposition of fluorescence traces obtained from a prolonged depolarizing pulse to 50 mV of oocytes expressing the conducting V234Anap mutant in absence (gray) or presence of 5 mM external 4-AP (red) and the nonconducting V234Anap mutant (black). The traces are normalized to the value at the end of the pulse. (Inset) Shown is the correlation between ionic current and fluorescence decay for the V234Anap-conducting mutant.

In a superposition of the fluorescence signals at voltages below pore opening, Anap fluorescence (lower S4) responded faster to a voltage change than the TMR fluorescence (upper S4; figure 3.2*C*). Fitting the traces to single exponentials revealed that the region around the lower S4 moved about twice as fast as the region around the upper S4 (figure 3.2*E*). Nevertheless, both signals followed the same voltage dependence (figure 3.2 *B* and *D*), signifying that both events are prompted by the same transition. If we had a sequential two-step process with the lower S4 region moving during the first and the upper during the second step, we would expect a temporal delay in the onset of the TMR signal, which is not observed. However, the delay would be

"hidden" if the TMR also senses the first transition to a small fraction. We would still observe only one exponential. Alternatively, two fully independent transitions both triggered by the positive charges in the S4 are possible. In either case, both regions do not undergo the conformational changes simultaneously, but the upper S4 region settles slower during charge movement after the initial transition in a second, voltage-independent step. Although accessibility studies suggest that the S4 itself moves during both steps [30], we can only detect movements relative to the surrounding with fluorescence. Therefore, we are not able to clearly distinguish whether also the upper and lower end of the S4 helix move differently or whether the S4 moves as one entity during one of the transitions followed by a relaxation of the surrounding around the N terminus.

3.3.2 C-Terminal S4 Region Moves During Opening and C-Type Inactivation.

In addition to the charge-related movement, the lower S4 region undergoes another conformational change as reported by the second component in the fluorescence voltage relation. During this second transition of V234Anap-W434F, the fluorescence is decreased, whereas it increased during gating charge movement. However, in the conducting mutant V234Anap, a second component occurred with the inversed sign, i.e., the fluorescence increased and, thus, changed in the same manner as during charge movement (figure 3.2*F*). Because the amplitude of this component was small, it remained uncertain whether both signals coincided exactly. Nevertheless, the only difference between these constructs is the mutation W434F, which is thought to render the channel instantaneously C-type inactivated [37], suggesting that the lower S4 region rearranges during C-type inactivation. To confirm this hypothesis, we monitored the fluorescence signal during prolonged depolarization (figure 3.2*G*) and, indeed, fluorescence in the conducting mutant underwent a slow fluorescence decay correlating with entry to the C-type inactivated state (figure 3.2*G*). Although the W434F mutant entered the inactivated state rapidly, we were able to follow this entry because the fluorescence follows the probability of a single subunit, whereas the current is already blocked when a single of the four subunits inactivates [37] and because pore opening is likely a prerequisite. Blocking the late transitions to pore opening with the potassium channel blocker 4-aminopyridine (4-AP; refs. [38] and [39]) prevented the fluorescence decrease during C-type inactivation (figure 3.2*G*).

Based on these results, we can speculate about the movement in the lower S4 region during gating. S1 and S4 likely move relative to one another during the first component, because charge movement coincides with S4 rearrangements [31] while our marker is located on the S1. The second fluorescence change occurs in the same direction, so it might be the S4 continuing in the same direction and might include the S4–S5 linker. The S4–S5 linker has been shown to move during gating [6]. It is covalently linked to the S5 and also anneals to the C terminus of the S6, which forms the cytosolic gate of the ion-conducting pore [30, 40-42]. Alternatively, the relative fluorescence change might be caused by a movement of the S1 or a surrounding helix. For instance, involvement of S1 and S2 in conformational changes of the voltage sensor has been demonstrated for BK [43] and Shaker channels [11]. Finally, in the C-type inactivated conformation, the helices are reoriented such that fluorescence of V234Anap reduces. This movement is probably associated with the S4, because movement of the N-terminal S4 during C-type inactivation and relaxation has been shown [30, 44-47].

3.3.3 Final Pore Opening Occurs in a Two-Step Process.

The synchronism of the voltage dependencies of the first component of the V234Anap fluorescence signal and the major charge movement signifies that lower S4 movement still occurred independently for each voltage sensor if we assume that major charge movement occurs independently for partially uncoupled mutants [32]. Thus, the S4 helix does not yet contribute to the cooperative pore opening.

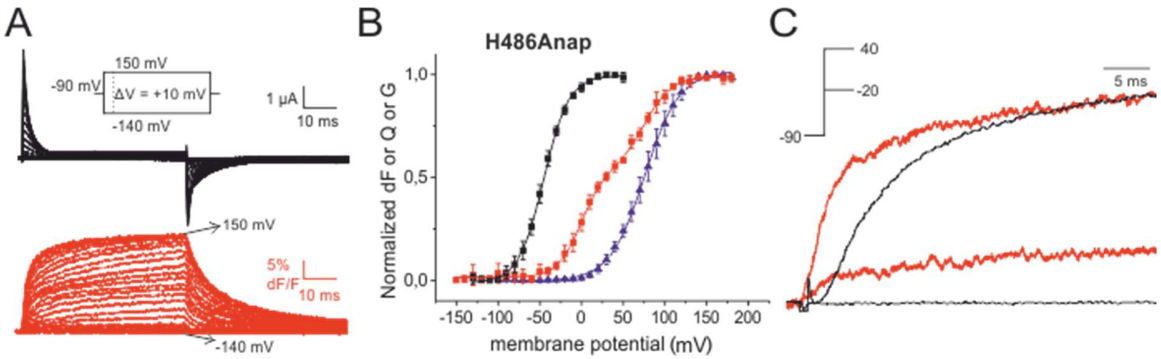

Figure 3.3
A) Fluorescence response and gating currents of H486Anap in response to pulses from −90 mV to potentials between −140 and 150 mV. **B)** Fluorescence voltage (FV, red circles), gating charge voltage (QV, black squares), and conductance voltage (GV, blue triangles) relations of H486Anap. QV and GV were fitted to Boltzmann relations (QV: $V_{1/2}$ = −47.2 mV, dV = 16.2 mV; GV: $V_{1/2}$ = 75.7mV, dV = 20.9 mV). The FV was fitted to a sum of two Boltzmann relations ($V_{1/2,1}$ = 0.5 mV, dV_1 = 14.2 mV, $V_{1/2,2}$ = 75.7 mV, dV_2 = 16.4 mV. **C)** Comparison of time dependence between conductance (black) and fluorescence (red) of H486Anap. Fluorescence changes are

observed in the absence of ion conduction and clearly precede ion conduction at −20 mV and +40 mV, respectively.

To find the location, which no longer shows independently but only cooperatively moving components, and to answer the question how this internal pore gate behaved with respect to the lower S4, we incorporated Anap at position H486 in the C-terminal S6 close to the attachment site to the S4–S5 linker [30, 40-42, 48] (figure 3.1*A*). The corresponding FV contained two components (figure 3.3 *A* and *B* and figure S3.1*B*): The first component was situated between QV and GV, whereas the second component was closely related to the GV. Because no component superposed with the QV directly, the associated movement at the internal gate of K_V did not occur independently for the four subunits. The C-terminal S6 may thus be interpreted as the first position in the gating path not to act independently but cooperatively as postulated [8]. However, this first transition did not coincide yet with the GV, indicating that, in contrast to previous models [8], the first cooperative step after activation of all four voltage sensors did not yet open the pore, but that a second transition of the internal gate is required as suggested by Schoppa and Sigworth [9] and Bezanilla et al. [7]. This finding is confirmed in a superposition of the fluorescence change with the ionic current; here, movement of the C-terminal S6 evidently preceded ion conduction (figure 3.3*C*). Pore opening (GV) is finally related to the second component of the FV (figure 3.3*B*). All in all, fluorescent tracking of the internal gate revealed two features for pore opening: (*i*) Movement of the C-terminal S6 is the first cooperative movement and (*ii*) the first cooperative transition of the internal pore gate is not yet sufficient for pore opening, but a second transition is required.

3.4 Discussion

If we combine the fluorescence results in this study, we are in a position to describe the structural dynamics of the entire gating sequence from the early “pregating” closed state transitions to pore opening. The gating sequence begins at strongly hyperpolarized potentials with closed-state transitions only observed at the N-terminal S4. It is followed by the predicted translocation and tilt of the S4 generating the two major gating charges. Despite identical voltage dependence of both the C- and N-terminal ends of S4 during the major charge movement, the conformational changes in both regions are not simultaneous. Instead, the upper S4 region

"slowly" eases into its final state. The movement observed around the C-terminal S4 still occurs independently for every voltage sensor. The first cooperative movement in the gating sequence, once all voltage sensors have activated, is the first transition of the C-terminal S6, during which the pore enters an additional permissive, nonconducting state. It is followed by the final pore opening step (second S6 transition). Finally, the voltage sensor undergoes a global rearrangement during C-type inactivation and the related relaxation.

We can also compare the structural information obtained by the fluorescence measurements with the kinetic models based on electrophysiology. Although initially a single concerted step during pore opening was proposed by kinetic modeling [8], two concerted steps had been predicted in some models [7, 9]. Schoppa and Sigworth [9] suggested three independent steps of each voltage sensor followed by two concerted transitions. In good agreement, we also found three transitions in the voltage sensor—one during the deep-closed states and two during major gating charge movement—followed by two concerted steps, which we detected at the C-terminal S6 in the pore domain.

Mannuzzu and Isacoff [32] found the second major charge movement in the S4 (Q_2) to show cooperativity, and they suggested this cooperativity either to be an intrinsic property of the voltage sensors or to be imposed by a cooperative subsequent transition. If the energetic coupling between pore domain and voltage sensor is strong, the cooperativity would be detected in the voltage sensor transitions although they are intrinsically independent. Energetic uncoupling of both domains in the L382V mutant removed the cooperativity in Q_2 confirming the intrinsically independent movement of the voltage sensors [32]. The partial uncoupling in V234Anap and H486Anap allowed us, too, to separate the late transitions leading to pore opening, and our data seem to confirm that the concerted movements begin in the pore domain.

This effect of partial uncoupling leads to the question of energetic coupling between voltage sensor and pore domain. Remarkably, the final pore opening step that we detected was not related to major charge movement in the voltage sensor but seemed to have its own voltage dependence. Such a final voltage-dependent step for pore opening was postulated in models explaining the coupling between voltage sensing and pore domains—the electromechanical coupling [10, 30, 48-50]. The separation between charge movement and pore opening by

uncoupling demonstrates that energy is transferred between voltage sensors and pore domain during gating. Because the first three voltage sensors move before pore opening, the generated energy has to be conserved in the system. It is transferred to the pore domain during gating most likely via the structure separating the independent from the concerted movements. According to our results, this structure would be the S4–S5 linker annealed to the C-terminal S6. This finding is in accordance with earlier ones that mutations in the S4–S5 linker, and the C-terminal S6 lead to energetic uncoupling of voltage sensing and pore domain [30, 40, 49-51].

Our use of a fUAA provided dynamic structural information collected from the cytosolic side of the channel. VCF from the cytosolic side of the channel was not possible with chemical labeling because of the large number of unwanted binding sites in the cytosol. Labeling with fUAAs also disposes of the need to construct cysteine-free mutants, which are often impaired in function and expression. Anap has a size comparable to tryptophan and may be introduced at virtually any position in the protein. The smaller size compared with organic dyes makes it more sensitive even to small rearrangements (as seen in A359Anap). Because fUAAs may be readily incorporated in any protein with minimal genetic manipulation, we expect voltage-clamp fluorometry in combination with fUAAs to find widespread application in structural biology.

3.5 Materials and Methods

3.5.1 Molecular Biology and Channel Expression.

Mutations were introduced into a plasmid encoding the *Drosophila* Shaker gene H4 in the pBSTA vector with N-type inactivation removed by deletion of amino acids 6–46 [52]. Gating currents and fluorescence traces were obtained from the nonconducting W434F mutant. The tRNA/AnapRS encoding plasmid and the fUAA Anap [29] were kindly provided by Peter G. Schultz (Scripps Research Institute, La Jolla, CA). For functional expression of channels harboring Anap, 0.5 ng of cDNA encoding the tRNA/AnapRS pair was injected into the nucleus of oocytes from *Xenopus laevis* situated in the animal pole and incubated for 24 h at 18 °C to allow tRNA transcription and synthetase expression. Subsequent steps were performed under light not exciting the fluorophore (>610 nm). 5–35 nanograms of in vitro transcribed RNA was coinjected with 23 nL of 1 mM Anap. Oocytes were incubated in Barth solution for 1–3 d at 18 °C. In the

absence of the tRNA/AnapRS pair and/or the fUAA, no channel expression was detected for all three mutants, verifying that only proteins with the inserted unnatural amino acids were trafficked to the membrane.

3.5.2 Voltage-Clamp Fluorometry

Voltage clamp was performed with a CA-1B amplifier (Dagan). Currents were recorded in the cut-open oocyte voltage-clamp configuration as described [30] and analyzed by using GPatch (Department of Anesthesiology, University of California, Los Angeles). Capacitive currents were subtracted from gating currents by using the P/4 protocol [53]. For fluorescence measurements, an upright fluorescence microscope (Axioskop 2FS; Zeiss) and a Photomax 200 photodetection system (Dagan) were used. Boltzmann relations were of the form $y = (1+\exp((V_{1/2}-V)/dV))^{-1}$ and $y = (1+\exp((V_{1/2,1}-V)/dV_1)(1+\exp((V_{1/2,2}-V)/dV_2))^{-1}$ for first (single transition) and second (for two sequential transitions) order, respectively. Data are shown as mean ± SD with n = 4–7 of at least two independent injections.

The external solution used for ionic current recordings contained 5 mM KOH, 110 mM NMDG, 10 mM Hepes, and 2 mM $Ca(OH)_2$, whereas for gating conditions, 115 mM NMDG, 10 mM Hepes, and 2 mM $Ca(OH)_2$ was used. The internal solution contained 115 mM NMDG (gating) or KOH (ionic), 10 mM Hepes, and 2 mM EDTA. TMR labeling was accomplished by incubating oocytes for 20 min in 5 µM TMR-maleimide (Invitrogen) in depolarizing solution [115 mM KOH, 10 mM Hepes, and 2 mM $Ca(OH)_2$]. All solutions were adjusted to pH 7.1 with Mes.

3.6 Acknowledgements

The plasmid encoding the tRNA/AnapRS pair and Anap were kind gifts from Dr. Peter G. Schultz (Scripps Research Institute, La Jolla, CA). We thank Dr. Abhishek Chatterjee for advice on plasmid preparation, Helène Klein for discussions on unnatural amino acid expression, and Yolaine Dodier and Yoan Lussier for technical assistance. This work was funded by the Canadian Institutes for Health Research Grant MOP-102689 (to R.B.) and Canadian Foundation for Innovation Grant 950-225005. Groupe d'Études des Protéines Membranaires is a research group funded by the Fonds de recherche du Québec–Santé. R.B. holds a Canada Research Chair on Molecular Mechanisms of Membrane Proteins.

3.7 Supporting information

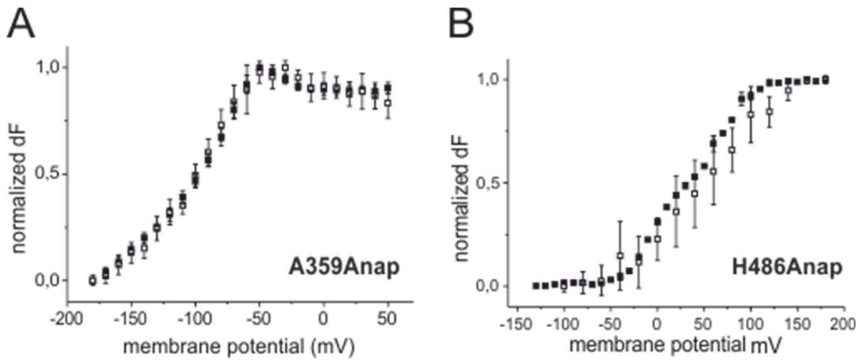

Figure S3.1
Comparison of fluorescence-voltage dependencies of the conducting (open squares) and nonconducting (filled squares) mutants of **A)** A359Anap and **B)** H486Anap.

3.8 References

1. Long, S.B., E.B. Campbell, and R. Mackinnon, *Crystal structure of a mammalian voltage-dependent Shaker family K+ channel.* Science, 2005. **309**(5736): p. 897-903.
2. Long, S.B., X. Tao, E.B. Campbell, and R. MacKinnon, *Atomic structure of a voltage-dependent K+ channel in a lipid membrane-like environment.* Nature, 2007. **450**(7168): p. 376-82.
3. Yarov-Yarovoy, V., P.G. DeCaen, R.E. Westenbroek, C.Y. Pan, T. Scheuer, D. Baker, and W.A. Catterall, *Structural basis for gating charge movement in the voltage sensor of a sodium channel.* Proc Natl Acad Sci U S A, 2012. **109**(2): p. E93-102.
4. Vargas, E., F. Bezanilla, and B. Roux, *In search of a consensus model of the resting state of a voltage-sensing domain.* Neuron, 2011. **72**(5): p. 713-20.
5. Jensen, M.O., V. Jogini, D.W. Borhani, A.E. Leffler, R.O. Dror, and D.E. Shaw, *Mechanism of voltage gating in potassium channels.* Science, 2012. **336**(6078): p. 229-33.
6. Faure, E., G. Starek, H. McGuire, S. Berneche, and R. Blunck, *A limited 4 A radial displacement of the S4-S5 linker is sufficient for internal gate closing in Kv channels.* J Biol Chem, 2012. **287**(47): p. 40091-8.
7. Bezanilla, F., E. Perozo, and E. Stefani, *Gating of Shaker K+ channels: II. The components of gating currents and a model of channel activation.* Biophys J, 1994. **66**(4): p. 1011-21.
8. Zagotta, W.N., T. Hoshi, and R.W. Aldrich, *Shaker potassium channel gating. III: Evaluation of kinetic models for activation.* J Gen Physiol, 1994. **103**(2): p. 321-62.
9. Schoppa, N.E. and F.J. Sigworth, *Activation of Shaker potassium channels. III. An activation gating model for wild-type and V2 mutant channels.* J Gen Physiol, 1998. **111**(2): p. 313-42.
10. Blunck, R. and Z. Batulan, *Mechanism of electromechanical coupling in voltage-gated potassium channels.* Front Pharmacol, 2012. **3**: p. 166.
11. Cha, A. and F. Bezanilla, *Characterizing voltage-dependent conformational changes in the Shaker K+ channel with fluorescence.* Neuron, 1997. **19**(5): p. 1127-40.
12. Mannuzzu, L.M., M.M. Moronne, and E.Y. Isacoff, *Direct physical measure of conformational rearrangement underlying potassium channel gating.* Science, 1996. **271**(5246): p. 213-6.
13. Cha, A. and F. Bezanilla, *Structural implications of fluorescence quenching in the Shaker K+ channel.* J Gen Physiol, 1998. **112**(4): p. 391-408.

14. Bannister, J.P., B. Chanda, F. Bezanilla, and D.M. Papazian, *Optical detection of rate-determining ion-modulated conformational changes of the ether-a-go-go K+ channel voltage sensor.* Proc Natl Acad Sci U S A, 2005. **102**(51): p. 18718-23.
15. Savalli, N., A. Kondratiev, L. Toro, and R. Olcese, *Voltage-dependent conformational changes in human Ca(2+)- and voltage-activated K(+) channel, revealed by voltage-clamp fluorometry.* Proc Natl Acad Sci U S A, 2006. **103**(33): p. 12619-24.
16. Claydon, T.W. and D. Fedida, *Voltage clamp fluorimetry studies of mammalian voltage-gated K(+) channel gating.* Biochem Soc Trans, 2007. **35**(Pt 5): p. 1080-2.
17. Blunck, R., D.M. Starace, A.M. Correa, and F. Bezanilla, *Detecting rearrangements of shaker and NaChBac in real-time with fluorescence spectroscopy in patch-clamped mammalian cells.* Biophys J, 2004. **86**(6): p. 3966-80.
18. Zheng, J. and W.N. Zagotta, *Gating rearrangements in cyclic nucleotide-gated channels revealed by patch-clamp fluorometry.* Neuron, 2000. **28**(2): p. 369-74.
19. Cha, A., P.C. Ruben, A.L. George, Jr., E. Fujimoto, and F. Bezanilla, *Voltage sensors in domains III and IV, but not I and II, are immobilized by Na+ channel fast inactivation.* Neuron, 1999. **22**(1): p. 73-87.
20. Meinild, A.K., B.A. Hirayama, E.M. Wright, and D.D. Loo, *Fluorescence studies of ligand-induced conformational changes of the Na(+)/glucose cotransporter.* Biochemistry, 2002. **41**(4): p. 1250-8.
21. Gagnon, D.G., A. Holt, F. Bourgeois, B. Wallendorff, M.J. Coady, and J.Y. Lapointe, *Membrane topology of loop 13-14 of the Na+/glucose cotransporter (SGLT1): a SCAM and fluorescent labelling study.* Biochim Biophys Acta, 2005. **1712**(2): p. 173-84.
22. Li, M., R.A. Farley, and H.A. Lester, *An intermediate state of the gamma-aminobutyric acid transporter GAT1 revealed by simultaneous voltage clamp and fluorescence.* J Gen Physiol, 2000. **115**(4): p. 491-508.
23. Li, M. and H.A. Lester, *Early fluorescence signals detect transitions at mammalian serotonin transporters.* Biophys J, 2002. **83**(1): p. 206-18.
24. Dahan, D.S., et al., *A fluorophore attached to nicotinic acetylcholine receptor beta M2 detects productive binding of agonist to the alpha delta site.* Proc Natl Acad Sci U S A, 2004. **101**(27): p. 10195-200.
25. Nowak, M.W., et al., *Nicotinic receptor binding site probed with unnatural amino acid incorporation in intact cells.* Science, 1995. **268**(5209): p. 439-42.
26. Tao, X., A. Lee, W. Limapichat, D.A. Dougherty, and R. MacKinnon, *A gating charge transfer center in voltage sensors.* Science, 2010. **328**(5974): p. 67-73.
27. Pless, S.A., J.D. Galpin, A.P. Niciforovic, and C.A. Ahern, *Contributions of counter-charge in a potassium channel voltage-sensor domain.* Nat Chem Biol, 2011. **7**(9): p. 617-23.
28. Pantoja, R., E.A. Rodriguez, M.I. Dibas, D.A. Dougherty, and H.A. Lester, *Single-molecule imaging of a fluorescent unnatural amino acid incorporated into nicotinic receptors.* Biophys J, 2009. **96**(1): p. 226-37.
29. Lee, H.S., J. Guo, E.A. Lemke, R.D. Dimla, and P.G. Schultz, *Genetic incorporation of a small, environmentally sensitive, fluorescent probe into proteins in Saccharomyces cerevisiae.* J Am Chem Soc, 2009. **131**(36): p. 12921-3.
30. Haddad, G.A. and R. Blunck, *Mode shift of the voltage sensors in Shaker K+ channels is caused by energetic coupling to the pore domain.* J Gen Physiol, 2011. **137**(5): p. 455-72.
31. Baker, O.S., H.P. Larsson, L.M. Mannuzzu, and E.Y. Isacoff, *Three transmembrane conformations and sequence-dependent displacement of the S4 domain in shaker K+ channel gating.* Neuron, 1998. **20**(6): p. 1283-94.

32. Mannuzzu, L.M. and E.Y. Isacoff, *Independence and cooperativity in rearrangements of a potassium channel voltage sensor revealed by single subunit fluorescence.* J Gen Physiol, 2000. **115**(3): p. 257-68.
33. Cole, K.S. and J.W. Moore, *Potassium ion current in the squid giant axon: dynamic characteristic.* Biophys J, 1960. **1**: p. 1-14.
34. Sigg, D., F. Bezanilla, and E. Stefani, *Fast gating in the Shaker K+ channel and the energy landscape of activation.* Proc Natl Acad Sci U S A, 2003. **100**(13): p. 7611-5.
35. Freites, J.A., E.V. Schow, S.H. White, and D.J. Tobias, *Microscopic origin of gating current fluctuations in a potassium channel voltage sensor.* Biophys J, 2012. **102**(11): p. L44-6.
36. Ledwell, J.L. and R.W. Aldrich, *Mutations in the S4 region isolate the final voltage-dependent cooperative step in potassium channel activation.* J Gen Physiol, 1999. **113**(3): p. 389-414.
37. Yang, Y., Y. Yan, and F.J. Sigworth, *How does the W434F mutation block current in Shaker potassium channels?* J Gen Physiol, 1997. **109**(6): p. 779-89.
38. McCormack, K., W.J. Joiner, and S.H. Heinemann, *A characterization of the activating structural rearrangements in voltage-dependent Shaker K+ channels.* Neuron, 1994. **12**(2): p. 301-15.
39. Loboda, A. and C.M. Armstrong, *Resolving the gating charge movement associated with late transitions in K channel activation.* Biophys J, 2001. **81**(2): p. 905-16.
40. Lu, Z., A.M. Klem, and Y. Ramu, *Ion conduction pore is conserved among potassium channels.* Nature, 2001. **413**(6858): p. 809-13.
41. Labro, A.J., A.L. Raes, A. Grottesi, D. Van Hoorick, M.S. Sansom, and D.J. Snyders, *Kv channel gating requires a compatible S4-S5 linker and bottom part of S6, constrained by non-interacting residues.* J Gen Physiol, 2008. **132**(6): p. 667-80.
42. Long, S.B., E.B. Campbell, and R. Mackinnon, *Voltage sensor of Kv1.2: structural basis of electromechanical coupling.* Science, 2005. **309**(5736): p. 903-8.
43. Pantazis, A. and R. Olcese, *Relative transmembrane segment rearrangements during BK channel activation resolved by structurally assigned fluorophore-quencher pairing.* J Gen Physiol, 2012. **140**(2): p. 207-18.
44. Pathak, M., L. Kurtz, F. Tombola, and E. Isacoff, *The cooperative voltage sensor motion that gates a potassium channel.* J Gen Physiol, 2005. **125**(1): p. 57-69.
45. Gandhi, C.S., E. Loots, and E.Y. Isacoff, *Reconstructing voltage sensor-pore interaction from a fluorescence scan of a voltage-gated K+ channel.* Neuron, 2000. **27**(3): p. 585-95.
46. Claydon, T.W., M. Vaid, S. Rezazadeh, S.J. Kehl, and D. Fedida, *4-aminopyridine prevents the conformational changes associated with p/c-type inactivation in shaker channels.* J Pharmacol Exp Ther, 2007. **320**(1): p. 162-72.
47. Villalba-Galea, C.A., W. Sandtner, D.M. Starace, and F. Bezanilla, *S4-based voltage sensors have three major conformations.* Proc Natl Acad Sci U S A, 2008. **105**(46): p. 17600-7.
48. Batulan, Z., G.A. Haddad, and R. Blunck, *An intersubunit interaction between S4-S5 linker and S6 is responsible for the slow off-gating component in Shaker K+ channels.* J Biol Chem, 2010. **285**(18): p. 14005-19.
49. Muroi, Y., M. Arcisio-Miranda, S. Chowdhury, and B. Chanda, *Molecular determinants of coupling between the domain III voltage sensor and pore of a sodium channel.* Nat Struct Mol Biol, 2010. **17**(2): p. 230-7.
50. Ding, S. and R. Horn, *Effect of S6 tail mutations on charge movement in Shaker potassium channels.* Biophys J, 2003. **84**(1): p. 295-305.
51. Schoppa, N.E. and F.J. Sigworth, *Activation of Shaker potassium channels. II. Kinetics of the V2 mutant channel.* J Gen Physiol, 1998. **111**(2): p. 295-311.

52. Hoshi, T., W.N. Zagotta, and R.W. Aldrich, *Biophysical and molecular mechanisms of Shaker potassium channel inactivation.* Science, 1990. **250**(4980): p. 533-8.
53. Armstrong, C.M. and F. Bezanilla, *Inactivation of the sodium channel. II. Gating current experiments.* J Gen Physiol, 1977. **70**(5): p. 567-90.

Chapter 4

The S4-S5 linker movement during activation and inactivation in voltage-gated K^+ channels

Tanja Kalstrup[1] and Rikard Blunck[1,2]

[1]Department of Physiology and Pharmacology, and [2]Department of Physics, Montreal University, Montreal, Quebec, Canada

Under revision. Submitted to *Proc Natl Acad Sci USA* on November 1, 2017.

Author contributions: T.K. and R.B. designed research, T.K. performed experiments, T.K. and R.B. analyzed data, T.K. wrote the first version which was edited by R.B.

4.1 Abstract

In voltage-gated ion channels, the electromechanical coupling between the peripheral voltage-sensing domains and the central ion conducting pore is mainly occurring at the cytosolic surface of the channels. The S4-S5 linker is the physical link between the voltage sensor and the pore domain and plays an important role in the electromechanical coupling. While numerous dynamical studies have been performed on voltage sensor movement, less have focused on the S4-S5 linker movement due to the inaccessibility for fluorophore labelling and lack of electric readout for the movement of the linker. To understand the movements of the gating machinery during activation and inactivation, we have incorporated a fluorescent unnatural amino acid at four positions in the S4-S5 linker of the Shaker K_V channel (L382, R387, K390 and A391). Using two-color voltage clamp fluorometry, we directly compared S4-S5 linker movements with charge displacement, S4 movement and pore opening. We found that the N-terminal portion of the linker moves together with the S4 helix throughout the gating process, while the C-terminal portion undergoes a separate motion related to late gating transitions. Both pore and S4-S5 linker undergo rearrangements during C-type inactivation, however, in presence of accelerated C-type inactivation (W434F mutation), the energetic coupling between movement of the C-terminus of the S4-S5 linker and pore opening disappears.

4.2 Introduction

Voltage-gated potassium (K_V) channels are responsible for repolarization of the membrane potential during neuronal and cardiac action potentials, and regulate neuronal excitability among many other physiological processes. Mutations in K_V channel genes thus result in severe neuronal and cardiac diseases such as episodic ataxia, epilepsy and cardiac arrhythmia, collectively named channelopathies. Its central role in heart and brain underscores the importance of understanding the mechanisms of K_V channels in detail. K_V channels thus constitute therapeutic drug targets for treatments of diverse diseases [1].

All mammalian Shaker-like K_V channels (K_V1 channel subfamily) share the characteristic assembly of four subunits which each consists of six transmembrane helices containing a voltage sensor (S1-S4) and a pore region (S5-S6, figure 4.1A) [2, 3]. The voltage sensor (VS) contains positively charged arginine residues in the S4 helix which are responsible for the generation of gating

currents as they rearrange according to changes in the electric field they sense across the membrane [4]. This conformational change results in pore opening through a mechanism called electromechanical coupling [5].

Although dynamic information lacks and the underlying molecular driving forces are not fully understood, a consensus model of the coupling process has emerged [5, 6]. First, initial S4 charge movements (Q1) occur independently in each VS upon membrane depolarization, applying a force onto the S4-S5 linker as they move upwards within the membrane. Then, during a second S4 charge movement (Q2), energy is released to the pore domain in a cooperative conformational change which finally results in widening of the bundlecross at the intracellular S6 gates. The opening step has been shown to occur cooperatively among the subunits [7, 8] and comprises at least two transitions [9]. In addition to being covalently bound to the pore domain via S5, the S4-S5 linker interacts directly with the S6 bundlecrossing via non-covalent interactions of both the same [10-13] and the neighboring subunit [14] . Since dynamics of the S4 helices and the inner S6 gate are associated with gating currents and ionic currents respectively, the role of each region in the activation process have been well established. The S4-S5 linker movement, on the contrary, is intrinsically not associated to any charge movement. Moreover, the intracellular position of the S4-S5 linker has made it inaccessible for fluorophore-labelling. Consequently, only limited dynamical information is available for the S4-S5 linker movement [15].

To investigate S4-S5 linker dynamics, we have made use of the stop codon suppression technique for the genetic incorporation of a fluorescent unnatural amino acid (Anap) [9, 16, 17], enabling specific labelling of intracellular sites for the use of voltage clamp fluorometry (VCF) in proteins expressed in *Xenopus* oocytes [9]. We aimed to address questions as to where the transition between the independent voltage sensor movement and the cooperative pore opening occurred; and whether the S4-S5 linker rearranges as a rigid body throughout the gating process, or with a degree of flexibility, allowing conservation of the energy provided by the voltage sensor. To this end, Anap was inserted into the S4-S5 linker of the Shaker K_V channel. By labelling the external part of the S4 helix with an thiol-reactive dye, we were able to compare movements of the voltage sensor and of the S4-S5 linker simultaneously.

4.3 Results

4.3.1 Assessment of functional expression with Anap

All 12 positions along the Shaker S4-S5 linker (residues 381-392) were scanned for Anap insertion (figure 4.1B). Proper protein maturation and folding were determined from the presence of both ionic and gating currents. Four positions resulted in robust expression and voltage-dependent fluorescence changes with Anap inserted at L382, R387, K390, A391, while four did not express (G381, Y385, T388, G392). The four remaining residues either showed limited expression (Q383, L389) or defective channel opening (I384, G386). In the available K_V channel crystal structures [2, 3], the non-expressing residues face inwards towards the center of the channel (*black* in figure 4.1B) while expressing residues point outwards, away from the channel (*red* in figure 4.1B). This finding agrees with the fact that a large amino acid like Anap is more likely to sterically disrupt protein folding at positions which interact with the protein versus positions which point outwards into the cytosol or into the lipid bilayer. I384 has been shown previously to be essential for electromechanical coupling [18].

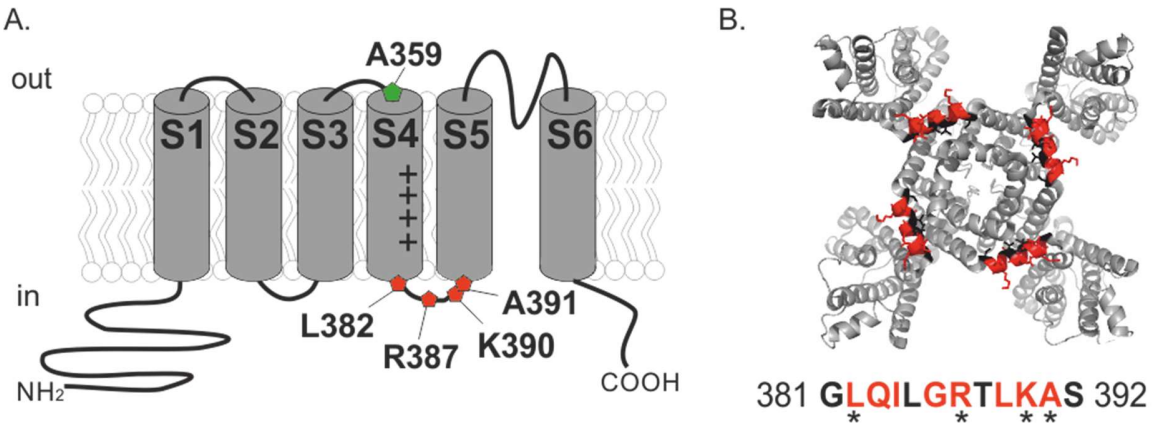

Figure 4.1 Overview of K_V channel structure
A) Topology of a Shaker subunit with relevant positions highlighted. A cysteine was inserted at position A359 for TMR labelling (green) and Anap was inserted into the S4-S5 linker (red). B) Bottom view of the K_V1.2-2.1 crystal structure of the homotetrameric transmembrane segment [3]. Below is the S4-S5 linker sequence which was scanned for Anap incorporation. Anap was successfully incorporated into positions marked in red but only those marked with an asterisk was used to characterize the S4-S5 linker movement.

It was recently shown that Shaker channels lacking the pore domain express as functional isolated voltage sensor domains (iVSD) giving rise to gating pore currents[19]. These currents were also observed in mutants with a stop-codon insertion in the S4-S5 linker in the absence of

Anap or pAnap (figure. S4.1A-B). However, while iVSD currents also occurred when Anap and pAnap were present, their amplitude depended on the success of Anap incorporation, such that iVSD current amplitudes were considerably smaller in oocytes expressing full length channels (4.4 µA ±6.7 at -170 mV) compared to oocytes in which full length channels were absent (20.4 µA ±7.9 at -170 mV, figure S4.1C). Having ensured that iVSD currents were not altering gating kinetics and did not form heterotetramers (see supplemental material), we were able to proceed to the analysis of the fluorescence signals.

4.3.2 The S4-S5 linker rearranges after S4 activation

The four S4-S5 linker mutants L382Anap, R387Anap, K390Anap and A391Anap of full length Shaker exhibited robust expression levels, with Anap changes showing relative fluorescence intensity changes (dF/F) in the range of 0.2-4% in response to depolarization (figure 4.2A). Since fluorescent labeling either by insertion of Anap or TMR might influence kinetics and energy of voltage sensor movement and pore opening, we can only directly compare voltage sensor movement, movement of the S4-S5 linker and pore opening in the same mutant, i.e. tracking all parameters simultaneously. However, we showed previously that fluorescence originating from TMR attached to the extracellular end of S4 reliably follows gating charge movement [18]. Therefore, the stop codons were inserted in the Shaker-A359C background, to compare S4-S5 linker movement (Anap signals) with voltage sensor movement (A359C-TMR signals), simultaneously. Pore opening was monitored electrically via development of ionic current.

As expected, the voltage dependence of voltage sensor movement (FV-TMR) for all four mutants developed at less depolarized potentials compared to pore opening (conductance voltage relation, GV; figure 4.2B-E). In contrast, comparison of the voltage dependencies of voltage sensor movement (FV-TMR) and movement at the S4-S5 linker (FV-Anap) varied with the monitored position in the S4-S5 linker. While the signals overlapped in L382Anap (figure 4.2B), the movements at R387, K390 and A391, in the S4-S5 linker, were shifted to more depolarized potentials compared to voltage sensor movement by 29 mV, 21 mV and 21 mV, respectively (figure 4.2C-E and table 1). However, movement at all three positions was still occurring at less depolarized potentials than pore opening (GV).

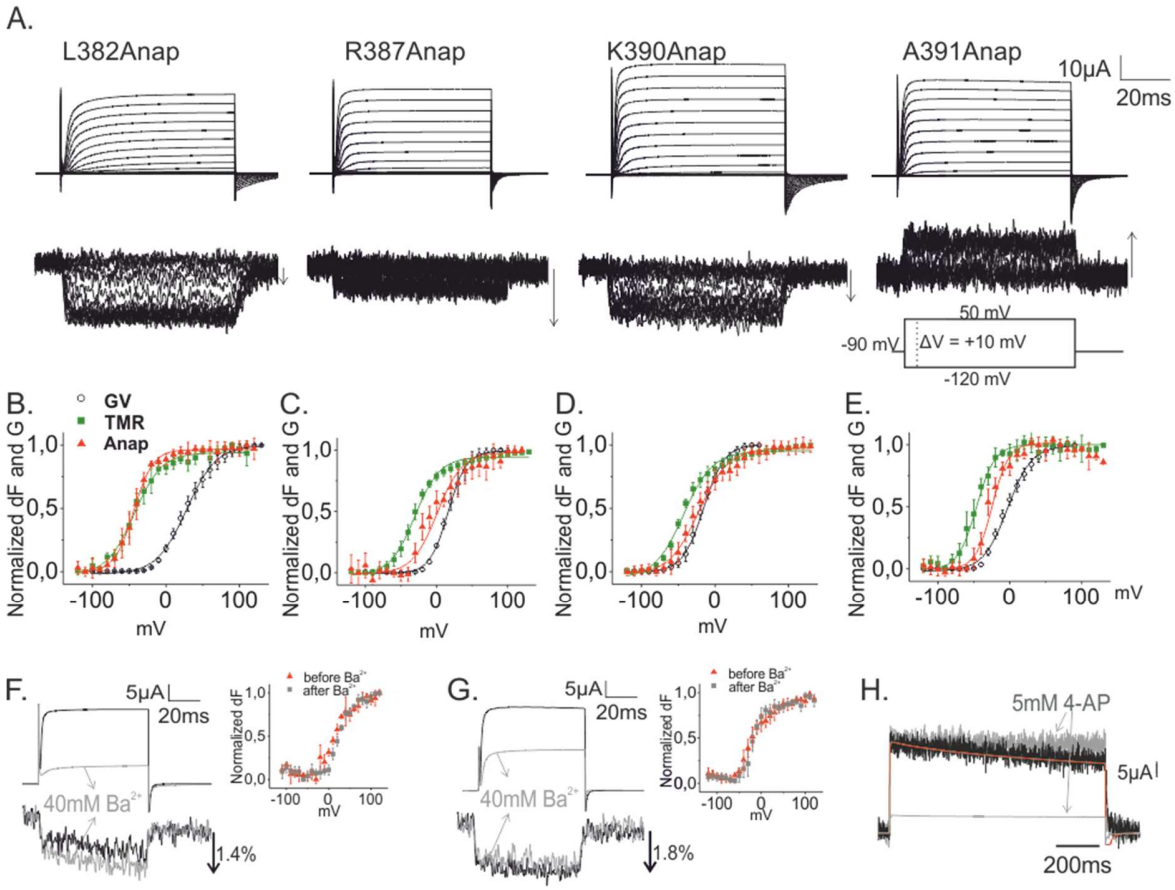

Figure 4.2 Fluorescence profile of conducting channels
A) VCF recordings of ionic currents (upper) and Anap fluorescence changes (lower) obtained from oocytes expressing each of the S4-S5 linker mutants. The arrow next to each fluorescence signal represents 1% dF/F. B-E) Anap FV, TMR FV and GV curves of B) L382Anap C) R387Anap D) K390Anap and E) A391Anap channels. Each data set is fitted to a Boltzman distribution (see methods and materials). Error bars indicate mean ±SD. F-G) Current and fluorescence output upon depolarization from -90mV to 20mV before and 30 min after external application of 40 mM Barium in F) R387Anap and G) K390Anap channels. Inset shows Anap FV obtained before and after block. H) Anap fluorescence and ionic currents of A391Anap-W434F channels upon prolonged 1 sec depolarisation from -90mV to 50mV before and after 5 mM external 4-AP block. The ionic current before 4-AP application is colored in red for clarity.

To ensure that the signal was caused by conformational changes at the labeling position, we excluded that the fluorescence was influenced by potassium flux through the nearby pore entrance. Conductance might alter local ion concentrations and, thereby, the local electric field, which could influence fluorescence signals. We used Ba^{2+} to block the ionic current. Ba^{2+} has a size similar to K^+ and can enter the pore but blocks conductance once it reaches the selectivity filter with minimal effects on voltage sensor activation[20]. Despite significant block by external Ba^{2+} in R387Anap and K390Anap channels, the total Anap fluorescence change was not

diminished, and the fluorescence time course and voltage dependency remained unaffected, indicating that the fluorescence signals were indeed caused by conformational changes at the labeling site (figure 4.2F-G). The results suggest that only the N-terminal part of the linker (L382) moves together with the S4 helix during activation while the more distal part of the linker rearranges later in the activation process.

	TMR FV		Anap FV		GV				
	$V_{1/2}$	dV	$V_{1/2}$	dV	$V_{1/2\,(1)}$	$dV_{(1)}$	$V_{1/2\,(2)}$	$dV_{(2)}$	n
L382Anap	-39.2 ±2.7	23.2 ±2.0	-44 ±0.7	13.1 ±0.8	27.8 ±1.0	20.3 ±0.9			9
R387Anap	-27.4 ±2.1	19.6 ±1.6	1.3 ±1.3	17.1 ±2.1	16.2 ±0.5	12.9 ±0.5			6
K390Anap	-43 ±1.9	19.8 ±1.6	-22 ±0.9	20.2 ±1.5	-15.6 ±0.7	14.4 ±0.5			12
A391Anap	-46 ±1.3	18.2 ±1.1	-24.6 ±1.0	12.1 ±1.3	-3.2 ±1.0	17.0 ±0.1			4
					QV				
L382Anap-W434F	-41.5 ±0.9	22.2 ±0.6	-51.0 ±0.4	15.8 ±0.5	-45.0 ±0.6	17.6 ±0.6	-	-	6
R387Anap-W434F	-38.5 ±0.8	11.0 ±0.5	-26.1 ±0.4	10.4 ±0.6	-58.4 ±14.2	6.0 ±9.6	-28.5 ±5.3	12.5 ±1.3	7
K390Anap-W434F	-48.1 ±0.2	9.7 ±0.2	-40.5 ±0.5	10.9 ±0.4	-77.4 ±10.2	6.3 ±4.2	-37.4 ±3.1	9.2 ±1.5	4
A391Anap-W434F	-42.9 ±0.4	10.6 ±0.2	-39.4 ±0.2	7.3 ±0.4	-59.2 ±7.6	7.4 ±2.2	-34.9 ±2.8	5.3 ±1.1	4

Table 2 $V_{1/2}$ and dV values obtained from single or double Boltzman fits of FV, QV and GV curves of conducting and non-conducting (W434F) mutants.

4.3.3 The S4-S5 linker experience C-type inactivation-related rearrangements

A second fluorescence component of opposite direction appeared in A391Anap at depolarizations more positive than 60 mV (figure 4.2E). An overlap of the current and fluorescence time course during a prolonged depolarization pulse revealed that the second fluorescence component correlated kinetically with C-type inactivation (figure 4.2H). Moreover, the second fluorescence component was sensitive to application of 4-aminopyridine (4-AP, figure 4.2H), which prevents K_V channels from entering the final concerted transition leading to pore opening and thus also prevents C-type inactivation [21].

This was confirmed in non-conducting W434F mutants, in which ionic currents are blocked due to accelerated C-type inactivation [22]. In agreement with the accelerated C-type inactivation, the second Anap fluorescence component in A391Anap-W434F channels appeared faster and larger than without W434F (figure 4.3A and 4.3E). The FV from A391Anap-W434F channels could no longer be fitted to a single Boltzmann relation because the onset for C-type inactivation now occurred at lower potentials than channel opening did (figure 4.3E). These findings indicate that

A391Anap probes rearrangements which are associated with C-type inactivation, in addition to those associated to activation.

Interestingly, a second smaller Anap component of opposite direction also appeared in K390Anap-W434F channels (figure 4.3D). For both K390Anap-W434F and A391Anap-W434F mutants, the second fluorescence component was 4-AP sensitive as demonstrated in the fluorescence time course and in the FV obtained before and after 4-AP application (figure 4.3F-I). Since the second fluorescence component in the conducting K390Anap channels is absent or too small to be measured, it was not possible to verify whether the kinetics of C-type inactivation correlated with the fluorescence signal as was the case with A391Anap (figure 4.2H). The W434F data, nonetheless, suggest that Anap is influenced by C-type inactivation at position K390 in the same way as at position A391.

4.3.4 C-type inactivation allows the S4-S5 linker to assume final position after voltage sensor activation

The most remarkable difference in the W434F background was that the shift between voltage sensor (TMR) and S4-S5 linker (Anap) movement was strongly diminished (figure 4.3C-E). The disappearance of the shift indicates that, in presence of W434F, the entire S4-S5 linker undergoes its conformational change upon voltage sensor activation. In the conducting channel, in contrast, the C-terminus of the S4-S5 linker cannot enter its final position yet after voltage sensor activation but is hindered by an additional energy barrier.

The question remains whether also the sequence of events has altered. To answer this, we considered the dynamic information. The time constants obtained from exponential fits of the fluorescence and gating currents were plotted as a function of the test pulse (figure 4.4A-D). The mutants exhibited similar patterns for TMR and gating currents, each with two components – one in the 1-10 ms range and one in the 10-100 ms range (*green* and *black* symbols, figure 4.4A-D) except for A391Anap-W434F gating currents which only could be fitted to one exponential (figure 4.4D). This could be either because the two components are kinetically similar (yet have different voltage dependencies as the QV was fitted to a double Boltzmann relation) and therefore appear indistinguishable, or because the slower component is too small or too slow to be detected during the test pulse. In fact, A391Anap-W434F generally expressed less than the

other linker mutants yielding maximum 1 µA of gating currents when depolarizing from -90 to 50 mV. It is therefore possible that the slow component in the gating currents disappeared within the experimental noise. Nevertheless, these findings suggest that the kinetics of the upper S4 movement and the charge displacement were not markedly affected by the relative position of Anap in the S4-S5 linker.

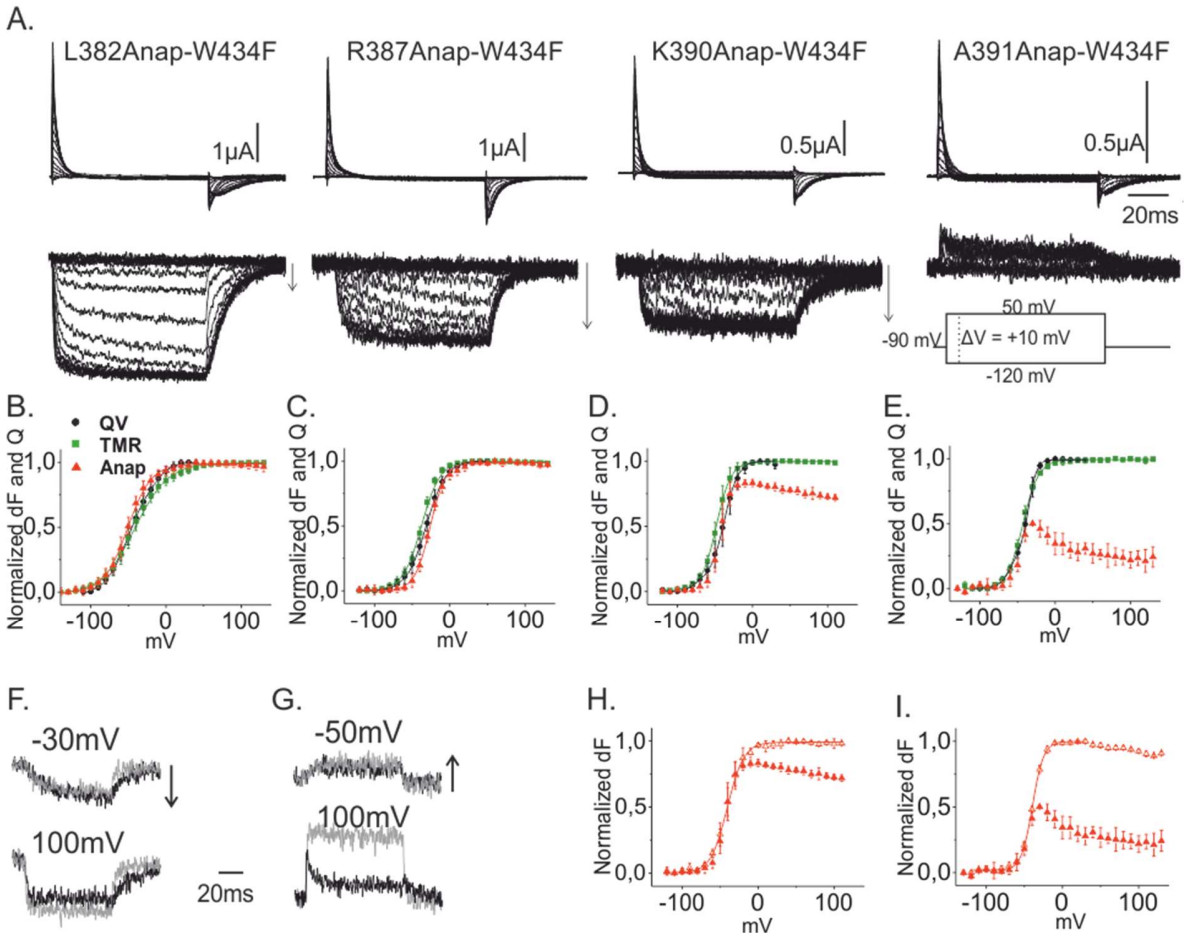

Figure 4.3 Fluorescence profile of non-conducting channels.
A) VCF recordings of gating currents (upper) and Anap fluorescence changes (lower) obtained from oocytes expressing each of the S4-S5 linker mutants with the W434F mutation. B-E) Anap FV, TMR FV and QV curves of B) L382Anap-W434F C) R387Anap-W434F D) K390Anap-W434F and E) A391Anap-W434F channels. Except for Anap FV in D) and E), each data set is fitted to a Boltzman distribution (see methods and materials). Error bars indicate mean ±SD. F) Anap fluorescence of K390Anap-W434F upon depolarisation from -90 mV before (black) and after (grey) external application of 5mM 4-AP. G) Same as F) but for A391Anap-W434F channels. H-I) Anap FV before (filled symbols) and after (open symbols) 4-AP from G) K390Anap-W434F and H) A391Anap-W434F channels. The FV obtained after 4-AP was fitted to a Boltzman distribution.

In L382Anap-W434F, two Anap components were observed- one in the 1-10 ms range and another in the 10-100 ms range (red symbols, figure 4.4A). Although the fast TMR component is 1-5 ms slower than the fast Anap component, the kinetics of TMR, Anap and gating currents are comparable. The result agrees with the overlapping FVs and QV for L382Anap-W434F (figure 4.3B). When overlapping the fluorescence time courses and charge displacement, it is seen that TMR relaxes slower than Anap, and that Anap is kinetically closer to the charge displacement in the first miliseconds where the fast component is dominant (arrow, figure 4.4E). Furthermore, the absence of a delay in the onset of the Anap fluorescence compared to TMR indicates that their movements are prompted simultanously (*black arrow*, figure 4.5A). In fact, these data are similar to earlier data of V234Anap on the S1 helix which is only 9.6 Å away [9] (figure 4.4F). Based on the kinetical analysis, and FV and QV comparisons, the results show that the L382 movement is similar to that of the voltage sensor.

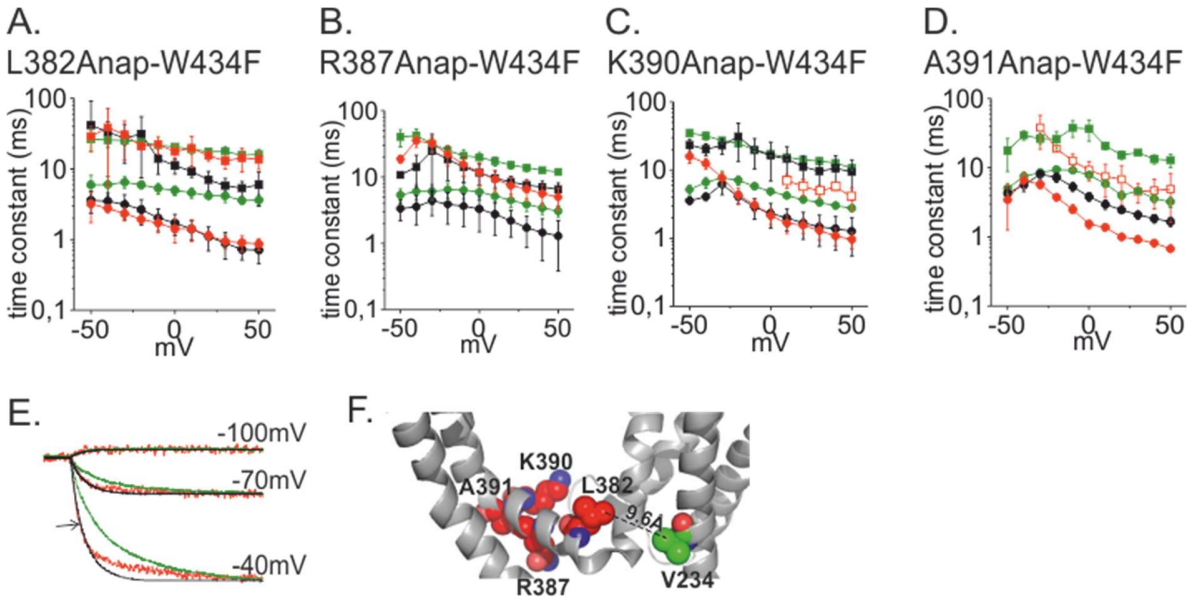

Figure 4.4 Kinetical analysis of fluorescence and gating current time course.
A-D) Time constants obtained from single or double exponentials fits of TMR fluorescence (green), Anap fluorescence (red) and gating currents (black) for each of the S4-S5 linker mutants during a test pulse similar to those in figure 3A. E) Overlapping TMR (green), Anap (red) and charge displacement (black) for an oocyte expressing L382Anap-W434F. Arrow highlights kinetic correlation between the fast component of Anap fluorescence and charge displacement. F) Structural view from the K_V1.2-2.1 crystal structure [3] showing the four S4-S5 linker positions in red and the distance from L382 to V234 in green in S1.

For the C-terminal part of the S4-S5 linker however, Anap fluorescence only exhibited a single time constant (*red circles*, figure 4.4B-D) when disregarding the 4-AP-sensitive slow component of opposite direction in K390Anap-W434F and A391Anap-W434F (*red open squares*, figure 4C-D). In contrast to L382Anap-W434F, superposition of the TMR and Anap fluorescence time courses revealed a delayed onset for Anap. This was best observed in R387Anap-W434F channels where it amounted to ~0.6 ms (*black bar*, figure 5B). The delay in K390Anap-W434F channels was shorter and only visible at small depolarizations (*black arrows*, figure 4.5C). The shorter delay was due to the overall faster kinetics of gating and ionic currents in K390Anap-W434F (figure 4.4B-C and 4.5). Due to the smaller Anap fluorescence change of A391Anap-W434F as a result of limited expression, a delay of less than a milisecond would not be detectable in the noise. The presence of a delayed onset in the Anap fluorescence of the C-terminal linker mutants means that at least one transition needs to occur prior to linker rearrangement also in the W434F background. Therefore, even though the S4-S5 linker is free to transition into its final position upon voltage sensor activation, it is not an independent movement like the voltage sensors.

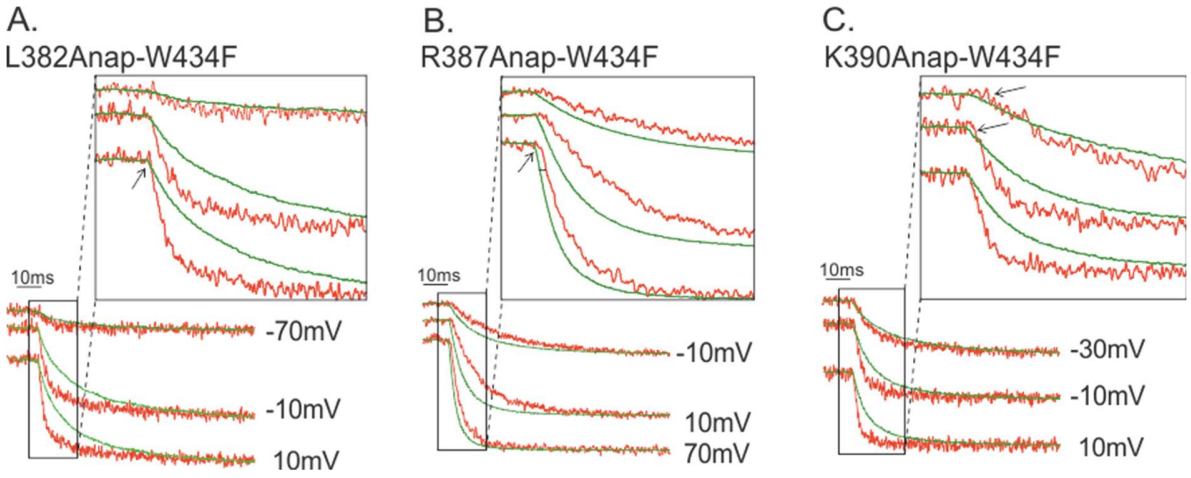

Figure 4.5 Comparison of onset of TMR and Anap fluorescence signal
A-C) Overlap of TMR (green) and Anap (red) fluorescence upon depolarisations from -90mV. Arrow in A) highlights the absense of a delayed onset, while arrows in B and C) highlights the presence of a delayed onset for Anap compared to TMR. The horisontal bar in B) indicates a time difference of 600µs. D-E) Time constants obtained from double exponential fits of gating currents (filled symbols) and ionic currents (open symbols) of D) R387Anap and E) K390Anap channels. F) To take into account the relative voltage-dependencies, the ratio of the maximum ionic time constant to the maximum gating time constant was determined for both the fast (T1) and slow (T2) component, showing that the ionic currents in K390Anap are slower than those in R387Anap relative to the gating current.

4.3.5 The C-terminal S4-S5 linker follows both early and late transitions

Except for L382Anap-W434F, the QVs (figure 4.3B-E) were best fit to a two-transition Boltzmann relation, reflecting the two major charge systems Q1 and Q2 [23]. There were subtle differences among the FVs of TMR and Anap and the QV. In fact, by comparing the midpoint values of Q1, Q2 and the FVs of the three C-terminal S4-S5 linker mutants, it is tempting to conclude that Anap follows Q2, while TMR is closer to Q1 (table 1). However, we would have to separate both charge movements to determine whether these subtle differences are significant. To this end, we inserted the F290A mutation into the R387Anap and K390Anap background.

F290 is situated in the S2 helix where it stabilizes the voltage sensor in the activated state, presumably by controlling the transfer of the fourth gating charge [24 , 25]. When mutated from phenylalanine to alanine, the early gating transitions remain nearly unaffected while the final transitions shift to higher potentials. In agreement with WT-F290A channels [25], the GV curve was shifted to higher potentials when F290A was inserted into R387Anap and K390Anap (*open black circles*, figure 4.6C-D) with GV midpoint values of 134.8 mV and 95.5 mV, respectively (table 2).

	Anap FV				QV				GV (no W434F)		
	$V_{1/2\,(1)}$	$dV_{(1)}$	$V_{1/2\,(2)}$	$dV_{(2)}$	$V_{1/2\,(1)}$	$dV_{(1)}$	$V_{1/2\,(2)}$	$dV_{(2)}$	$V_{1/2}$	dV	n
F290A-R387Anap-W434F	-28.0 ±5.1	12.2 ±3.4	73.9 ±7.1	21.0 ±6.5	-40.3 ±0.3	11.2 ±0.3	129.9 ±6.4	28.0 ±2.9	134.8 ±2.7	15.5 ±1.0	5
F290A-K390Anap-W434F	-48.9 ±0.7	10.9 ±0.7	70.7 ±3.4	21.4 ±3.0	-58.0 ±0.3	9.8 ±0.2	79.2 ±1.7	10.7 ±1.5	95.5 ±1.2	19.4 ±0.8	4

Table 2 $V_{1/2}$ and dV values obtained from single or double Boltzman fits of FV, QV and GV curves of F290A mutants.

In the W434F background, wildtype (F290A-W434F) and both mutants, R387Anap-F290A-W434F and K390Anap-F290A-W434F, exhibited a biphasic QV in which ~ 20% of the charge activated at higher potentials (figure 4.6A-B) [24]. The second charge movement developed in the voltage range of channel opening with Q2 (table 2). The Anap FV also split into two components (figure 4.6C-D). The first component (F1) remained shifted by 10-12 mV to potentials more depolarized than Q1 , whereas the second component (F2) developed in the voltage range of Q2. The slight shift between Q2 and F2 is caused by the shift of the off-gating currents versus the on-gating currents [18]. The Q2 had to be obtained from off-gating currents because the oocytes exhibit endogenous K^+ currents at potentials more positive than +50 mV [26, 27] (*black arrows*, figure 6A-B), making it challenging to determine the displaced charge during depolarization more

positive than +50 mV. The F290A data show that the C-terminal part of the S4-S5 linker rearranges at least twice during activation. The first rearrangement occurs with a voltage dependence falling between Q1 and Q2, and the second rearrangement coincided with Q2.

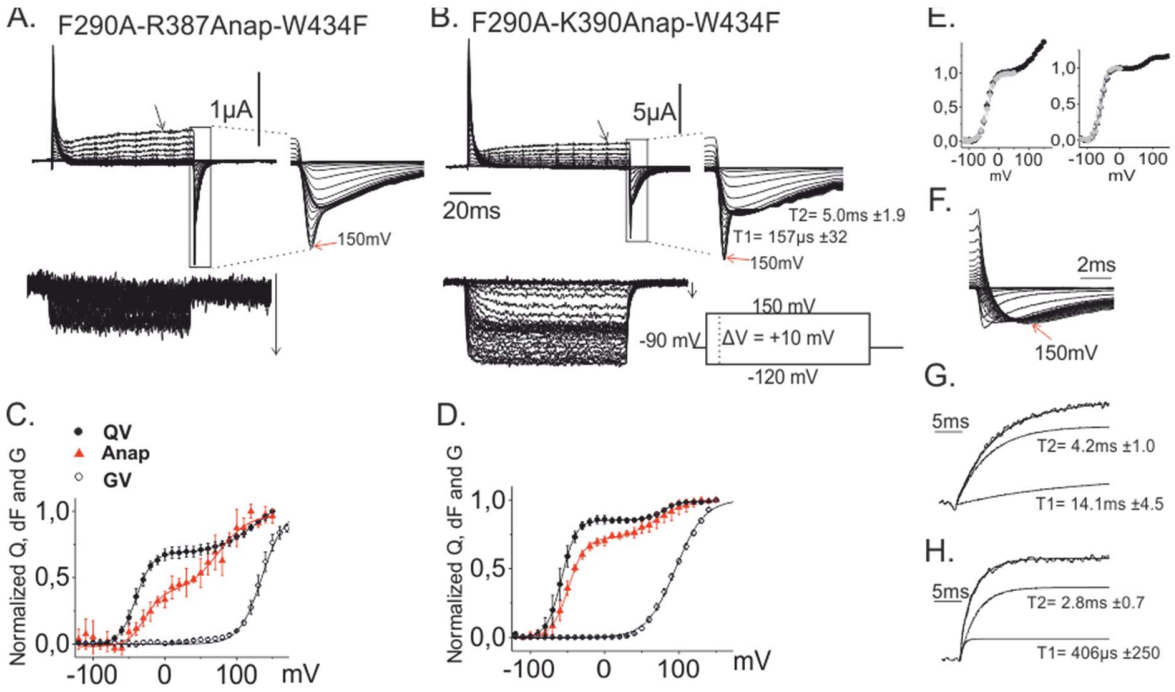

Figure 4.6 Separation of the final gating transition using F290A
A-B) Gating currents (upper) and Anap fluorescence changes (lower). The arrows highlight endogenous leak currents during high depolarisations. C-D) Anap FV and QV for C) F290A-R387Anap-W434F and D) F290A-K390Anap-W434F plotted together with the GV obtained from the respective conducting mutants. E) QV_{on} (grey) and QV_{off} (black) obtained from the gating currents in A) and B), respectively. F) Off-gating currents from R387Anap-W434F channels highlighting the slow component when repolarising from high potentials, as in contrast to the fast component present in F290A channels. G-H) Anap fluorescence of G) K390Anap-W434F and H) F290A-K390Anap-W434F upon repolarisation from 120mV to -90mV, fitted to a double exponential relation. The two components of the fit, T1 and T2, are shown as lines. Insertion of F290A accelerated the slow time constant from 14.1ms to a fast time constant of 406µs.

4.3.6 Kinetical analysis of F290A deactivation

The off-gating currents exhibited a remarkably fast component (with a time constant T1 of 157 µs ±32 µs in F290A-K390Anap-W434F, *red arrow* figure 4.6A-B) which was absent in channels without the F290A mutation (figure 4.6F). The same fast component also occurred in WT-F290A-W434F channels (figure S4.3A). The fast kinetics only developed upon repolarization from high potentials, and could be isolated from the slow kinetics by repolarizing to 0 mV instead of -90 mV (figure S4.3B). Moreover, as the fast component was only visible upon repolarization and not upon depolarization, it is the rate-limiting step only during deactivation. The QV curve of the off-

gating currents obtained from 0 mV holding potential overlapped with that of Q2 obtained at -90 mV holding potential (figure S4.3C). These findings suggest that the return of the final gating charge is accelerated in F290A channels. Deactivation currents in F290A channels were previously also found to dramatically accelerate the deactivation currents as determined from weighted time constants [24]. This finding led the authors to conclude that F290A destabilize the active state due to a diminution of the deactivation energy barrier [28]. Here, we demonstrate that the fast component caused by F290A is clearly visible in the off-gating currents and results in an isolated peak which develops in the µs-range.

In the absence of F290A, the fluorescence time course of K390Anap-W434F channels during repolarization to -90 mV was fitted to two exponential components with the time constants T1 and T2 (figure 4.6G). In the presence of F290A, the fluorescence time course was also fitted to two exponentials, but T1 was significantly faster with a time constant of 0.4 ms ± 0.25 ms, which is in the same range as the fast component in corresponding off-gating currents. Moreover, the other time constant (T2) of 2.8 ms ± 0.7 ms corresponded to T2 in the off-gating current of 5.0 ms ± 1.9 ms (figure 4.6H and B). These data suggest that Anap reports on both the rate-limiting and the subsequent step during deactivation, which is in agreement with the findings of the previous section, that Anap in the S4-S5 C-terminal linker probes both early and final gating transitions.

4.4 Model for the cytosolic gating machinery

In this study, the fluorescent unnatural amino acid Anap was site-specifically incorporated into various positions in the S4-S5 linker of the Shaker channel. Two-color voltage clamp fluorometry was used for detection of voltage-gated fluorescence changes, allowing the dynamical study of protein rearrangements from two regions in the same protein simultaneously. Anap was successfully inserted into both the N-terminal part (L382) and the C-terminal part (R387, K390, A391) of the S4-S5 linker. In a previous work, we already studied the movement of the cytosolic end of the VSD (V234Anap) and pore opening (H486Anap) [9]. By combining these results, we are now in a position to follow the progression of the voltage-gated rearrangements throughout the voltage-gated K^+ channel Shaker: the extracellular end of the VSD (A359C-TMRM), the cytosolic end of the VSD (V234Anap), the N- and C-termini of the S4-S5 linker (L382Anap, R387Anap, K390Anap, A391Anap) and the cytosolic pore gate (H486Anap).

We found that the VSD moves independently coinciding with the gating charge movement. The cytosolic end of VSD moves faster than the external surface but they share their voltage dependence[9]. Here, we found that the N-terminus of the S4-S5 linker also follows the gating charge movement. The C-terminus of the S4-S5 linker, in contrast, moves at potentials intermediate between gating charge movement and pore opening (figure 4.2). The difference in movement of the N- and C-termini indicate that, due to flexibility between L382 and R387, energy is briefly stored in this region until the S4-S5 linker responds by relaxing into its final state. The S4-S5 linker thus constitutes the transition between the independently acting voltage sensors and the cooperative pore opening step.

Pore opening, monitored at H486, occurred in two steps, one of which also precedes conduction (GV) [9]. The sequence of events would thus begin with VSD activation and S4-S5 linker bending. This is followed by "tension" or energy relief in the S4-S5 linker and preactivation of the pore, and finally pore opening and C-type inactivation. While the essential step of C-type inactivation occurs in the selectivity filter [29], it has been shown to interact with the cytosolic pore gate at the helical bundlecrossing [30]. We found accordingly rearrangements correlating with C-type inactivation in both the N- and C-terminal end of the S4-S5 linker (figure 4.2) and the S4 (V234Anap) [9]. We therefore verified the rearrangements at the helical bundlecrossing at H486Anap and found, indeed, a slow fluorescence change correlating with entry into C-type inactivation upon prolonged depolarization (figure 4.7). C-type inactivation thus leads to conformational changes in the cytosolic pore gate, the entire S4-S5 linker and the VSD.

The question remains whether the sequence of events is fixed or whether it may be exchanged, in other words, what is the driving force? In the presence of the W434F mutation, Shaker C-type inactivation was shown to be significantly increased [22]. Here, we found that there is no shift between voltage sensor movement and S4-S5 linker rearrangements anymore (figure 4.3). However, the S4-S5 linker rearrangements are temporally delayed versus the voltage sensor movement, indicating that they do occur subsequently. In contrast, the movement of the cytosolic pore gate (H486) is not affected by W434F and still shows two transitions that occur at potentials more depolarized than gating charge movement [9]. These results suggest that the S4-S5 linker is no longer hindered to directly enter its final conformation, and that it induces no change in pore gate opening.

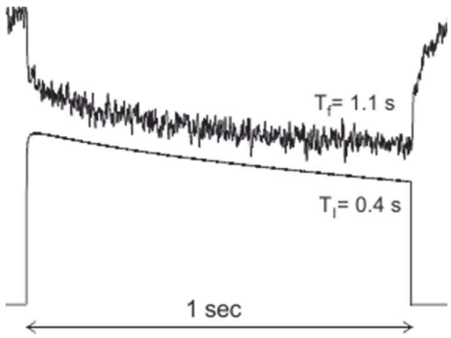

Figure 4.7 C-type inactivation of H486Anap
Current and fluorescence change elicited upon a 1 sec depolarization from -90 mV to +100 mV to induce C-type inactivation in H486Anap channels. The slow time constant in both signals was obtained by fitting with a single exponential function.

4.5 Discussion

Our findings provide us with a detailed picture about the rearrangements following membrane depolarization in voltage-gated K^+ channels including the voltage sensing domain, S4-S5 linker and cytosolic pore gate. Temporally correlating the signals with electrical signals from gating charge movement and ion conduction allowed us to establish a sequence of events.

It was remarkable that the C-terminal S4-S5 linker and the cytosolic pore gate react differently to the presence of W434F. While the S4-S5 linker is free to move with the voltage sensor in W434F, the cytosolic pore gate still opens at more depolarized potentials. Our data suggest that in spite of an uncoupling of S4-S5 linker movement from S6 movement in the presence of W434F, the channel still opens normally. This seems to contradict our current understanding of electromechanical coupling, according to which the annealing of the S4-S5 linker and the complementary C-terminal S6 leads to coinciding movements [10, 13, 18, 31-33]. A mechanism similar to what we see here, where uncoupling of the S4-S5 linker from S6 is linked to pore inactivation has been suggested for closed state inactivation in Kv4 channels [34], and it will thus be interesting to investigate S4-S5 linker movement in Kv4 as well as the fast inactivating Herg channels.

An interesting feature in the C-terminal S4-S5 linker rearrangements was that we still observed a slow conformational change even in the presence of W434F. This component was sensitive to 4-AP but occurred at potentials more depolarized than pore opening. It might be an indication that

the S4-S5 linker, in spite not entering a "strained" state in presence of W434F, only enters its final state after pore opening.

By breaking down the sequence of molecular events during protein conformational changes, we can shed light on the underlying energies and forces and get closer to the ultimate goal of understanding protein structure and function. Fluorescence spectroscopy remains today a valuable tool to investigate protein dynamics in living cells and with the use of fluorescent unnatural amino acids, the VCF technique will likely continue to add cutting-edge information to the field in the future. We think that our findings in the Shaker K^+ channel can be applied to a wide range of members of the voltage-gated ion channel family.

4.6 Methods and Materials

4.6.1 Xenopus oocyte injection

All mutations were introduced into the *Drosophila* Shaker H4 gene in the pBSTA vector with a deletion of amino acids 6-46 to remove N-type inactivation[14]. For Anap incorporation, 9.2nl of 0.1 ng/nL cDNA encoding the tRNA/AnapRS pair (pAnap)[9, 17] was injected into the nucleus of *Xenopus laevis* oocytes 6-24 hours prior to coinjection of 23 nL 1mM Anap (Abzena TCRS, custom synthesis TCRS-170) and 35ng *in vitro* transcribed RNA. All steps during and after Anap injection were performed under red light to avoid bleaching. Oocytes were then incubated for 1-3 days at 18°C in Barth's solution supplemented with 5% horse serum.

4.6.2 Electrophysiology

Voltage clamp was performed with a CA-1B amplifier (Dagan). Currents were recorded in the cut-open oocyte voltage-clamp configuration as described [18] and analyzed by using GPatch (Department of Anesthesiology, University of California, Los Angeles). Linear capacitance currents were subtracted online using the P/4 protocol[35], or offline using a negative pulse from -100mV to -120mV (F290A mutants). For ionic recordings the external solution contained in mM: 5 KOH, 110 NMDG, 10 Hepes, and 2 $Ca(OH)_2$, and the internal solution contained in mM: 115 KOH, 10 Hepes, and 2 EDTA. For gating current recordings, KOH was replaced by NMDG. For blocking experiments, 5mM NMDG or KOH was replaced by 5mM 4-aminopyridine (4-AP), and the command potential was held at 0 mV for 5 seconds prior to recordings. All solutions were

adjusted to pH 7.1 with methane sulfonic acid (MES). Conductance (G) was calculated from the steady state currents (I) via $G=I/(V-V_{rev})$, where V_{rev} is the reversal potential. Conductance-voltage relationships (GV) were fitted to a Boltzmann relation of the form $G/G_{max} = (1 + \exp(-(V - V_{1/2})/dV))^{-1}$. The total gating charge (Q) was calculated from the gating currents by integration, and charge-voltage relationships (QV) where fitted to a double-Boltzmann relation of the form $Q/Q_{max} = (1 + \exp(-(V - V_{1,1/2})/dV_1))^{-1} + (1 + \exp(-(V - V_{2,1/2})/dV_2))^{-1}$.

4.6.3 Voltage clamp fluorometry

For two-color VCF, oocytes were incubated in 5µM TMR-maleimide in depolarizing labeling solution (in mM: 115 KOH, 10 Hepes, and 2 $Ca(OH)_2$, pH 7.1 with MES) for 20 minutes at room temperature, prior to recordings. The oocytes were washed three times in labelling solution to remove excess dye. Fluorescence intensities were recorded with a photodiode detection system (Photomax 200, Dagan) using ex-545/25, dc-570, em-605/70 (TMR) or ex-377/50, dc-409, em-470/40 (Anap) filter sets. Fluorescence-voltage (FV) relationships were fitted to a single or double Boltzmann relation of the form $dF/dF_{max} = (1 + \exp(-(V - V_{1/2})/dV))^{-1}$ and $dF/dF_{max} = (1 + \exp(-(V - V_{1,1/2})/dV_1))^{-1} + (1 + \exp(-(V - V_{2,1/2})/dV_2))^{-1}$, respectively. Bleaching effects during step protocols were accounted for by scaling fluorescence traces using the first sweep as reference. See Kalstrup & Blunck 2017[36] for visual demonstration of two-color VCF.

4.7 Acknowledgements

This work was funded by the Canadian Institutes for Health Research Grants MOP-102689 and MOP-136894 (to R.B.) and Canadian Foundation for Innovation Grant 950-225005. We thank Mireille Marsolais for help on mutant preparation.

4.8 Supplementary Material

Effect of iVSD on full length channels and potential heteromerization.

The voltage range in which iVSD conducts is opposite to that of full length channels, allowing separation of the two current phenotypes when they express in the same oocyte (figure S4.1D). However, oocytes never exhibited high expression of both phenotypes simultaneously, but generally showed high full length with little or no iVSD, and vice versa. This observation can be

explained by two scenarios. Either the full length and iVSD synthesis are competing for the translation capacity of the oocyte, or the full length and iVSD assemble into functionally silent heterotetramers. The latter scenario will be discussed below.

Next, to see whether iVSD affected the gating machinery of full length channels, expression of both full length channels and iVSD were induced by mixing WT Shaker mRNA with and without K390stop in a 1:1 ratio (in the absence of pAnap and Anap). Also, A359C which is situated on the extracellular part of S4 was inserted for TMR-labeling to probe the voltage sensor movement[37], and the W434F mutation was used in order to measure gating currents[22]. Following expression, voltage-dependent ionic currents, gating currents and fluorescence-changes were measured using standard K_V activation protocols. The oocytes exhibited outward K^+ currents upon depolarization which were indistinguishable from WT currents (figure S4.1E). If the oocytes also exhibited inward iVSD currents upon hyperpolarisation they were similar to the currents of iVSD-only oocytes shown in figure S4.1A. These findings indicate that the two current phenotypes are functionally independent. In agreement with this, the conductance-voltage (GV), charge-voltage (QV) and fluorescence-voltage (FV) relationships of the full length population were identical to those obtained from oocytes injected only with WT (figure S4.1F). When the iVSD current amplitude was too significant, the full length recordings were impaired due to current run-down, low membrane resting potential and leaky oocytes. The maximum iVSD current amplitude at which full length currents could be reliably measured was estimated to be 10 µA when pulsing from a holding potential of 0 mV to -170 mV. Fortunately, iVSD rarely expressed above 10 µA when Anap was succesfully incorporated (figure S4.1C). Taken together, these results show that the gating machinery of full length channels (VS movement, charge displacement, pore opening) remained unaffected by the presence of iVSD

.

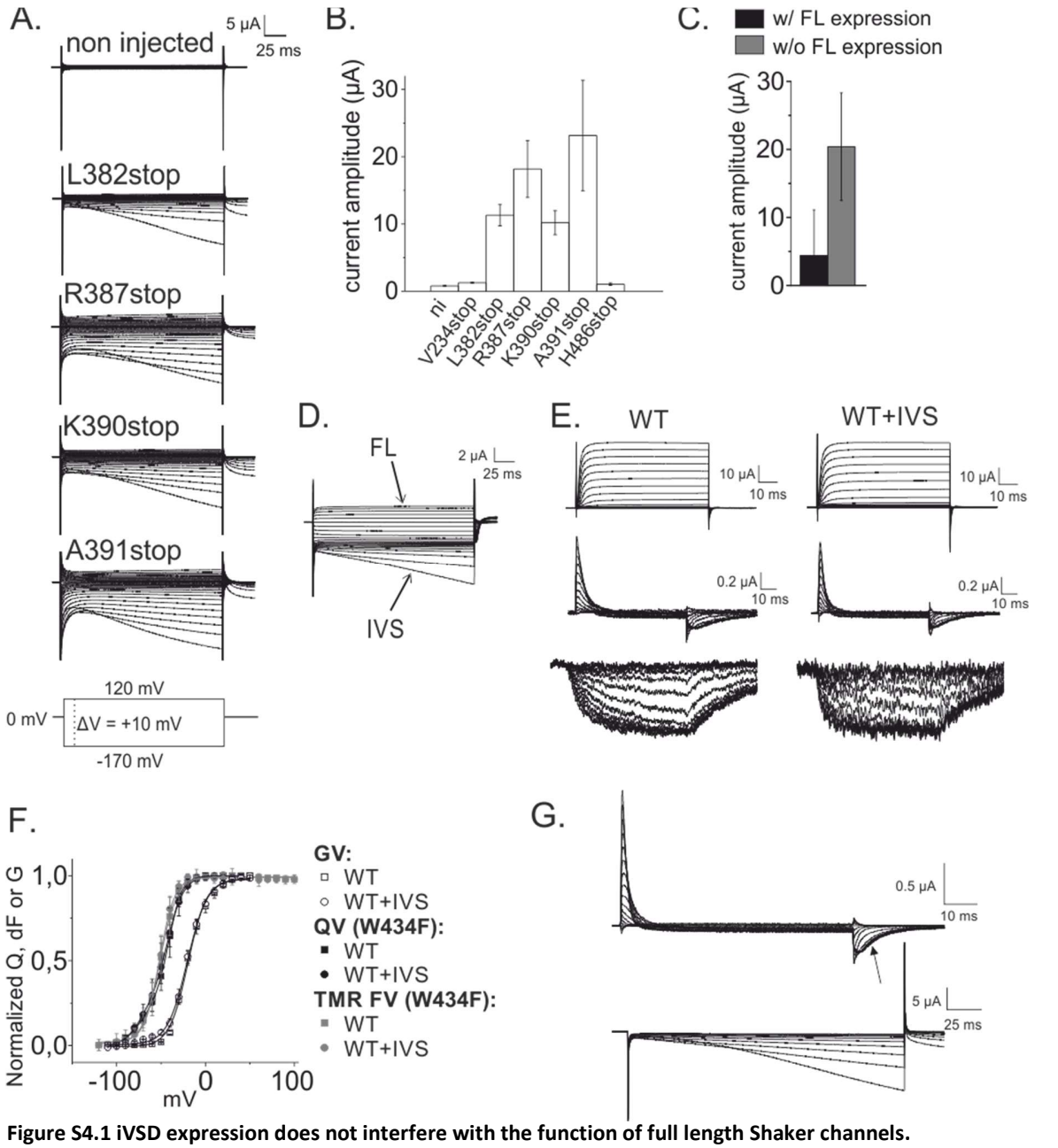

Figure S4.1 iVSD expression does not interfere with the function of full length Shaker channels.
A) Examples of oocytes expressing iVSD two days after RNA injection, as a result of translation stop in the S4-S5 linker at position L382, R387, K390 or A391. B) Demonstration of the amount of iVSD expression, shown as recorded current amplitude, upon hyperpolarisation from 0 mV to -170 mV. No iVSD currents are detected when the stop codon is placed in S1 (V234) or in the S6 (H486). C) For experiments with Anap and pAnap using R387stop, oocytes were placed in two groups regarding the presence or absence of full length ionic currents detected during a standard K_V activation protocol. Then, the amount of iVSD (if any) was determined as in B). D) Example of an oocyte which has been injected with K390stop in presence of Anap and pAnap, and expresses both full length and iVSD. Currents were activated as in A. E) Ionic currents, gating currents and TMR fluorescence changes of WT-only and WT+K390stop oocytes. F) QV, TMR-FV and GV of WT A359C channels compared to those of WT A359C channels in the presence of limited iVSD expression (less than 10 µA).

If full length and iVSD subunits were to express as stable and mature heterotetramers at the membrane, the channel complex would either form an obstructed constitutively open pore with little or no voltage dependency and with no ion-selectivity, or be constitutively closed by virtue of an absent pore. The findings that the oocytes which expressed a mixed population exhibited two current phenotypes reminiscent of the sum of WT full length and WT iVSD channels (figure S4.1D), argues against the possibilty of a conductive heteromeric channel. Therefore, if heteromerization occurs, it would be as a non-conducting channel, possibly with iVSD gating pore currents.

The N-terminal T1 domains in Shaker-like K_V channels are responsible for initial assembly of the subunits [38, 39], while other interactions are responsible for subsequent channel assembly and folding, including the C-terminal portion and intersubunit interactions provided by the transmembrane helices from S1 to S6 [40-42]. Some of these intersubunit transmembrane interactions would be impaired in a heterotetramer of iVSD and full length, and it is therefore likely that the four subunits fold independently, although they are brought together as tetramers. By virtue of the independent nature of the VSD, it is possible that in such a heterotetramer, the iVSD subunits would function normally and the full length subunits would exhibit gating currents. However, the gating currents originating from full length subunits in heterotetramers would be different from WT gating currents and lack the slow component in the off-gating currents which reflects the stabilization of the open pore[43] caused by intersubunit interactions between the S4-S5 linker and S6[14] and has been linked to C-type inactivation[44]. Since all three mechanisms necessitate the presence of S5 and S6, the slow component would be absent in gating currents originating from full length subunits in heterotetramers. However, the gating currents elicited by oocytes which expressed both iVSD currents and full length gating currents exhibited a slow component in the off-gating current – reminiscent of a functional pore (figure S4.1G). Moreover, the four S4-S5 linker Anap-mutants also exhibited the slow component (figure 4.3A). We conclude that no evidence existed for heterotetramerization. Taken together, the results show that experiments with incorporation of Anap into the S4-S5 linker are not compromised by iVSD (if any). In agreement with this conclusion, Anap fluorescence changes were indeed not affected by the presence of IVS, even above the IVS limit of 10 μA (figure S4.2A-B).

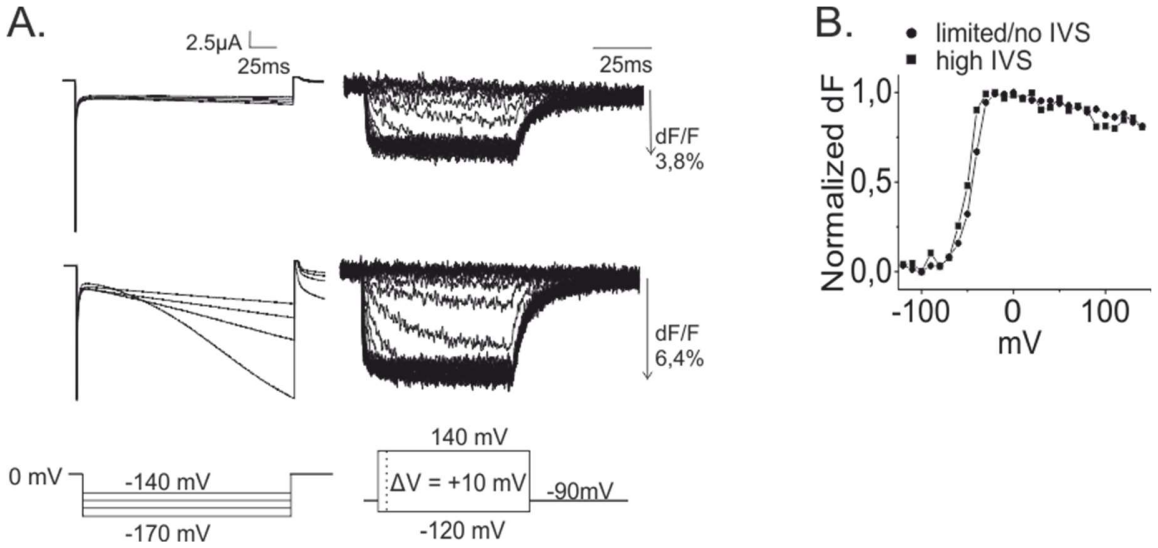

Figure S4.2 Supplementary figure 2. Anap fluorescence in K390Anap oocytes is not affected by iVSD
A) A K390Anap-expressing oocyte with limited iVSD expression compared to a K390Anap-expressing oocyte with high iVSD expression, and to the right is shown Anap fluorescence changes during standard Shaker activation protocol of the same oocyte. B) Anap FV curves obtained from the oocytes in A.

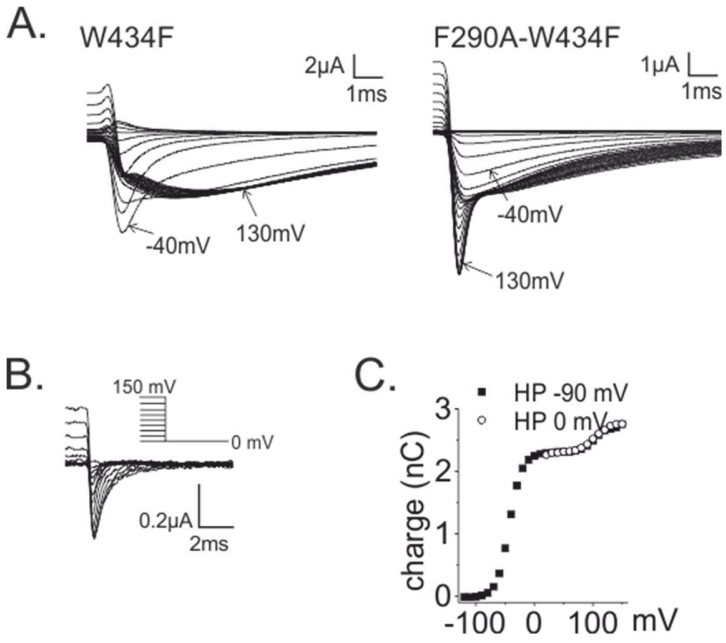

Figure S4.3 Characterization of the final gating transition separated by F290A.
A) Off-gating currents in WT-W434F compared to W434F-F290A. B) Visualization of the fast component separated from the slow component by repolarizing to 0mV in F290A-K390Anap-W434F. C) Charge displacement obtained from the gating currents in B) overlapped with those obtained during repolarization to -90 mV.

4.9 References

1. Wulff, H., N.A. Castle, and L.A. Pardo, *Voltage-gated potassium channels as therapeutic targets.* Nat Rev Drug Discov, 2009. **8**(12): p. 982-1001.
2. Long, S.B., E.B. Campbell, and R. Mackinnon, *Crystal structure of a mammalian voltage-dependent Shaker family K+ channel.* Science, 2005. **309**(5736): p. 897-903.
3. Long, S.B., X. Tao, E.B. Campbell, and R. MacKinnon, *Atomic structure of a voltage-dependent K+ channel in a lipid membrane-like environment.* Nature, 2007. **450**(7168): p. 376-82.
4. Bezanilla, F., *How membrane proteins sense voltage.* Nat Rev Mol Cell Biol, 2008. **9**(4): p. 323-32.
5. Blunck, R. and Z. Batulan, *Mechanism of electromechanical coupling in voltage-gated potassium channels.* Front Pharmacol, 2012. **3**: p. 166.
6. Chowdhury, S. and B. Chanda, *Perspectives on: conformational coupling in ion channels: thermodynamics of electromechanical coupling in voltage-gated ion channels.* J Gen Physiol, 2012. **140**(6): p. 613-23.
7. Pathak, M., L. Kurtz, F. Tombola, and E. Isacoff, *The cooperative voltage sensor motion that gates a potassium channel.* J Gen Physiol, 2005. **125**(1): p. 57-69.
8. Mannuzzu, L.M. and E.Y. Isacoff, *Independence and cooperativity in rearrangements of a potassium channel voltage sensor revealed by single subunit fluorescence.* J Gen Physiol, 2000. **115**(3): p. 257-68.
9. Kalstrup, T. and R. Blunck, *Dynamics of internal pore opening in K(V) channels probed by a fluorescent unnatural amino acid.* Proc Natl Acad Sci U S A, 2013. **110**(20): p. 8272-7.
10. Labro, A.J., A.L. Raes, A. Grottesi, D. Van Hoorick, M.S. Sansom, and D.J. Snyders, *Kv channel gating requires a compatible S4-S5 linker and bottom part of S6, constrained by non-interacting residues.* J Gen Physiol, 2008. **132**(6): p. 667-80.
11. Long, S.B., E.B. Campbell, and R. Mackinnon, *Voltage sensor of Kv1.2: structural basis of electromechanical coupling.* Science, 2005. **309**(5736): p. 903-8.
12. Labro, A.J., A.L. Raes, and D.J. Snyders, *Coupling of voltage sensing to channel opening reflects intrasubunit interactions in kv channels.* J Gen Physiol, 2005. **125**(1): p. 71-80.
13. Lu, Z., A.M. Klem, and Y. Ramu, *Coupling between voltage sensors and activation gate in voltage-gated K+ channels.* J Gen Physiol, 2002. **120**(5): p. 663-76.
14. Batulan, Z., G.A. Haddad, and R. Blunck, *An intersubunit interaction between S4-S5 linker and S6 is responsible for the slow off-gating component in Shaker K+ channels.* J Biol Chem, 2010. **285**(18): p. 14005-19.
15. Faure, E., G. Starek, H. McGuire, S. Berneche, and R. Blunck, *A limited 4 A radial displacement of the S4-S5 linker is sufficient for internal gate closing in Kv channels.* J Biol Chem, 2012. **287**(47): p. 40091-8.
16. Lee, H.S., J. Guo, E.A. Lemke, R.D. Dimla, and P.G. Schultz, *Genetic incorporation of a small, environmentally sensitive, fluorescent probe into proteins in Saccharomyces cerevisiae.* J Am Chem Soc, 2009. **131**(36): p. 12921-3.
17. Chatterjee, A., J. Guo, H.S. Lee, and P.G. Schultz, *A genetically encoded fluorescent probe in mammalian cells.* J Am Chem Soc, 2013. **135**(34): p. 12540-3.
18. Haddad, G.A. and R. Blunck, *Mode shift of the voltage sensors in Shaker K+ channels is caused by energetic coupling to the pore domain.* J Gen Physiol, 2011. **137**(5): p. 455-72.
19. Zhao, J. and R. Blunck, *The isolated voltage sensing domain of the Shaker potassium channel forms a voltage-gated cation channel.* Elife, 2016. **5**.

20. Hurst, R.S., M.J. Roux, L. Toro, and E. Stefani, *External barium influences the gating charge movement of Shaker potassium channels.* Biophys J, 1997. **72**(1): p. 77-84.
21. Claydon, T.W., M. Vaid, S. Rezazadeh, S.J. Kehl, and D. Fedida, *4-aminopyridine prevents the conformational changes associated with p/c-type inactivation in shaker channels.* J Pharmacol Exp Ther, 2007. **320**(1): p. 162-72.
22. Yang, Y., Y. Yan, and F.J. Sigworth, *How does the W434F mutation block current in Shaker potassium channels?* J Gen Physiol, 1997. **109**(6): p. 779-89.
23. Bezanilla, F., E. Perozo, and E. Stefani, *Gating of Shaker K+ channels: II. The components of gating currents and a model of channel activation.* Biophys J, 1994. **66**(4): p. 1011-21.
24. Lacroix, J.J. and F. Bezanilla, *Control of a final gating charge transition by a hydrophobic residue in the S2 segment of a K+ channel voltage sensor.* Proc Natl Acad Sci U S A, 2011. **108**(16): p. 6444-9.
25. Tao, X., A. Lee, W. Limapichat, D.A. Dougherty, and R. MacKinnon, *A gating charge transfer center in voltage sensors.* Science, 2010. **328**(5974): p. 67-73.
26. Parker, I. and I. Ivorra, *A slowly inactivating potassium current in native oocytes of Xenopus laevis.* Proc R Soc Lond B Biol Sci, 1990. **238**(1293): p. 369-81.
27. Lu, L., C. Montrose-Rafizadeh, T.C. Hwang, and W.B. Guggino, *A delayed rectifier potassium current in Xenopus oocytes.* Biophys J, 1990. **57**(6): p. 1117-23.
28. Lacroix, J.J., H.C. Hyde, F.V. Campos, and F. Bezanilla, *Moving gating charges through the gating pore in a Kv channel voltage sensor.* Proc Natl Acad Sci U S A, 2014. **111**(19): p. E1950-9.
29. Berneche, S. and B. Roux, *A gate in the selectivity filter of potassium channels.* Structure, 2005. **13**(4): p. 591-600.
30. Cuello, L.G., et al., *Structural basis for the coupling between activation and inactivation gates in K(+) channels.* Nature, 2010. **466**(7303): p. 272-5.
31. Lu, Z., A.M. Klem, and Y. Ramu, *Ion conduction pore is conserved among potassium channels.* Nature, 2001. **413**(6858): p. 809-13.
32. Wall-Lacelle, S., M.I. Hossain, R. Sauve, R. Blunck, and L. Parent, *Double mutant cycle analysis identified a critical leucine residue in the IIS4S5 linker for the activation of the Ca(V)2.3 calcium channel.* J Biol Chem, 2011. **286**(31): p. 27197-205.
33. Muroi, Y., M. Arcisio-Miranda, S. Chowdhury, and B. Chanda, *Molecular determinants of coupling between the domain III voltage sensor and pore of a sodium channel.* Nat Struct Mol Biol, 2010. **17**(2): p. 230-7.
34. Barghaan, J. and R. Bahring, *Dynamic coupling of voltage sensor and gate involved in closed-state inactivation of kv4.2 channels.* J Gen Physiol, 2009. **133**(2): p. 205-24.
35. Bezanilla, F. and C.M. Armstrong, *Inactivation of the sodium channel. I. Sodium current experiments.* J Gen Physiol, 1977. **70**(5): p. 549-66.
36. Kalstrup, T. and R. Blunck, *Voltage-clamp Fluorometry in Xenopus Oocytes Using Fluorescent Unnatural Amino Acids.* J Vis Exp, 2017(123).
37. Mannuzzu, L.M., M.M. Moronne, and E.Y. Isacoff, *Direct physical measure of conformational rearrangement underlying potassium channel gating.* Science, 1996. **271**(5246): p. 213-6.
38. Shen, N.V., X. Chen, M.M. Boyer, and P.J. Pfaffinger, *Deletion analysis of K+ channel assembly.* Neuron, 1993. **11**(1): p. 67-76.
39. Li, M., Y.N. Jan, and L.Y. Jan, *Specification of subunit assembly by the hydrophilic amino-terminal domain of the Shaker potassium channel.* Science, 1992. **257**(5074): p. 1225-30.
40. Raja, M., *The role of extramembranous cytoplasmic termini in assembly and stability of the tetrameric K(+)-channel KcsA.* J Membr Biol, 2010. **235**(1): p. 51-61.

41. Tu, L., V. Santarelli, Z. Sheng, W. Skach, D. Pain, and C. Deutsch, *Voltage-gated K+ channels contain multiple intersubunit association sites.* J Biol Chem, 1996. **271**(31): p. 18904-11.
42. Jenke, M., A. Sanchez, F. Monje, W. Stuhmer, R.M. Weseloh, and L.A. Pardo, *C-terminal domains implicated in the functional surface expression of potassium channels.* EMBO J, 2003. **22**(3): p. 395-403.
43. Kanevsky, M. and R.W. Aldrich, *Determinants of voltage-dependent gating and open-state stability in the S5 segment of Shaker potassium channels.* J Gen Physiol, 1999. **114**(2): p. 215-42.
44. Chen, F.S., D. Steele, and D. Fedida, *Allosteric effects of permeating cations on gating currents during K+ channel deactivation.* J Gen Physiol, 1997. **110**(2): p. 87-100.

Chapter 5

Probing dynamics of the ball and chain in K_V channels during N-type inactivation

Tanja Kalstrup[1] and Rikard Blunck[1,2]

[1]Department of Physiology and Pharmacology, and [2]Department of Physics, Montreal University, Montreal, Quebec, Canada

Unpublished.

Author contributions: T.K. and R.B. designed research, T.K. performed experiments, T.K. and R.B. analyzed data, T.K. wrote the first version which was edited by R.B.

5.1 Abstract

N-type inactivation is a mechanism in certain voltage-gated potassium channels where the N-terminal cytosolic inactivation particle (IP) binds to the open pore, resulting in block of ionic currents (ball-and-chain mechanism). Such regulation of K^+ currents balances the excitability of neurons. Numerous mutational studies have characterized N-type inactivation functionally, while X-ray crystal structures have yet to include the ball-and-chain structure. By incorporating a fluorescent unnatural amino acid (Anap) into the N-terminus and into a receptor site (T1 window), we tracked the movement of the IP during inactivation using voltage clamp fluorometry in Xenopus oocytes. The findings suggest a sequential-step model in which the chain region undergoes a movement which precedes occlusion of the pore, whereas the hydrophobic tip undergoes an additional movement which causes the final pore block. Moreover, a receptor site in the T1-S1 linker experiences relative movements which corresponds to that of the chain region, affirming its role in accommodating the IP close to the pore.

5.2 Introduction

When voltage-gated potassium (K_V) channels open in response to membrane depolarisation they allow the passage of K^+ ions and repolarize the cell within miliseconds during an action potential. The duration and pattern of action potentials in excitable cells can be regulated by an inactivation mechanism in which the cytosolic N-terminus binds to the open pore and blocks the entry of ions (N-type inactivation) [1-4]. The N-terminus, or the inactivation particle (IP), is either part of the transmembrane α-subunit (Shaker, K_V1.4, K_V3.4) or of the β-subunit which co-assembles with the K_V1 subfamily. The IPs of N-type inactivating channels have no sequence similarity but they all contain a hydrophobic tip region of approximately the first 10 amino acids which, in the Shaker K_V channel, have been suggested to inactivate the channel by interacting with hydrophobic pore-lining residues [3, 4]. The downstream hydrophilic region which carries a net positive charge, is responsible for increasing the diffusion rate of the IP towards the pore region via long-range electrostatic interactions [3, 5-7].

Below the transmembrane region in Shaker-related K_V1 channels is situated the conserved cytoplasmic T1 domain which is responsible for subunit tetramerization [8-10]. The T1 domain is

attached to the first transmembrane helix S1 via the T1-S1 linker, so that four windows form between the T1 domain and the transmembrane domain (figure 5.1A). The N-terminus enters the window of its own subunit in order to reach the inner pore cavity [11, 12]. The T1-S1 linker contains conserved negative charges important for accommodating the positively charged chain region [5, 12, 13].

Even though the mechanism of N-type inactivation is functionally well characterized, any dynamic information about the pathway by which the IP travels is lacking. By inserting a fluorescent unnatural amio acid (Anap) into the IP using the amber stop codon suppression technique [14-16], we were able to probe relative movements using voltage clamp fluorometry. This procedure allowed us to compare tip motion (A3 and Y8) and chain motion (K19 and E35). Anap was also inserted into the T1-S1 linker receptor site (E201) to probe the arrival of the IP through the T1 window.

5.3 Results

5.3.1 Anap incorporation does not inhibit N-type inactivation

In order to probe movements of the IP during N-type inactivation, Anap was inserted into selective sites in the Shaker channel via the amber codon suppression technique using the Anap-specific tRNA synthethase/tRNA (RS/tRNA) pair [14, 16]. To this end, two positions in the tip region, A3 and Y8, and two positions in the chain region, K19 and E35, were used as sites for Anap incorporation (figure 5.1A). Since N-terminal insertion of stop codon can lead to translational reinitiation at downstream start codons, nine start codons were silently mutated as previously described [17]. Anap was succesfully incorporated into the four positions as determined from the robust expression in presence of Anap and poor expression in the absence of Anap (figure 5.1B-C). All mutants exhibited functional N-type inactivation (figure 5.1B) with WT-like inactivation voltage dependencies (figure 5.1D).

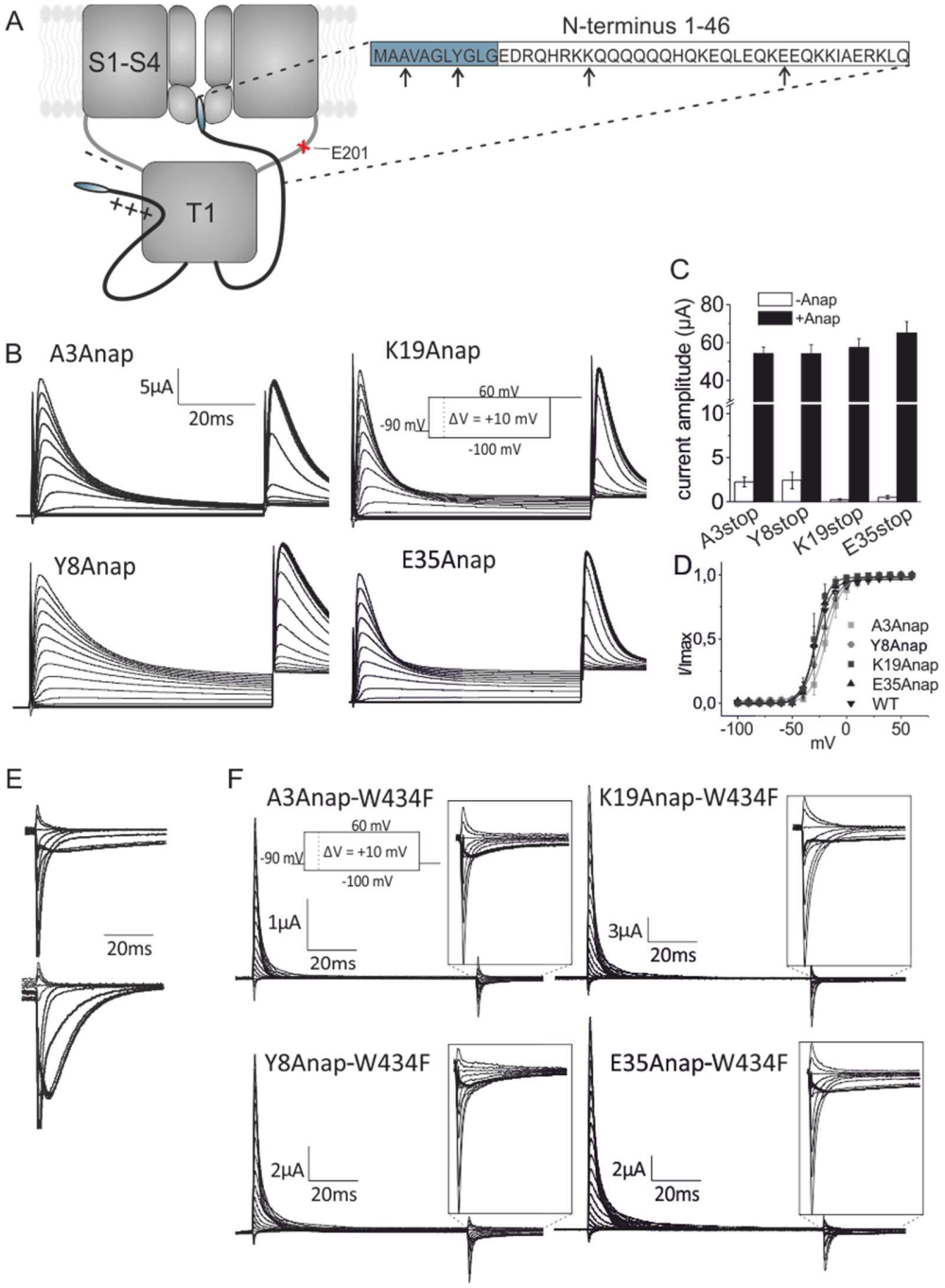

Figure 5.1 Functional expression with Anap in N-terminus
A) Cartoon of the Shaker channel inactivated by the N-terminus. Only two subunits are shown for clarity. Residues used in this study are marked arrows in the N-terminus and a red cross in the T1-S1 linker. **B)** Currents obtained from each N-terminal mutant upon a standard activation step protocol followed by a second pulse to +60 mV. **C)** Expression levels shown as current peak amplitudes upon depolarising from -90 mV to +40 mV for each mutant in the absence and presence of Anap. Adapted from Kalstrup and Blunck 2015 [17] **D)** IV curve for inactivation obtained by plotting the peak current during the second pulse in at +60 mV in C). **E)** Off-gating currents obtained with W434F in WT full length (upper) and Δ6-46 channels (lower). **F)** Gating currents obtained during a standard activation step protocol. Insets show the presence of charge immobilization.

It has previously been shown that when the IP binds to the pore in the inactivated state, the voltage sensors are unable to return to their resting state, making unbinding of the IP the rate-limiting step upon repolarisation [18]. In W434F channels, where ionic currents are blocked but the gating machinery remains normal [19], voltage sensor immobilization is visualized as a slow off-gating current during repolarisation which disappears in the Δ6-46 deletion mutant (figure 5.1E) [18]. We used this feature to verify whether the tip properly reaches the final docking site in the Anap mutants. Indeed, charge immobilization was unaffected in all mutants as shown by the presence of a slow component in the off-gating currents with a time course similar to the one found in WT (figure 5.1F). The finding that the IP reaches the final docking site agrees with the functional current phenotypes seen during N-type inactivation (figure 5.1B). These results show that the presence of Anap in the tip and the chain region did not inhibit the ability of IP to reach the pore and block the ionic currents.

5.3.2 Anap in the tip region probes final step in N-type inactivation

A3Anap and Y8Anap exhibited small voltage dependent fluorescence changes at expression levels above 50 µA when depolarising to 40 mV (supplementary figure S5.1A-B). The slow inactivation kinetics seen in figure S5.1A-B are caused by accumulation of external K^+ at dense channel population [20]. The presence of two fluorescence components of opposite direction made the analysis of A3Anap and Y8Anap challenging due to low dF/F values. In order to enhance the fluorescence signal, we therefore decided to use the non-conducting Shaker W434F mutant [21], which allows higher expression levels than the conducting channels. The fluorescence changes in W434F channels were similar to those of the conducting channels and did also exhibit two components of opposite direction (figure S5.1C-D and figure 5.2A-B, upper traces). In order to verify whether the fluorescence changes were caused by binding of the tip region to the pore, we used the K_V channel blocker 4-aminopyridine (4-AP) which inhibits the final transitions during channel activation [22-24]. Since pore opening needs to occur for the IP to reach the final docking site, we were able to identify fluorescence changes sensitive to the ability of the IP in blocking the pore. Indeed, application of 5mM 4-AP resulted in inhibition of the second fluorescence component, suggesting that the final blocking step is monitored by Anap (figure 5.2A-B, middle traces).

By subtraction of the signal in presence of 4-AP from the original signal, the slow 4-AP sensitive component was obtained (figure 5.2A-B, lower traces). Interestingly, in Y8Anap, the fluorescence time course upon repolarisation followed the slow kinetics of charge immobilization with a time constant $t_f = 73 \pm 4$ ms and $t_g = 74 \pm 2$ ms obtained from exponential fits (figure 5.2C). This indicates that the slow fluorescence component directly probes conformational changes during the final blocking step, in agreement with being sensitive to 4-AP. The 4-AP sensitive component in A3Anap was too small to confidently fit to an exponential and was therefore not analyzed kinetically. Plotting the 4-AP insensitive (fast) and 4-AP sensitive (slow) component as a function of voltage (FV) for both mutants, revealed that the voltage dependency of both components are similar to that of inactivation (figure 5.2D-E). Taken together, these results strongly suggest that Anap at position 3 and 8 in the IP probes a movement which causes the docking of the tip into the final receptor site.

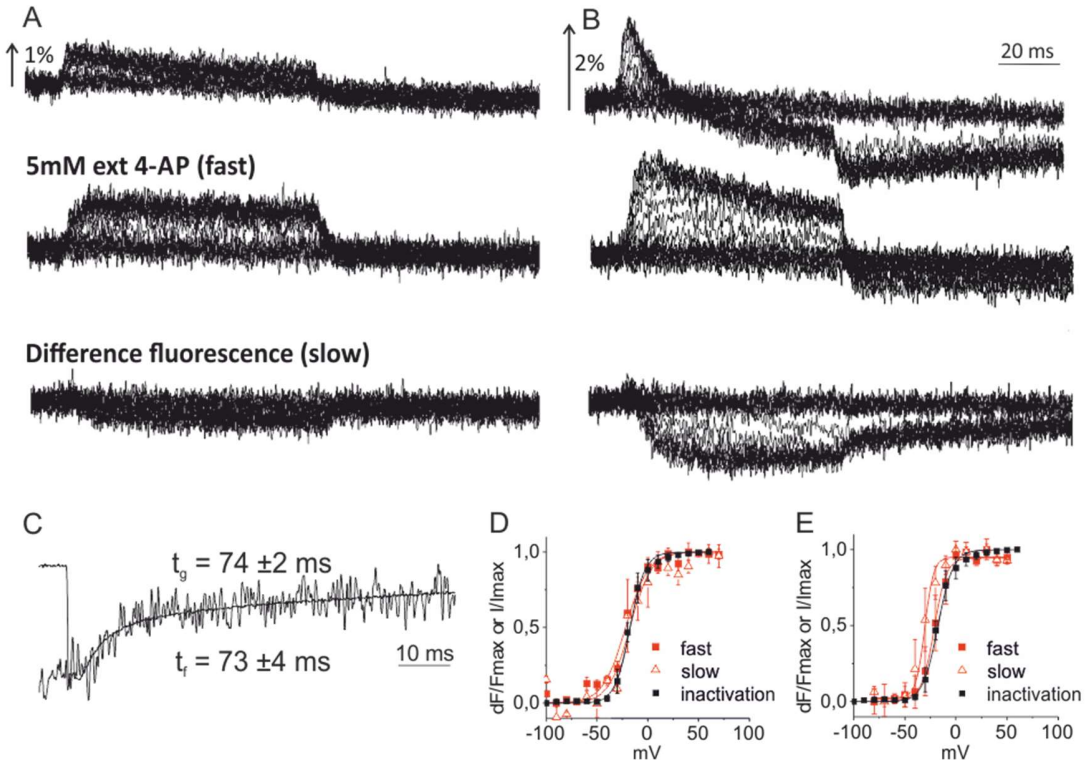

Figure 5.2 VCF results for the tip region mutants A3Anap and Y8Anap
A-B) Voltage-dependent fluorescence changes obtained during recordings of the gating currents in figure 5.1F for A3Anap-W434F A) and Y8Anap-W434F B). Middle traces are obtained in the presence of 5 mM external 4-AP, and the lower traces are the 4-AP sensitive components obtained via subtraction **C)** Overlap of Y8Anap-W434F off-gating current and fluorescence time course during repolarisation from 0 mV to -90 mV. **D-E)**

A3Anap-W434F (D) and Y8Anap-W434F (E) FV curves of the 4-AP insensitive (slow) and insensitive (fast) components plotted together with the IV of inactivation from figure 5.1D.

5.3.3 Anap in the chain region probes movements preceding final block

Next, we performed the same procedure for the chain mutants, K19Anap and E35Anap, which also required high expression levels in order to see fluorescence changes (figure 5.3A-B).

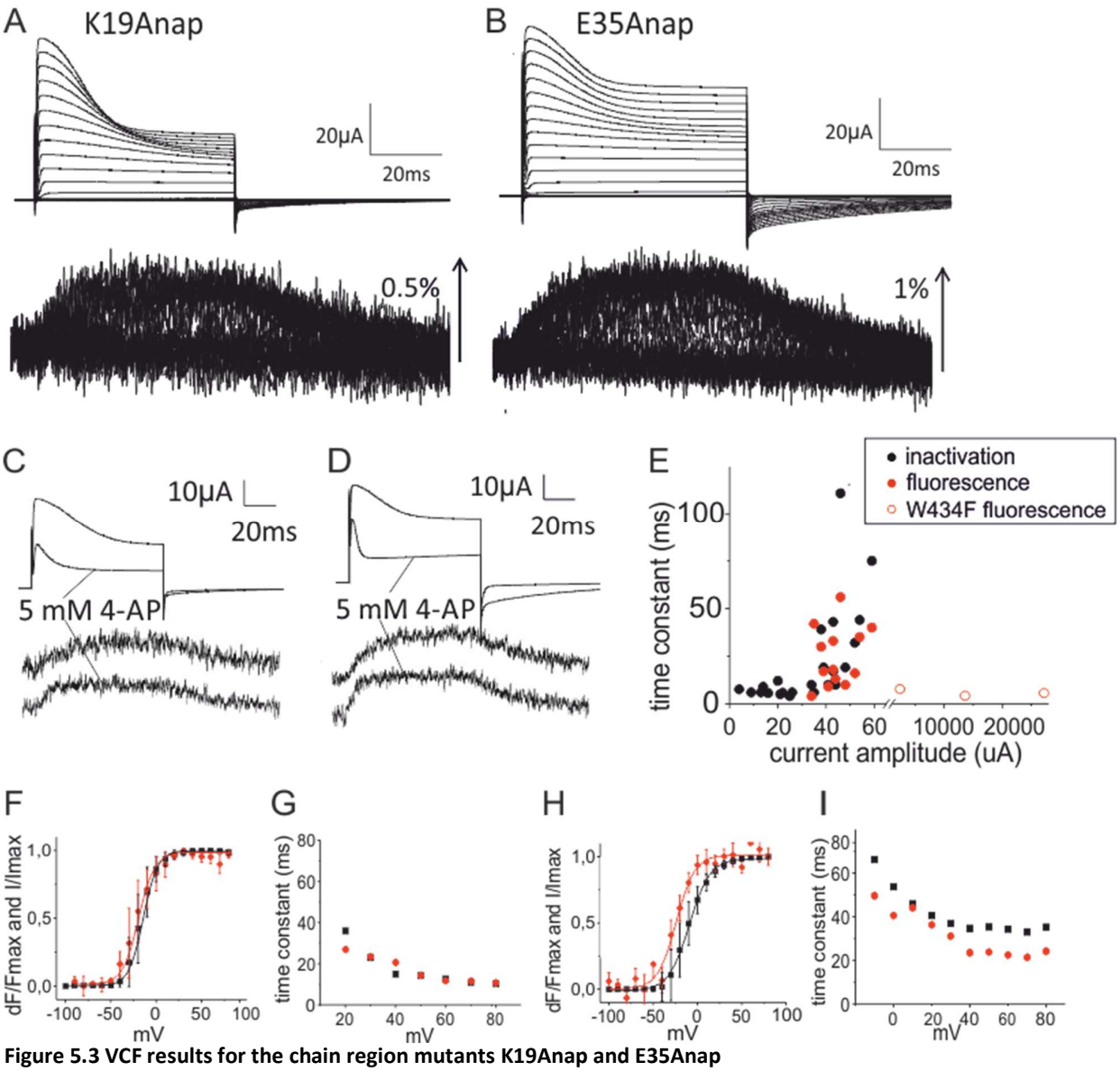

Figure 5.3 VCF results for the chain region mutants K19Anap and E35Anap
Examples of inactivating currents elicited by the chain mutants K19Anap **A)** and E35Anap **B)** and their respective fluorescence changes. **C-D)** Comparison of currents and fluorescence changes before and after application of external 4-AP during depolarisation from -90 mV to + 40 mV. **E)** Time constants obtained from exponential fits of E35Anap current inactivation and fluorescence changes during depolarisation from -90 mV to +40 mV, are plottet as a function of current amplitude (expression level). The corresponding ionic current of W434F gating currents was calculated using 13 elementary charges pr channel [25, 26] with a unitary conductance of 20 pS. **F)** FV (red) and IV (black) curves obtained from K19Anap expressing oocytes. **G)** Time constants obtained from

exponential fits of inactivation currents (black) and fluorescence (black) time courses of K19Anap expressing oocytes. **H-I)** Same as F-G) but for E35Anap expressing oocytes.

In contrast to the tip mutants, they only exhibited one fluorescence component which made the fluorescence signal easier to analyze and thus excluded the need for using W434F. The fluorescence intensity of K19Anap and E35Anap was insensitive to 4-AP (figure 5.3C-D), suggesting that it reports a movement prior to pore block. The FV of K19Anap correlated with the IV curve for inactivation with midpoint values of -19.3 mV and -14.3 mV respectively, as obtained from Boltzmann fits (figure 5.3F). On the other hand, the FV of E35Anap was more left-shifted with respect to inactivation with midpoint values of -24.0 mV and -9.3 mV, respectively (figure 5.3H). The kinetics of inactivation and fluorescence were highly variable from oocyte to oocyte with slower inactivation at increased expression as mentioned earlier (an effect which disappears with W434F, figure 5.3E). We therefore could not directly compare mean time constants. Nevertheless, when comparing inactivation and fluorescence kinetics of single oocytes, the data suggests that fluorescence and inactivation exhibit similar kinetics in K19Anap, whereas, in E35Anap, the time constant of fluorescence is approximately 10 ms faster than the one of inactivation (figure 5.3G and I). Taken together, the results indicate that, in both mutants, Anap is probing a transition which precedes final block, due to their 4-AP insensitivity. However, the two movements are not nessecarily the same. The K19Anap movement develops closely with inactivation whereas E35Anap fluorescence signal is both left-shifted to and faster than inactivation. A possible mode-of-action which could explain these results could be a sequential transition mechanism. First, the downstream chain region movement (E35) sets in motion, which then is followed by a second movement involving the upstream part of the chain (K19).

5.3.4 Probing the reception of the inactivation particle

In order to probe the reception of the N-terminus as it enters through the T1 side window, Anap was inserted into position E201 in the T1-S1 linker (red mark, figure 5.1A). Like the N-terminal mutants, E201Anap exhibited functional N-type inactivation (figure 5.4A) and displayed fluorescence changes at high expression levels (figure 5.4B). As the T1-S1 linker is situated close to the voltage sensor, it is possible that the fluorescence changes of E201Anap originate from channel activation, and not inactivation. To verify this, the experiments were repeated in inactivation-removed channels lacking the N-terminus (IR, Δ6-46). IR-E201Anap channels

exhibited no fluorescence changes, demonstrating that the movement, probed by Anap in E201Anap is caused by N-type inactivation. In agreement with this, both the $V_{½}$ values (-21.6 mV and -15.8 mV, respectively) and the time constants of fluorescence signal and inactivation correlated well (figures 5.4D-E). As with the chain mutants, the total fluorescence change was insensitive to blocking by 4-AP (figure 5.4F). We also attempted to probe reception of the IP within the pore. To that end, Anap was inserted into selected pore-lining residues (I470, V478, Y485). Unfortunately, all the pore mutants exhibited dysfunctional pore opening or N-type inactivation, and were therefore inadequate for further investigation in relation to this study (data not shown). Nevertheless, the results for E201Anap suggest that Anap is probing the reception of the IP – a movement which is not causing the final block.

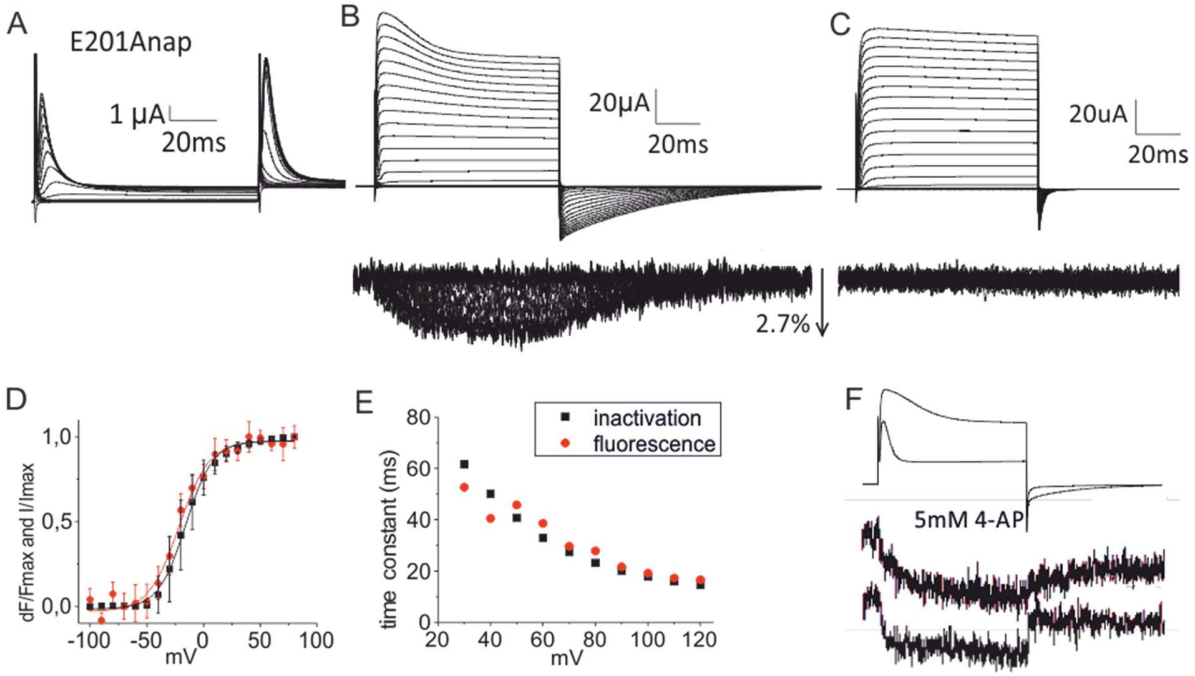

Figure 5.4 VCF results for the receptor site mutant E201Anap in the T1-S1 linker
A) Currents obtained from an E201Anap expressing oocyte from a step protocol as in figure 5.1B. **B)** Example of an oocyte expressing E201Anap showing fluorescence changes upon a standard depolarisation protocol. **C)** Same protocol as in B except that the oocyte is expressing an E201Anap mutant in which the N-terminus has been removed (Δ6-46). **D)** Comparison of FV (red) and IV for inactivation (black) of E201Anap. **E)** Time constants of exponential fits obtained from the oocyte shown in B. **F)** Currents and fluorescence during a depolarisation step from -90 mV to +40 mV before and after application of external 4-AP.

5.4 Discussion

By genetically incorporating a fluorescent unnatural amino acid on the cytoplasmic side of the Shaker K_V channel, we were able to directly probe conformational changes underlying N-type

inactivation. The experiments provide the first dynamic information about the IP movement during N-type inactivation. Our findings suggest a sequential-step model during which the IP undergoes at least two transitions, which is in agreement with previous functional studies that suggest an initial binding of the IP to the T1 domain [12], followed by a second binding to the inner pore [3].

Based on our VCF results we suggest that, upon depolarization, both tip and chain region initially moves (transition 1 in figure 5.5). We found that, relative to inactivation, the movement of the downstream chain region (E35) preceded the movement of the upstream chain region (K19) which suggests the presence of two pre-inactivation steps. Then, a final movement is responsible for docking the IP tip into the pore, and this movement only involves the tip region (A3 and Y8, transition 2 in figure 5.5). Molecular dynamics of a Shaker IP have recently shown that the IP adopts a helical structure which inserts spontaneously into the intracellular cavity of the pore and subsequently "snakes" deep into the pore when driven by voltage [27]. It is possible that the slow fluorescence component of A3Anap and Y8Anap represent this last transition.

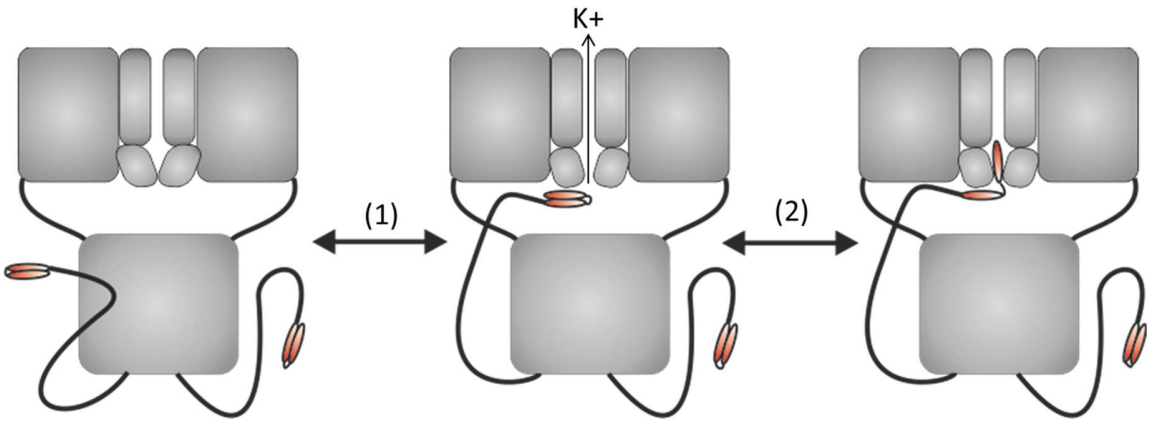

Figure 5.5 Proposed model for N-type inactivation
Binding of the IP to the open pore involves at least two conformational changes. The first involves both tip and chain (2), whereas the second only involves the tip (2).

The finding of two pre-inactivation steps is consistent with previous work on $K_V1.4$ channels, where a downstream intra-chain electrostatic interaction was identified and suggested to be responsible for initially shortening the distance between the IP and the T1-S1 linker [5, 28]. It is therefore possible that position E35 in Shaker lies within a region that is part of a similar interaction as an initial step upon depolarisation.

It is worth mentioning that the E201Anap and K19Anap fluorescence data are similar relative to inactivation. This suggests that Anap experiences the same transition at both positions (ie. E201Anap probes the reception of K19, and K19Anap probes the movement of the IP towards E201). This interpretation agrees with findings in two other Shaker-related K_V channels where the three conserved glutamates in the T1-S1 linker (199-EEE-201) have been shown to interact electrostatically with positive charges in the early region of the chain which corresponds to the 17-RKK-19 region in Shaker (R18 in AK_V1 and 26-RARERER-32 in $K_V1.4$) [5, 13].

VCF results only report on relative movements from which we cannot deduce the exact position of the tip and chain before and during N-type inactivation. For example, the current model for N-type inactivation generally implies that the N-terminus rests randomly in the cytosol and enters through the side windows upon depolarization. But it is also possible that the N-terminus is already bound near or at the T1 windows. One way to reconstruct the IP movement is to specifically insert tryptophans along putative binding sites (T1 domain, T1-S1 linker) in the background of a tip mutant and a chain mutant (eg. Y8Anap and E35Anap) to induce quenching (or unquenching) of Anap. Since quenching by tryptophan requires contact formation and depends on van-der-Walls radii [29], the method is useful for determination of short range distances [30, 31]. Such experiments would allow accurate estimates of the position of the IP with respect to the T1 domain, which especially during resting state is unknown. Moreover, the direction of the fluorescence change would allow us to determine whether the IP moves towards or away from the inserted tryptophans. To this end, we have selected 7 residues in the T1 domain and 3 residues in the putative binding site region, for tryptophan insertion in the Y8Anap background (figure 5.6). So far, G159W, K178W, E192W, I470W and A391W did not result in any quenching (not shown).

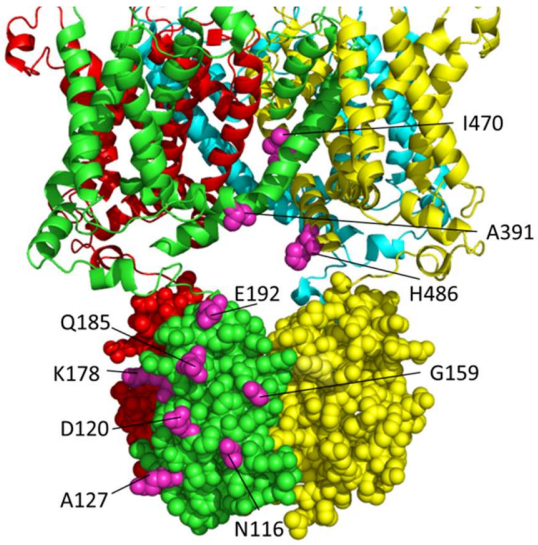

Figure 5.6 Overview of residues selected for Trp insertion.
The T1 domain in the Kv channel is shown as spheres and residues for Trp insertion are highlighted in pink.

5.5 Methods and materials

5.5.1 Xenopus oocyte injection

The mutations were introduced into the full-length *Drosophila Shaker* H4 gene in the pBSTA vector. The N-terminal stop codons (A3, Y8, K19, E35) were inserted into a 9LL background in which 9 noncanonical start codons have been removed via silent mutations as previously described [17]. For Anap incorporation, 9.2 nl of 0.1 ng/nL cDNA encoding the tRNA/AnapRS pair (pAnap) [14] was injected into the nucleus of *Xenopus laevis* oocytes 6-24 hours prior to coinjection of 23 nL 1 mM Anap (Abzena TCRS, custom synthesis TCRS-170) and 35 ng *in vitro* transcribed RNA [16]. All steps during and after Anap injection were performed under red light to avoid bleaching. Oocytes were then incubated for 1-3 days at 18°C in Barth's solution supplemented with 5% horse serum. See Kalstrup & Blunck, 2017 [32] for detailed description and visualisation of this procedure.

5.5.2 Electrophysiology

Voltage clamp was performed with a CA-1B amplifier (Dagan). Currents were recorded in the cut-open oocyte voltage-clamp configuration [33] and analyzed by using GPatch (Department of Anesthesiology, University of California, Los Angeles). For ionic recordings the external solution contained in mM: 5 KOH, 110 NMDG, 10 Hepes, and 2 $Ca(OH)_2$, and the internal solution

contained in mM: 115 KOH, 10 Hepes, and 2 EDTA. For gating recordings the KOH was replaced by NMDG. All solutions were adjusted to pH 7.1 with MES. For 4-AP blocking experiments, 5mM NMDG (gating) or KOH (ionic) was replaced by 5 mM 4-AP, and the command potential was held at 0 mV for 5 seconds prior to recordings. Conductance (G) was calculated from the steady state currents (I) via $G=I/(V-V_{rev})$, where V_{rev} is the reversal potential. Conductance-, charge- and fluorescence-voltage relationships (GV, QV, FV) were fitted to a Boltzmann relation of the form $y = (1 + \exp(-(V - V_{1/2})/dV))^{-1}$.

5.5.3 Voltage clamp fluorometry

Fluorescence intensities were recorded with a photodiode detection system (Photomax 200, Dagan) using a ex-377/50, dc-409, em-470/40 filter set for Anap fluorescence. Bleaching effects during step protocols were accounted for by scaling fluorescence traces using the first sweep as reference.

5.6 Supporting information

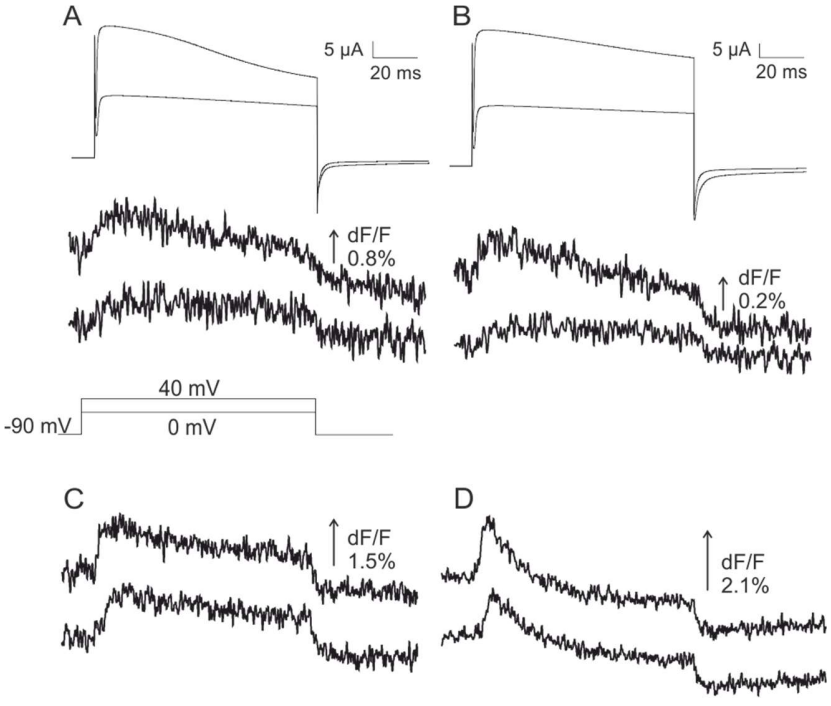

Figure S5.1 Two fluorescence components present in A3Anap and Y8Anap

Currents and fluorescence changes elicited by depolarisations of **A)** A3Anap and **B)** Y8Anap channels, obtained at high expression levels. The same protocol was performed with **C)** A3Anap-W434F and **D)** Y8Anap-W434F channels.

5.7 Acknowledgements

This work was funded by the Canadian Institutes for Health Research Grants MOP-102689 and MOP-136894 (to R.B.). We thank Mireille Marsolais for assistance on mutant preparation.

5.8 References

1. Hoshi, T., W.N. Zagotta, and R.W. Aldrich, *Biophysical and molecular mechanisms of Shaker potassium channel inactivation.* Science, 1990. **250**(4980): p. 533-8.
2. Zagotta, W.N., T. Hoshi, and R.W. Aldrich, *Restoration of inactivation in mutants of Shaker potassium channels by a peptide derived from ShB.* Science, 1990. **250**(4980): p. 568-71.
3. Zhou, M., J.H. Morais-Cabral, S. Mann, and R. MacKinnon, *Potassium channel receptor site for the inactivation gate and quaternary amine inhibitors.* Nature, 2001. **411**(6838): p. 657-61.
4. Demo, S.D. and G. Yellen, *The inactivation gate of the Shaker K+ channel behaves like an open-channel blocker.* Neuron, 1991. **7**(5): p. 743-53.
5. Fan, Z., X. Ji, M. Fu, W. Zhang, D. Zhang, and Z. Xiao, *Electrostatic interaction between inactivation ball and T1-S1 linker region of Kv1.4 channel.* Biochim Biophys Acta, 2012. **1818**(1): p. 55-63.
6. Murrell-Lagnado, R.D. and R.W. Aldrich, *Interactions of amino terminal domains of Shaker K channels with a pore blocking site studied with synthetic peptides.* J Gen Physiol, 1993. **102**(6): p. 949-75.
7. Prince, A. and P.J. Pfaffinger, *Conserved N-terminal negative charges support optimally efficient N-type inactivation of Kv1 channels.* PLoS One, 2013. **8**(4): p. e62695.
8. Kreusch, A., P.J. Pfaffinger, C.F. Stevens, and S. Choe, *Crystal structure of the tetramerization domain of the Shaker potassium channel.* Nature, 1998. **392**(6679): p. 945-8.
9. Li, M., Y.N. Jan, and L.Y. Jan, *Specification of subunit assembly by the hydrophilic amino-terminal domain of the Shaker potassium channel.* Science, 1992. **257**(5074): p. 1225-30.
10. Shen, N.V., X. Chen, M.M. Boyer, and P.J. Pfaffinger, *Deletion analysis of K+ channel assembly.* Neuron, 1993. **11**(1): p. 67-76.
11. Venkataraman, G., D. Srikumar, and M. Holmgren, *Quasi-specific access of the potassium channel inactivation gate.* Nat Commun, 2014. **5**: p. 4050.
12. Gulbis, J.M., M. Zhou, S. Mann, and R. MacKinnon, *Structure of the cytoplasmic beta subunit-T1 assembly of voltage-dependent K+ channels.* Science, 2000. **289**(5476): p. 123-7.
13. Prince-Carter, A. and P.J. Pfaffinger, *Multiple intermediate states precede pore block during N-type inactivation of a voltage-gated potassium channel.* J Gen Physiol, 2009. **134**(1): p. 15-34.
14. Chatterjee, A., J. Guo, H.S. Lee, and P.G. Schultz, *A genetically encoded fluorescent probe in mammalian cells.* J Am Chem Soc, 2013. **135**(34): p. 12540-3.
15. Lee, H.S., J. Guo, E.A. Lemke, R.D. Dimla, and P.G. Schultz, *Genetic incorporation of a small, environmentally sensitive, fluorescent probe into proteins in Saccharomyces cerevisiae.* J Am Chem Soc, 2009. **131**(36): p. 12921-3.
16. Kalstrup, T. and R. Blunck, *Dynamics of internal pore opening in K(V) channels probed by a fluorescent unnatural amino acid.* Proc Natl Acad Sci U S A, 2013. **110**(20): p. 8272-7.

17. Kalstrup, T. and R. Blunck, *Reinitiation at non-canonical start codons leads to leak expression when incorporating unnatural amino acids.* Sci Rep, 2015. **5**: p. 11866.
18. Bezanilla, F., E. Perozo, D.M. Papazian, and E. Stefani, *Molecular basis of gating charge immobilization in Shaker potassium channels.* Science, 1991. **254**(5032): p. 679-83.
19. Yang, Y., Y. Yan, and F.J. Sigworth, *How does the W434F mutation block current in Shaker potassium channels?* J Gen Physiol, 1997. **109**(6): p. 779-89.
20. Grigoriev, N.G., J.D. Spafford, and A.N. Spencer, *The effects of level of expression of a jellyfish Shaker potassium channel: a positive potassium feedback mechanism.* J Physiol, 1999. **517**: p. 25-33.
21. Perozo, E., R. MacKinnon, F. Bezanilla, and E. Stefani, *Gating currents from a nonconducting mutant reveal open-closed conformations in Shaker K+ channels.* Neuron, 1993. **11**(2): p. 353-8.
22. Claydon, T.W., M. Vaid, S. Rezazadeh, S.J. Kehl, and D. Fedida, *4-aminopyridine prevents the conformational changes associated with p/c-type inactivation in shaker channels.* J Pharmacol Exp Ther, 2007. **320**(1): p. 162-72.
23. Pathak, M., L. Kurtz, F. Tombola, and E. Isacoff, *The cooperative voltage sensor motion that gates a potassium channel.* J Gen Physiol, 2005. **125**(1): p. 57-69.
24. Armstrong, C.M. and A. Loboda, *A model for 4-aminopyridine action on K channels: similarities to tetraethylammonium ion action.* Biophys J, 2001. **81**(2): p. 895-904.
25. Schoppa, N.E., K. McCormack, M.A. Tanouye, and F.J. Sigworth, *The size of gating charge in wild-type and mutant Shaker potassium channels.* Science, 1992. **255**(5052): p. 1712-5.
26. Seoh, S.A., D. Sigg, D.M. Papazian, and F. Bezanilla, *Voltage-sensing residues in the S2 and S4 segments of the Shaker K+ channel.* Neuron, 1996. **16**(6): p. 1159-67.
27. Vergara-Jaque, A., F. Palma-Cerda, H. Poblete, A. Lowet, A. Sukharev, J. Comer, and M. Holmgren, *A Structural Model of the Inactivation Gate of Voltage Activated Potassium Channels.* Biophysical Journal, 2017. **112**(3): p. 247a.
28. Fan, Z., L.J. Bi, G. Jin, and Z. Qi, *Electrostatic interaction in the NH(2)-terminus accelerates inactivation of the Kv1.4 channel.* Biochim Biophys Acta, 2010. **1798**(11): p. 2076-83.
29. Mansoor, S.E., H.S. McHaourab, and D.L. Farrens, *Mapping proximity within proteins using fluorescence spectroscopy. A study of T4 lysozyme showing that tryptophan residues quench bimane fluorescence.* Biochemistry, 2002. **41**(8): p. 2475-84.
30. Islas, L.D. and W.N. Zagotta, *Short-range molecular rearrangements in ion channels detected by tryptophan quenching of bimane fluorescence.* J Gen Physiol, 2006. **128**(3): p. 337-46.
31. Pantazis, A. and R. Olcese, *Relative transmembrane segment rearrangements during BK channel activation resolved by structurally assigned fluorophore-quencher pairing.* J Gen Physiol, 2012. **140**(2): p. 207-18.
32. Kalstrup, T. and R. Blunck, *Voltage-clamp Fluorometry in Xenopus Oocytes Using Fluorescent Unnatural Amino Acids.* 2017(123): p. e55598.
33. Stefani, E. and F. Bezanilla, *Cut-open oocyte voltage-clamp technique.* Methods Enzymol, 1998. **293**: p. 300-18.

Chapter 6

Reinitiation at non-canonical start codons leads to leak expression when incorporating unnatural amino acids

Tanja Kalstrup[1] and Rikard Blunck[1,2]

[1]Department of Physiology and Pharmacology, and [2]Department of Physics, Montreal University, Montreal, Quebec, Canada

Accepted June 5, 2015 (received for review February 26, 2015).

Scientific Reports, Vol. 5, Article number: 11866, July 8, 2015

Author contributions: T.K. and R.B. designed research, T.K. performed experiments, T.K. and R.B. analyzed data, T.K. wrote the first version which was edited by R.B.

6.1 Abstract

With the rapid development of a continuously growing selection of unnatural amino acids (UAAs), UAA insertion becomes increasingly popular for investigating proteins. However, it can prove problematic to ensure the homogeneity of the expressed proteins, when homogeneity is compromised by "leak expression". Here, we show that leak expression may be mediated by reinitiation and can result in unwanted proteins when stop codons for UAA insertion are mutated into the N-terminus of proteins. We demonstrate that up to 25% of leak expression occurs through reinitiation in the Shaker-Kv channel when stop codons are located within the first 70 amino acids. Several non-canonical start codons were identified as translation reinitaition sites, and by removing the start codons, we were able to decrease leak expression to less than 1%. Our study emphasizes the need to carefully inspect for leak expression when inserting UAAs and demonstrates how leak expression can be eliminated.

6.2 Introduction

Genetic incorporation of unnatural amino acids (UAA) is a powerful tool to investigate protein structure and function. Through nonsense suppression of stop codons, UAAs are incorporated into proteins using chemically-charged tRNAs or orthogonal tRNA/tRNA synthetase (tRNA/RS) pairs [1]. With this method, numerous UAAs with different chemical and biophysical properties have been used as probes in E. coli, yeast, plant, amphibians and mammalian cells [1, 2]. When using UAAs, it is crucial to have control of the protein translation process in order to get reliable results. Indeed, the orthogonal tRNA/RS pair provides site-specific incorporation of the UAA, with no or only a negligible fraction of unwanted proteins lacking the UAA, which may result from crosstalk with endogenous tRNAs or synthetases.

Also cellular mechanisms can generate leak expression when using UAA mutagenesis, in spite of the orthogonality of the tRNA/RS pair. Eukaryotic cellular mRNA is mainly translated via a linear scanning model which consists of initiation, elongation and termination. During initiation, the 40S ribosomal subunit is equipped with initiation factors and Met-tRNA, and binds to the 5'-terminal mRNA 7-methylguanosine cap structure (Fig. 6.1A). The complex then scans in the 5' to 3' direction in a base-by-base inspection until it encounters the first AUG start codon, where elongation begins with recruitment of the large 60S subunit and release of initiation factors [3]

(Fig. 6.1A). When the ribosome encounters a stop codon during elongation, translation is terminated. The ribosome disassembles from the mRNA and prepares for a second round of translation.

However, under some circumstances, translation does not strictly follow the linear scanning model. One example is stop codon readthrough, where a tRNA inserts its amino acid at the stop codon [4], or the stop codon can be ignored due to ribosomal sliding [5]. The efficiency of stop codon readthrough includes complex combinations of stop codon identity, sequence context and RNA structure [6-8], and such recoding strategies are especially used by viruses to generate a rich and varied protein synthesis. Therefore, translational stop codon readthrough is best understood in viruses, but has also been observed in yeast, Drosophila and humans [9, 10]. Another recoding strategy is reinitiation, where multiple initiation sites can result in mRNAs harboring more than one open reading frame (ORF) [11]. If the eukaryotic ribosome encounters a stop codon shortly after initiation, a fraction of the initiation factors are still associated to the ribosome [12, 13]. This allows the 40S subunit to remain on the mRNA and as a result, the 40S subunit continues scanning for a downstream start codon and reinitiates translation, resulting in a downstream ORF (dORF). Reinitiation only occurs when the distance between the first start codon and the next stop codon is short [13, 14], likely increasing the probability that initiation factors are still present. As a result, N-terminal truncated proteins can be translated from the upstream ORF (uORF). In eukaryotes, the ribosomal initiation complex involves 13 initiation factors (eIFs) [15] but the identity and number of eIFs required for reinitiation is unknown. Reinitiation occurs in viruses [16] and throughout the eukaryotic kingdom [17-19]. Reinitiation also occurs in prokaryotes, but the mechanism is different due to a distinct initiation machinery [17].

In contrast to readthrough, reinitiation is more common in eukaryotes, and approximately 40% of mammalian mRNAs have a short uORF, although not all of them necessarily involve translation of both ORFs [20, 21]. Examples of functional reinitiation at downstream methionines include regulation of Aquaporin-4 isoforms [22] and LQT2 mutations in hERG channels leading to altered gating properties [23] and defective trafficking [24].

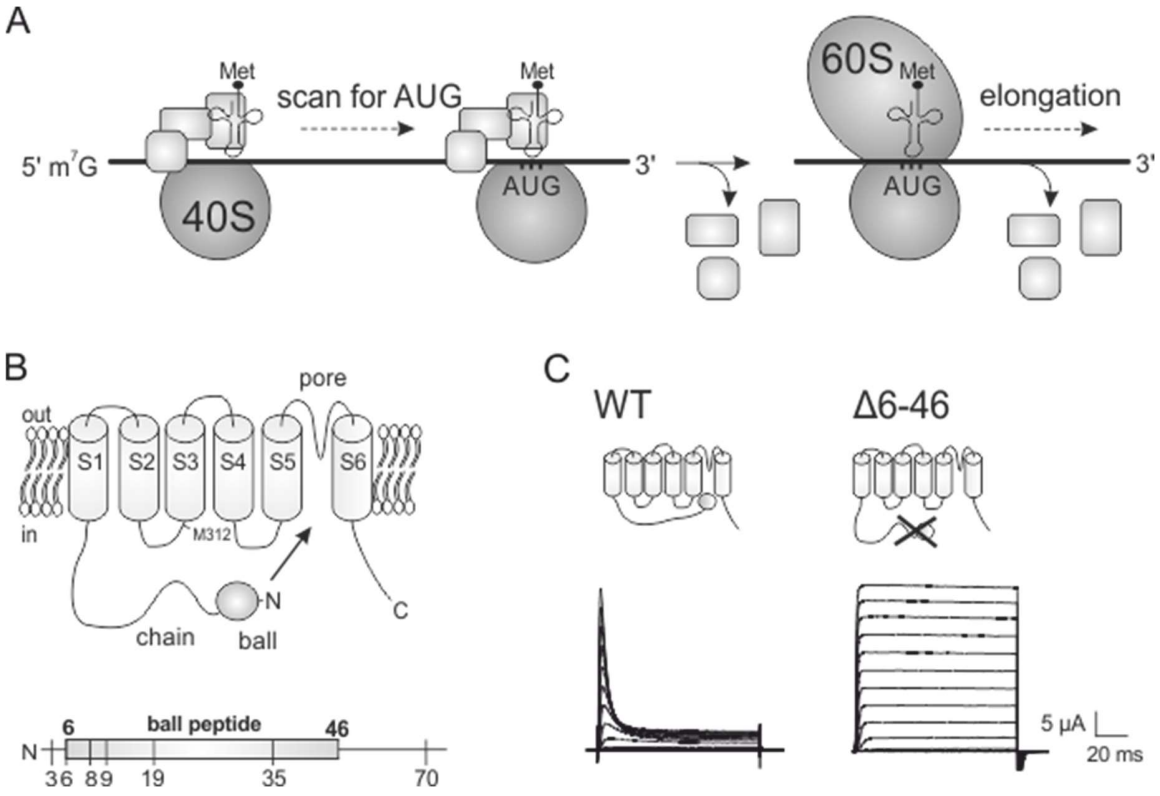

Figure 6.1 Translation reinitiation, *Shaker* channel topology, and current phenotypes
A) Simplified model for translation initiation in eukaryotes. First, the 40S small ribosomal subunit associates with initiation factors (shown as squares) and Met-tRNA^{Met} on the mRNA 5' cap structure. The assembled complex then scans the mRNA sequence until it meets the first AUG codon, after which a fraction of initiation factors are released and the 60S large ribosomal subunit is recruited. Elongation of peptide bonds can then begin and the rest of the initiation factors are released. For a more detailed view see Jackson, *et al.*[15] **B)** Topology of the Shaker Kv channel (top) and the N-terminal (below) with annotated positions used in this study. **C)** Ionic currents from WT and Δ6-46 Shaker channels upon depolarization from −100 mV to +60 mV in steps of +10 mV from a holding potential of –90 mV. The corresponding structures of each constructs are shown.

Previously, we successfully incorporated a fluorescent UAA into the Shaker voltage-gated potassium (Kv) channel [2]. The nonsense stop codons were located either central or C-terminal, and no leak expression was detected in the absence of the UAA, reflecting a strong orthogonality of the tRNA/RS pair used. Here, we show that when stop codons are introduced in the region near the N-terminus of the same Kv channel, a considerable amount of leak expression results from translation reinitiation which do not reinitiate at downstream methionines, but rather uses non-canonical (non-AUG) start codons.

The Kv channel is a homotetramer where each subunit consists of six transmembrane segments (S1–S6) containing the voltage sensor (S1–S4) and the pore (S5–S6). The N-terminal region (amino acids 1–46) of each subunit is a cytosolic soluble "ball-and-chain" region responsible for

fast N-type inactivation (Fig. 6.1B) [25, 26], where the N-terminus move into the pore region and occludes the pore in response to sustained depolarization (Fig. 6.1C). When the N-terminus of a Shaker Kv channel is deleted (Δ6-46), the inactivation is disrupted such that the channel remains open (Fig. 6.1C) [25]. The different current phenotypes of full length and N-terminal deletion channels allowed us to determine the absence or presence of the N-terminus in various Shaker mutants expressed in Xenopus oocytes using the cut-open voltage clamp technique [27].

6.3 Results

6.3.1 Functional channels are translated despite stop codons in the N-terminus.

In contrast to our previous findings where we introduced stop codons in the central and C-terminal part of the protein [2], leak expression was present when stop codons were inserted within the first 70 amino acids in the Shaker Kv channel (A3stop, G6stop, Y8stop, G9stop, K19stop, E35stop and D70stop, Fig. 6.1B, Fig. 6.2A). No leak expression was measured for any stop codons tested downstream of residue D70 (L170stop, F196stop and V234stop shown in Fig. 6.2A, and A359stop and H486stop in Kalstrup & Blunck 20132), which indicates that the mechanism responsible for leak expression is specific for N-terminal positions. D70stop expressed less than 1% whereas the other mutants expressed between 5 and 25% (Fig. 6.2C).

The leak expression presented in Fig. 6.2A occurs in the presence of the channel RNA only, and the mechanism leading to expression here therefore cannot be attributed to crosstalk between the modified tRNA/synthetase pair and endogenous amino acids. The observed leak expression could be due to readthrough or translational reinitiation beyond the inserted stop codon. One indication was the dependence of leak expression on the position of the stop codon. When stop codons are inserted proximal to the N-terminus, a short uORF is generated in the case of reinitiation. Due to the short length of the uORF, the likelihood is high that (some of) the initiation factors are still attached, allowing a second initiation to take place at the next start codon. The further downstream a stop codon is located, the longer the translated uORF will be and the higher will be the chance that all initiation factors separated from the ribosome, such that reinitiation cannot occur. Readthrough, on the other hand, is not dependent on the presence of initiation factors and should have no dependence on the relative position. We only

found leak expression for N-terminal stop codons, pointing towards reinitiation as the prevalent mechanism for leak expression.

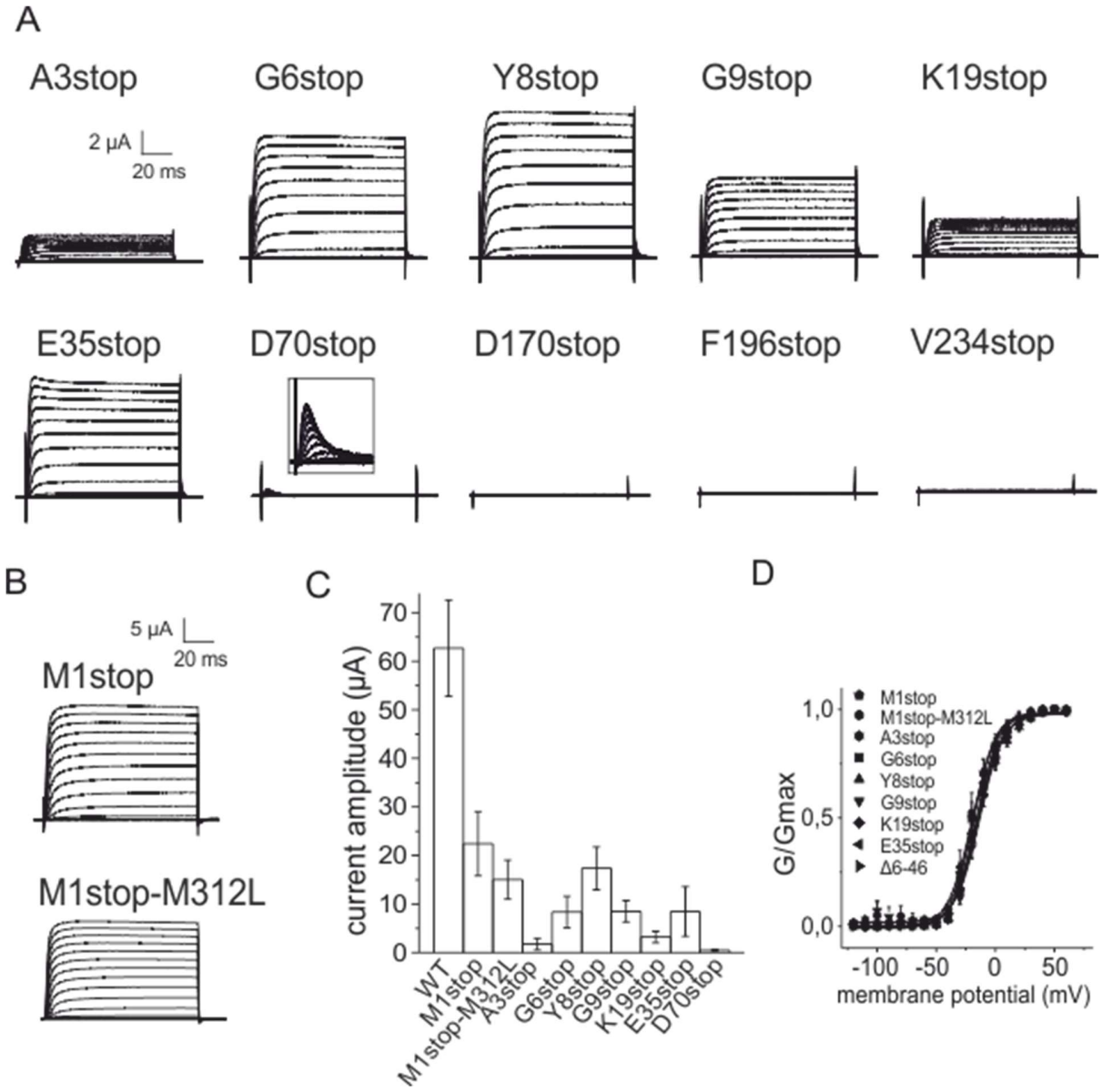

Figure 6.2
A–B) Ionic currents from Shaker mutants obtained with the same protocol as in 1C. **C)** Comparison of peak current amplitudes at +60 mV. Error bars indicate SEM with n =10–20 oocytes. **D)** Conductance-voltage (GV) relationships were fitted to a Boltzmann equation ($V_{½,M1stop}$ = −19.1 mV, dV_{M1stop} = 9.9 mV, $V_{½,M1stop\text{-}M312L}$ = −23.0 mV, $dV_{M1stop\text{-}M312L}$ = 11.3 mV, $V_{½,A3stop}$ = −18.1 mV, dV_{A3stop} = 9.1 mV, $V_{½,G6stop}$ = −15.5 mV, dV_{G6stop} = 9.7 mV, $V_{½,Y8stop}$ = −14.6 mV, dV_{Y8stop} = 10.8 mV, $V_{½,G9stop}$ = −13.0 mV, dV_{G9stop} = 10.0 mV, $V_{½,K19stop}$ = −16.3 mV, $dV_{K19stop}$ = 9.3 mV, $V_{½,E35stop}$ = −14.5 mV, $dV_{E35stop}$ = 10.1 mV, $V_{½,Δ6\text{-}46}$ = −15.8 mV, $dV_{Δ6\text{-}46}$ = 10.6 mV).

We were able to further corroborate this indication by investigating expression of the uORF. In the Shaker Kv channel, used in this study, we were also able to determine whether the uORF has been expressed because the N-terminus forms the ball peptide responsible for N-type inactivation and its presence is visible in the functional data. Deletion of residues 6–46 removes inactivation (Fig. 6.1C) while synthetic N-terminal Shaker peptides of the first 20 amino acids can restore inactivation in Δ6-46 channels [28].

In the case of reinitiation, an N-terminal peptide and an N-terminal truncated channel are translated. Depending on the length of the peptide and where the second translation begins, such N-terminal truncation could lead to disrupted N-type inactivation. E35stop and D70stop exhibited weak and complete N-type inactivation, respectively, while the other mutants did not undergo any N-type inactivation and were identical to Δ6-46 channels (Figs 6.1C and 6.2A,D). It seems that the uORFs generated in E35stop and D70stop were responsible for the inactivation of truncated channels, while the uORFs in the other mutants were too short to inactivate (<19 amino acids, Fig. 6.1B). We elaborate on this in the next section.

Principally, inactivation in E35stop and D70stop could also be due to stop codon readthrough, where full length channels are translated, and thus undergo N-type inactivation. However, readthrough would also have led the mutants with a shorter uORF to inactivate (Fig. 6.2A). In addition, removal of the start codon (M1stop) did not reduce leak expression (Fig. 6.2B–C), indicating that ribosomes are indeed capable of initiating translation downstream in the sequence. Taken together, these results indicate that the most likely mechanism causing leak expression here is reinitiation. The question remained at what site translation was reinitiated.

One possibility would be initiation at a downstream methionine; it was for instance previously reported that Kv1.4 channels with a stop codon at residue 19 exhibited leak currents from truncated channels which were eliminated by removal of a methionine at residue 108 [29]. However, here, removal of the next downstream methionine (M312L) in Shaker did not significantly influence leak expression (Fig. 6.2B). We ignored later methionines since the resulting translated protein would not yield functional channels, lacking most of or the entire voltage sensor. Reinitiation thus has to occur at sites other than the standard start codon AUG.

6.3.2 Non-canonical start codons are used as translation reinitiation sites.

Increasing evidence from the literature has underscored the use of non-canonical start codons which deviate from the canonical AUG codon by one nucleotide, except AAG and AGG [30-32]. We therefore screened the Shaker mRNA sequence for such non-canonical codons and found 9 in-frame codons within the first 121 amino acids at position I40, L45, L47, L63, L66, I89, I101, T114 and T121 (highlighted in bold in Fig. 6.3A). To verify that these codons were used as start codons in reinitiation, silent mutations were introduced into the E35stop background. First, we mutated L47 (#1 in Fig. 6.3A), then both L47 and L45 (#2) and then L47, L45 and I40 (#3). Each mutation led to a decreased expression level in a stepwise manner (Fig. 6.3B). Therefore, all ribosomes do not nessecarily reinitiate at the first codon they encounter (I40). For the subsequent mutations of L63 (#4), L66 (#5) and I89 (#6), only #5 led to a decreased expression. When the last three codons were removed in addition (#9), expression levels further decreased. Expression could partially be restored upon reinsertion of I40 into the #9 background (#9-1) confirming that reinitiation is not limited to the first start codon. As a control, the unnatural amino acid Anap was incorporated in response to the stop codon using the orthogonal tRNA/Anap-RS pair (pAnap) [2, 33, 34]. With Anap, wildtype expression levels and N-type inactivation were fully recovered, reflecting full length channels (Fig. 6.3B–C). The expression levels with Anap did not decrease with the removal of start codons, excluding the possibility that RNA stability might play a role in the decreased expression. If the RNA had become instable by silently removing the non-canonical start codons, also expression in presence of Anap would have been reduced. Therefore, our experiments demonstrate that several non-canonical start codons in the region of amino acids 40–121 are recognized by the ribosome to reinitiate translation in E35stop channels.

The sequence context of start codons has significant influence on the initiation efficiency of both canonical and non-canonical start codons [35, 36]. The Kozak consensus sequence gccRccAUGG is the optimal context in eukaryotes, with the nucleotides in capital letters at position − 3 and +4 (relative to AUG) being most important. The purine (R = A or G) at −3 is more important than a G at +4, and the other nucleotides only play a role if there is neither a purine at −3 or a G at +4 [37]. For the 9 codons tested here, L47, L63 and I89 have the weakest Kozak sequence (Fig. 6.3A), which could explain why L63 and I89 are not used as initiation sites. The codon for L47 (CTG) is

one of the most probable non-AUG codons [30] and may explain why it is recognized by the ribosome despite a weak Kozak sequence.

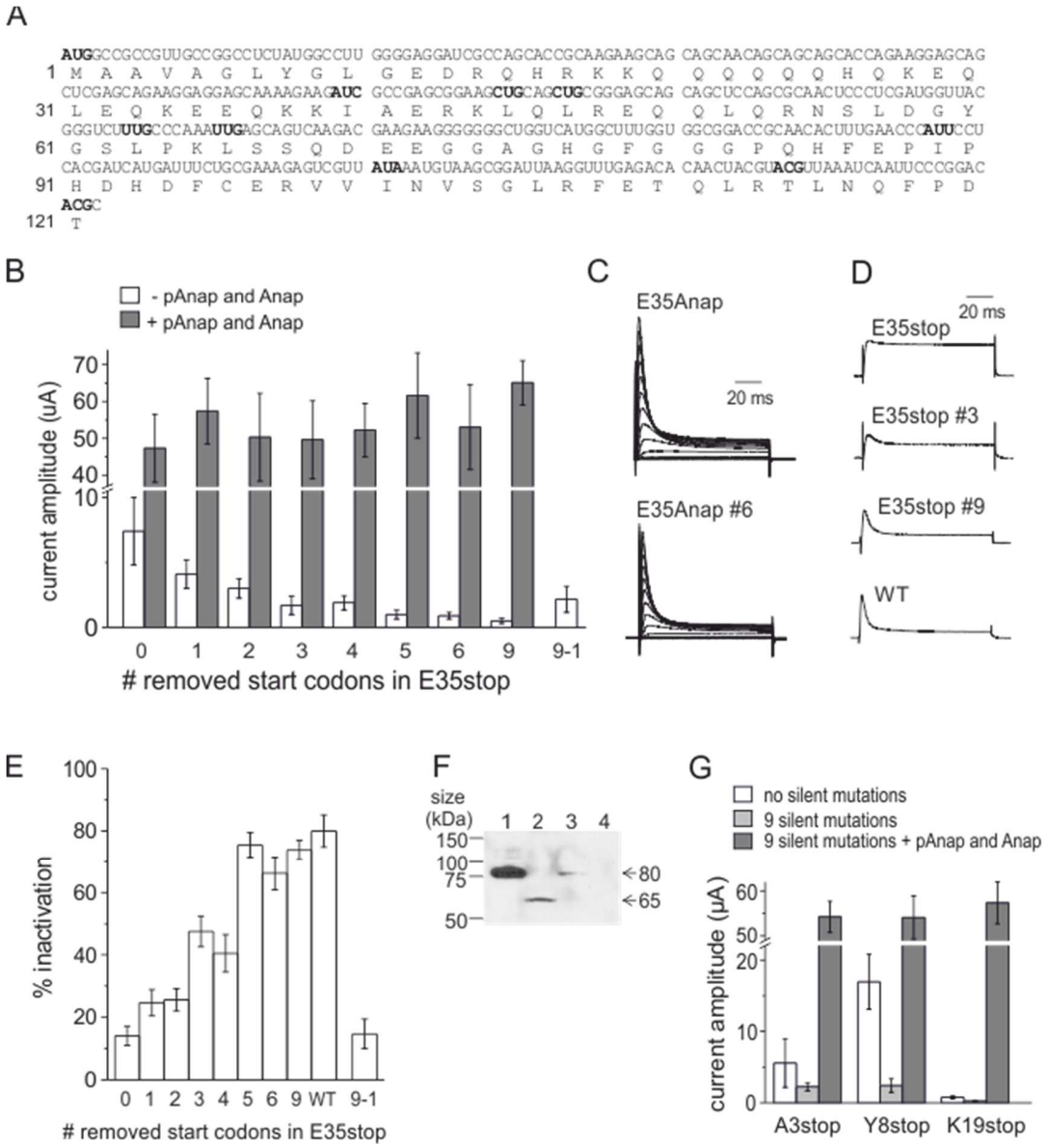

Figure 6.3

A) Sequence of amino acids 1−121 and the corresponding mRNA nucleotides in Shaker. The nucleotides of the canonical start codon (M1) and the following 9 downstream non-canonical start codons (I40, L45, L47, I89, L36, L66, I101, T114, and T121) are shown in bold. AAG and AGG codons were ignored. Numbers refer to the amino acid sequence. **B)** Comparison of peak current amplitudes at +60 mV of E35stop with silent mutations, without and with Anap incorporation. Numbers refer to the number of mutated start codons such that 1 is E35stop-L45L, 2 is E35stop-L45L-L47L, 3 is E35stop-I40L-L45L-L47L, 4 is E35stop-I40L-L45L-L47L-L63L, 5 is E35stop-I40L-L45L-L47L-L63L-L66L, 6 is E35stop-I40L-L45L-L47L-L63L-L66L-I89L and 9 is E35stop-I40L-L45L-L47L-L63L-L66L-I89L-I101L-T114T-T121T. Error bars indicate SEM with n = 20–30 oocytes. **C)** Inactivation is recovered with Anap incorporation. Shown are examples of ionic currents from E35Anap and E35Anap #6 (six mutated start codons). Voltage protocols are the same as in figure figure 1C **D)** Comparison of inactivation measured as the ratio between the current amplitude at the end of the +60 mV pulse, and the maximum current amplitude. Error bars

indicate SEM with n = 10–20 oocytes. **E)** Depolarization from −90 mV to +60 mV is shown for E35stop mutants and WT showing how inactivation increases when channel expression decreases. **F)** Western blot of isolated Xenopus oocytes membranes expressing Shaker WT (lane 1, 30 oocytes), E35stop (lane 2, 70 oocytes), E35Anap (lane 3, 30 oocytes) and non injected (lane 4, 70 oocytes). **G)** Comparison of peak current amplitudes at +60 mV for A3stop, Y8stop and K19stop, and removal of 9 start codons without and with Anap incorporation. Error bars indicate SEM with n = 5–10 oocytes.

When we reduce the translation efficiency of reinitiated channels, only the dORF is affected, while the short uORF is not. Therefore, the ratio of free N-terminal peptides to truncated channels will become larger when expression of the truncated channels decreases. This would explain why the slight inactivation of E35stop channels increases and almost reaches WT levels when the alternative start codons are removed (Fig.6.3D–E). These findings are supported by the fact that the efficiency of N-type inactivation indeed depends on both the length and the concentration of the N-terminal peptide [28]. We estimated the intracellular concentration of the uORF (amino acids 1–34) to be at least 2 μ M (see Methods), which is in agreement with previous peptide concentrations, where application of free peptides (amino acids 1–20) to Δ6-46 Shaker channels resulted in partial and full inactivation at concentrations of 10 μ M and 100 μ M, respectively [28]. Alternatively, the residual expression could be caused by readthrough, which would also show complete inactivation.

To confirm protein truncation in E35stop, a Western blot was performed for direct visualization of protein lengths with C-terminal myc-tagged Shaker constructs (Fig. 6.3F). Full-length wildtype Shaker exists in core-glycosylated (~80 kDa) and mature (~110 kD) form [38, 39]. For wildtype and E35Anap, we mainly see the core-glycosylated band at 80 kDa since the mature form only appears after longer expression times. E35stop in contrast, shows one band at ∼ 65 kDa. At 65 kD, we can exclude the possibility that E35stop leads to inefficient glycosylation as unglycosylated Shaker channels migrate at ∼ 75 kDa [38].

The expected truncated proteins can be ordered into two groups: Those which reinitiate at I40, L45, L47 or L66 would theoretically be ∼ 5–7 kDa shorter than wildtype. Those which reinitiate at I101, T114 or T121 would be ∼ 11–14 kDa shorter than wildtype. We only observed a single band at 65 kDa, despite loading 10 times more of E35stop on the SDS-PAGE gel compared to wildtype (not shown). The band at 65 kDa agrees with core-glycosylated truncated channels, reinitiating at I101, T114 and T121. From reinserting only the first non-canonical start codon, we know, however, that also the first start codons are used. It is possible that low expression combined

with different constructs resulted in protein concentrations too low to detect on a western blot. Alternatively, the small differences in length may result in truncated versions to migrate collectively.

To verify that reinitiation resulted in leak expression in the other mutants, we removed the same 9 alternative start codons in A3stop, Y8stop and K19stop. The expression levels decreased for all three mutants when removing the alternative start codons in the same manner as for E35stop (Fig. 6.3G). In addition, Anap incorporation rescued succesfully the full length channels with WT expression levels in presence of the 9 silent mutations, confirming that reinitiation is a general mechanism causing leak expression.

6.4 Discussion

In this study, we have identified translation events which require attention when UAAs are incorporated specifically in the N-terminal region of a protein. The efficient Xenopus oocyte expression system and the high sensitivity of electrophysiological recordings allowed us to measure low expression levels (<5%) which typically are difficult to resolve without direct access to protein function. Our system also allowed to efficiently discriminate between truncated and full-length proteins.

Based on the expression levels in Fig. 6.2C, we estimate that reinitiated translations can generate 5–25% leak expression when the length of the uORF is between 3 and 35 codons. Since cis-acting mRNA sequences and RNA structure can affect reinitiation efficiency [13, 40], the lengths mentioned here cannot be exactly extrapolated to other proteins and remain approximations. Our results are consistent with studies of the length and time dependence of reinitiation at downstream methionines, where expression levels decreased to 30% in the presence of a 13-codon uORF13, or to 50% in the presence of a 28-codon uORF [14]. The same studies showed that reinitiation was optimal for a certain uORF length, and reduced gradually when the uORF was lengthened further, most likely due to loss of initiation factors. Examples include reduction in reinitiation when a 13-codon uORF was lengthened to 33 codons [13], or a complete inhibition when a 24-codon uORF was lengthened to 40 codons [14]. These reported magnitudes of reinitiation inhibition by uORF lengths also correlate with our results, where reinitiation decreased to less than 1% when the uORF was lengthened to 70 codons (Fig. 6.2C). Our results

thus indicate that the nature of the reinitiation site (canonical versus non-canonical) does not play a major role.

Leak expression was reduced from 14% to less than 1% in E35stop channels when 9 non-canonical start codons between codon 40 and 121 were removed. Although the remaining leak expression was very subtle, it means nevertheless that the 40S ribosomal subunit is capable of scanning at least 258 nt (the length in nucleotides between residue 35 and 121) for a downstream non-canonical start codon. Comparison with scanning lengths for reinitiation at methionines shows similar results with 63 nt and 129 nt in hERG [23, 24] and 270 nt in Kv1.4 channels [29].

Kozak showed that reinitiation does not happen when the distance between the stop codon and the next start codon is short (ie. 8 nt) and that reinitiation is not limited to the closest downstream ATG codon [11], because the 40S subunit only gradually becomes capable of reinitiation. This is confirmed by our results for non-canonical start codons, which show that the first start codon (I40) is only used by a fraction of the ribosomes, while others continue scanning to reinitiate at later start codons.

Our results let us conclude that the established conditions for reinitiation at methionines also apply to non-canonical start codons. Taken together, the likeliness for reinitiation is balanced between the length of the uORF (optimal length is 2–50 codons), the scanning length between the stop and the next start codon (between 8 and 300 nt) and the Kozak sequence context. During the first initiation process, the 40S subunit scans base-by-base for a start codon. It is therefore likely that during scanning for reinitiation, the 40S subunit also scans base-by-base and thus has no memory of the codon-frame of the uORF. As a result, it is not unlikely that out-of-frame start codons can serve as reinitiation sites. In that case, the translated dORF would be non-functional and thus be of no concern for UAA experiments. In the quadruplet codon technique for UAA insertion [41], a frame-shift occurs during termination, but since the 40S subunit does not scan in codons, but in a base-by-base fashion, reinitiation is likely equally prone to occur.

In cases where full length and N-terminal truncated proteins are functionally identical, it can be difficult to differentiate between stop codon readthrough and reinitiation when leak expression exists in the absence of both UAA and the tRNA/RS pair. With the present study, we emphasize

the importance of translation reinitiation when using UAA mutagenesis. Since reinitiation only occurs when the uORF is short, the issue is particularly relevant when UAAs are incorporated near the N-terminus of the protein of interest. Furthermore, we underline that attention should not be limited to downstream methionines, but that non-canonical start codons also serve as reinitiation sites.

Our results provide evidence that when modifying the genetic code for incorporation of UAAs, other cellular mechanisms may be affected as well. The high level of regulation at the translation initiation step is sensitive to minimal changes at the 5' end of the mRNA sequence in terms of codons, sequence context and secondary structure. As a result, all these factors must be considered when inserting UAAs into the first 100 amino acids of any protein and especially in proteins where the function is not as readily visible as in ion channels.

It is possible that the efficiency of reinitiation-mediated leak expression is lower in the presence of UAAs than in their absence, and as a consequence low enough to be neglected. Nevertheless, in order to avoid N-terminal truncated proteins and proteins lacking the UAA to co-express with the UAA containing protein – in particular in multimeric proteins, – caution should be exercised against reinitiation, and removal of downstream start codons may decrease or eliminate such leak expression.

6.5 Methods and materials

6.5.1 Molecular Biology and Oocyte Injection.

All mutations were introduced into the Drosophila Shaker H4 gene in the pBSTA vector [42]. The tRNA/AnapRS synthetase pair were encoded on a cDNA (pAnap) with CMV promoter for the synthetase2; kind gift of P.G. Schultz, Scripps Research Institute. Xenopus laevis oocytes were injected with 35ng of in vitro transcribed RNA and incubated for 2 days at 18 °C in Barth solution. For incorporation with Anap, 9.2 nl of 0.1 ng/nL cDNA encoding the tRNA/AnapRS pair [2] was injected into the oocyte nucleus 6–24 hours prior to coinjection of 23 nL 1 mM Anap and 35 ng RNA. For leucine and threonine silencing, CTC and ACT codons were used, respectively. Isoleucines were mutated to leucines using CTC, since all isoleucine codons are potential start codons. The codon used for the M312L mutation was CTC.

6.5.2 Electrophysiology.

Voltage clamp was performed with a CA-1B amplifier (Dagan). Currents were recorded in the cut-open oocyte voltage-clamp configuration as described [43] and analyzed by using GPatch (Department of Anesthesiology, University of California, Los Angeles). Linear capacitance currents were subtracted online using the P/4 protocol [44]. The external solution contained in mM: 5 KOH, 110 NMDG, 10 Hepes, and 2 Ca(OH)2, and the internal solution contained in mM: 115 KOH, 10 Hepes, and 2 EDTA. Both solutions were adjusted to pH 7.1 with MES. Conductance (G) was calculated from the steady state currents (I) via G = I/(V− Vrev), where Vrev is the reversal potential. Conductance-voltage relationships (GV) were fitted to a Boltzmann relation of the form G/Gmax = (1 + exp(− (V − V1/2)/dV))−1.

6.5.3 Estimation of the intracellular inactivation peptide concentration.

To estimate a lower limit for the concentration of the intracellular inactivation peptides, we determined how many of the original constructs (Shaker-W434F) express under identical conditions. The N-terminal peptide should, as a short cytosolic peptide, reach at least the same concentration. The number of intracellular uORFs (the number of N-termini) per channel equals the number of subunits. The number of subunits n, expressed at the surface, can be calculated using 3.3 elementary charges per subunit [45-47] ($n = \frac{Q}{3.3e}$), where Q is the total gating charge (26 nC) obtained with cut-open voltage clamp after 2 days of RNA incubation with Shaker-W434F. Since only part of the oocyte is clamped in cut-open voltage clamp, the ratio of whole oocyte surface to clamped sherical cap surface was calculated using an oocyte radius of 0.5 mm and an angle of 30° from the center of the oocyte to the spherical cap edge. The final concentration of N-termini is then given by equation 1, where V is the oocyte volume (0.52 µl) as calculated from the radius.

$$[peptide] = n/N_A \cdot \frac{area_{oocyte}}{area_{cap}} \cdot \frac{1}{V} \quad (6.1)$$

6.5.4 Western blot.

For detection of Shaker, we generated myc-tagged Shaker constructs with Glu-Gln-Lys-Leu-Ile-Ser-Glu-Glu-Asp-Leu inserted in the COOH terminus (after Val650). Oocytes were injected with myc-Shaker RNA and incubated at 18 °C for 4 days. Membrane isolations were optained as previously described with minor modifications [48]. 30–70 oocytes were homogenized in 1 ml

HEDP buffer (100 mM HEPES, 1 mM EDTA, pH 7.6 with NaOH) supplemented with 0.5 mM phenylmethanosulfonyl fluoride, 0.5 ug/ml aprotonin, 0.5 ug/ml leupeptin and 0.7 ug/ml pepstatin, and centrifuged at 3.000 g for 10 min. All steps were performed at 4°C. The lipid layer on the surface was removed, and the supernatant centrifuged at 18.000 g for 30 min. The pellet was suspended in external recording solution and 4xSDS sample buffer with 50 mM DTT, and incubated for 10 min at 70°C. The samples were loaded on an 8% SDS gel. Running buffer contained 190 mM glycine, 25 mM Tris base and 0.1% SDS for electrophoresis. Precision Plus Protein Standard (Bio-Rad) was used as protein weigth marker. Wet transfer onto a nitrocellulose membrane was performed with a transfer buffer containing 190 mM glycine, 25 mM Tris base and 20% methanol. The membrane was then incubated with the anti-myc antibody (Invitrogen) and protein was detected using SuperSignal West Dura Substrate (Invitrogen).

6.6 Acknowledgements

We thank Mireille Marsolais for technical assistance and Dr. Hélène Klein for valuable advice. Anap and the plasmid encoding the tRNA/AnapRS pair (pAnap) were kind gifts from Dr. Peter G. Schultz (Scripps Research Institute, La Jolla, CA). This work was funded by the Canadian Institutes for Health Research Grants MOP-102689 and MOP-136894 (to R.B.) and Canadian Foundation for Innovation Grant 950-225005. Groupe d'Études des Protéines Membranaires is a research group funded by the Fonds de recherche du Québec–Santé. R.B. holds a Canada Research Chair on Molecular Mechanisms of Membrane Proteins.

6.7 References

1. Liu, C.C. and P.G. Schultz, *Adding new chemistries to the genetic code.* Annu Rev Biochem, 2010. **79**: p. 413-44.
2. Kalstrup, T. and R. Blunck, *Dynamics of internal pore opening in K(V) channels probed by a fluorescent unnatural amino acid.* Proc Natl Acad Sci U S A, 2013. **110**(20): p. 8272-7.
3. Kozak, M., *The scanning model for translation: an update.* J Cell Biol, 1989. **108**(2): p. 229-41.
4. von der Haar, T. and M.F. Tuite, *Regulated translational bypass of stop codons in yeast.* Trends Microbiol, 2007. **15**(2): p. 78-86.
5. Herr, A.J., C.C. Nelson, N.M. Wills, R.F. Gesteland, and J.F. Atkins, *Analysis of the roles of tRNA structure, ribosomal protein L9, and the bacteriophage T4 gene 60 bypassing signals during ribosome slippage on mRNA.* J Mol Biol, 2001. **309**(5): p. 1029-48.

6. Napthine, S., C. Yek, M.L. Powell, T.D. Brown, and I. Brierley, *Characterization of the stop codon readthrough signal of Colorado tick fever virus segment 9 RNA.* RNA, 2012. **18**(2): p. 241-52.
7. Bonetti, B., L. Fu, J. Moon, and D.M. Bedwell, *The efficiency of translation termination is determined by a synergistic interplay between upstream and downstream sequences in Saccharomyces cerevisiae.* J Mol Biol, 1995. **251**(3): p. 334-45.
8. Cassan, M. and J.P. Rousset, *UAG readthrough in mammalian cells: effect of upstream and downstream stop codon contexts reveal different signals.* BMC Mol Biol, 2001. **2**: p. 3.
9. Dunn, J.G., C.K. Foo, N.G. Belletier, E.R. Gavis, and J.S. Weissman, *Ribosome profiling reveals pervasive and regulated stop codon readthrough in Drosophila melanogaster.* Elife, 2013. **2**: p. e01179.
10. Namy, O., G. Duchateau-Nguyen, I. Hatin, S. Hermann-Le Denmat, M. Termier, and J.P. Rousset, *Identification of stop codon readthrough genes in Saccharomyces cerevisiae.* Nucleic Acids Res, 2003. **31**(9): p. 2289-96.
11. Kozak, M., *Effects of intercistronic length on the efficiency of reinitiation by eucaryotic ribosomes.* Mol Cell Biol, 1987. **7**(10): p. 3438-45.
12. Poyry, T.A., A. Kaminski, and R.J. Jackson, *What determines whether mammalian ribosomes resume scanning after translation of a short upstream open reading frame?* Genes Dev, 2004. **18**(1): p. 62-75.
13. Kozak, M., *Constraints on reinitiation of translation in mammals.* Nucleic Acids Res, 2001. **29**(24): p. 5226-32.
14. Luukkonen, B.G., W. Tan, and S. Schwartz, *Efficiency of reinitiation of translation on human immunodeficiency virus type 1 mRNAs is determined by the length of the upstream open reading frame and by intercistronic distance.* J Virol, 1995. **69**(7): p. 4086-94.
15. Jackson, R.J., C.U. Hellen, and T.V. Pestova, *The mechanism of eukaryotic translation initiation and principles of its regulation.* Nat Rev Mol Cell Biol, 2010. **11**(2): p. 113-27.
16. Powell, M.L., *Translational termination-reinitiation in RNA viruses.* Biochem Soc Trans, 2010. **38**(6): p. 1558-64.
17. Kozak, M., *Initiation of translation in prokaryotes and eukaryotes.* Gene, 1999. **234**(2): p. 187-208.
18. von Arnim, A.G., Q. Jia, and J.N. Vaughn, *Regulation of plant translation by upstream open reading frames.* Plant Sci, 2014. **214**: p. 1-12.
19. Hinnebusch, A.G., B.M. Jackson, and P.P. Mueller, *Evidence for regulation of reinitiation in translational control of GCN4 mRNA.* Proc Natl Acad Sci U S A, 1988. **85**(19): p. 7279-83.
20. Kochetov, A.V., A. Sarai, I.B. Rogozin, V.K. Shumny, and N.A. Kolchanov, *The role of alternative translation start sites in the generation of human protein diversity.* Mol Genet Genomics, 2005. **273**(6): p. 491-6.
21. Rogozin, I.B., A.V. Kochetov, F.A. Kondrashov, E.V. Koonin, and L. Milanesi, *Presence of ATG triplets in 5' untranslated regions of eukaryotic cDNAs correlates with a 'weak' context of the start codon.* Bioinformatics, 2001. **17**(10): p. 890-900.
22. Pisani, F., A. Rossi, G.P. Nicchia, M. Svelto, and A. Frigeri, *Translational regulation mechanisms of aquaporin-4 supramolecular organization in astrocytes.* Glia, 2011. **59**(12): p. 1923-32.
23. Stump, M.R., Q. Gong, J.D. Packer, and Z. Zhou, *Early LQT2 nonsense mutation generates N-terminally truncated hERG channels with altered gating properties by the reinitiation of translation.* J Mol Cell Cardiol, 2012. **53**(5): p. 725-33.

24. Stump, M.R., Q. Gong, and Z. Zhou, *LQT2 nonsense mutations generate trafficking defective NH2-terminally truncated channels by the reinitiation of translation.* Am J Physiol Heart Circ Physiol, 2013. **305**(9): p. H1397-404.
25. Hoshi, T., W.N. Zagotta, and R.W. Aldrich, *Biophysical and molecular mechanisms of Shaker potassium channel inactivation.* Science, 1990. **250**(4980): p. 533-8.
26. Aldrich, R.W., *Fifty years of inactivation.* Nature, 2001. **411**(6838): p. 643-4.
27. Taglialatela, M., L. Toro, and E. Stefani, *Novel voltage clamp to record small, fast currents from ion channels expressed in Xenopus oocytes.* Biophys J, 1992. **61**(1): p. 78-82.
28. Zagotta, W.N., T. Hoshi, and R.W. Aldrich, *Restoration of inactivation in mutants of Shaker potassium channels by a peptide derived from ShB.* Science, 1990. **250**(4980): p. 568-71.
29. Wang, W., et al., *Genetically encoding unnatural amino acids for cellular and neuronal studies.* Nat Neurosci, 2007. **10**(8): p. 1063-72.
30. Peabody, D.S., *Translation initiation at non-AUG triplets in mammalian cells.* J Biol Chem, 1989. **264**(9): p. 5031-5.
31. Starck, S.R., V. Jiang, M. Pavon-Eternod, S. Prasad, B. McCarthy, T. Pan, and N. Shastri, *Leucine-tRNA initiates at CUG start codons for protein synthesis and presentation by MHC class I.* Science, 2012. **336**(6089): p. 1719-23.
32. Ivanov, I.P., A.E. Firth, A.M. Michel, J.F. Atkins, and P.V. Baranov, *Identification of evolutionarily conserved non-AUG-initiated N-terminal extensions in human coding sequences.* Nucleic Acids Res, 2011. **39**(10): p. 4220-34.
33. Lee, H.S., J. Guo, E.A. Lemke, R.D. Dimla, and P.G. Schultz, *Genetic incorporation of a small, environmentally sensitive, fluorescent probe into proteins in Saccharomyces cerevisiae.* J Am Chem Soc, 2009. **131**(36): p. 12921-3.
34. Chatterjee, A., J. Guo, H.S. Lee, and P.G. Schultz, *A genetically encoded fluorescent probe in mammalian cells.* J Am Chem Soc, 2013. **135**(34): p. 12540-3.
35. Kozak, M., *An analysis of 5'-noncoding sequences from 699 vertebrate messenger RNAs.* Nucleic Acids Res, 1987. **15**(20): p. 8125-48.
36. Kozak, M., *Context effects and inefficient initiation at non-AUG codons in eucaryotic cell-free translation systems.* Mol Cell Biol, 1989. **9**(11): p. 5073-80.
37. Kozak, M., *Point mutations define a sequence flanking the AUG initiator codon that modulates translation by eukaryotic ribosomes.* Cell, 1986. **44**(2): p. 283-92.
38. Schulteis, C.T., S.A. John, Y. Huang, C.Y. Tang, and D.M. Papazian, *Conserved cysteine residues in the shaker K+ channel are not linked by a disulfide bond.* Biochemistry, 1995. **34**(5): p. 1725-33.
39. Santacruz-Toloza, L., Y. Huang, S.A. John, and D.M. Papazian, *Glycosylation of shaker potassium channel protein in insect cell culture and in Xenopus oocytes.* Biochemistry, 1994. **33**(18): p. 5607-13.
40. Munzarova, V., J. Panek, S. Gunisova, I. Danyi, B. Szamecz, and L.S. Valasek, *Translation reinitiation relies on the interaction between eIF3a/TIF32 and progressively folded cis-acting mRNA elements preceding short uORFs.* PLoS Genet, 2011. **7**(7): p. e1002137.
41. Wang, K., W.H. Schmied, and J.W. Chin, *Reprogramming the genetic code: from triplet to quadruplet codes.* Angew Chem Int Ed Engl, 2012. **51**(10): p. 2288-97.
42. Batulan, Z., G.A. Haddad, and R. Blunck, *An intersubunit interaction between S4-S5 linker and S6 is responsible for the slow off-gating component in Shaker K+ channels.* J Biol Chem, 2010. **285**(18): p. 14005-19.
43. Haddad, G.A. and R. Blunck, *Mode shift of the voltage sensors in Shaker K+ channels is caused by energetic coupling to the pore domain.* J Gen Physiol, 2011. **137**(5): p. 455-72.

44. Bezanilla, F. and C.M. Armstrong, *Inactivation of the sodium channel. I. Sodium current experiments.* J Gen Physiol, 1977. **70**(5): p. 549-66.
45. Seoh, S.A., D. Sigg, D.M. Papazian, and F. Bezanilla, *Voltage-sensing residues in the S2 and S4 segments of the Shaker K+ channel.* Neuron, 1996. **16**(6): p. 1159-67.
46. Schoppa, N.E., K. McCormack, M.A. Tanouye, and F.J. Sigworth, *The size of gating charge in wild-type and mutant Shaker potassium channels.* Science, 1992. **255**(5052): p. 1712-5.
47. Aggarwal, S.K. and R. MacKinnon, *Contribution of the S4 segment to gating charge in the Shaker K+ channel.* Neuron, 1996. **16**(6): p. 1169-77.
48. Geering, K., I. Theulaz, F. Verrey, M.T. Hauptle, and B.C. Rossier, *A role for the beta-subunit in the expression of functional Na+-K+-ATPase in Xenopus oocytes.* Am J Physiol, 1989. **257**(5 Pt 1): p. C851-8.

Chapter 7

Discussion

This thesis describes the successful implementation of a fluorescent unnatural amino acid for the use of VCF. While conventional VCF only allows for the study of extracellular regions, the Anap-VCF technique permits fluorophore labelling also in buried and intracellular regions. This has opened for possibilities to address new questions as many key functional regions in membrane proteins are located on the intracellular side. Here, the Anap-VCF method was used to reveal intracellular dynamics in K_V channels during activation and inactivation. For each study, the *Drosophila* Shaker K_V channel was used as a model and *Xenopus laevis* oocytes were used as expression system. The movements of the cytosolic part of the voltage sensor, the S6 gates, the S4-S5 linker and the N-terminus were probed and evaluated with respect to the functional state of the channel.

7.1 Dynamics of internal pore opening probed by a fluorescent unnatural amino acid

In this study, the implementation of Anap expression in Shaker channels using the in vivo amber suppression technique was established. Three positions exhibited both robust expression and high fluorescence changes (5-10% dF/F), and no leak expression was present in the absence of Anap or the tRNA/synthetase pair. This demonstrates that the Anap-VCF method has the potential to open up for studies of previously non-characterized protein rearrangements.

The first position, Ala359 on top of S4, has already been extensively studied with traditional VCF in which the fluorescence time course and voltage dependency correlate with charge displacement [1, 2]. However, when labeled with Anap at the same position, we show that rearrangements between closed transitions are detected in addition to charge displacement

related movements. It is foreseeable that the fluorescence signal changes with the fluorophore, because the fluorescence change is only an indirect measure of the conformational change, and it is important to remember that the detected fluorescence is first and foremost a measure of the fluorophore's dipole moment's interaction with the surroundings (solvent relaxation), or the ability of the fluorophore to fluoresce in a given environment (quenching). Both mechanisms depend on the chemical structure of the fluorophore, which in the case of Anap and TMR are very different (figure 7.1). It is, nonetheless, likely that the additional rearrangement probed by Anap is due to a higher sensitivity to fast protein rearrangements because Anap is, compared to TMRM, smaller and closer to the protein backbone (figure 7.1).

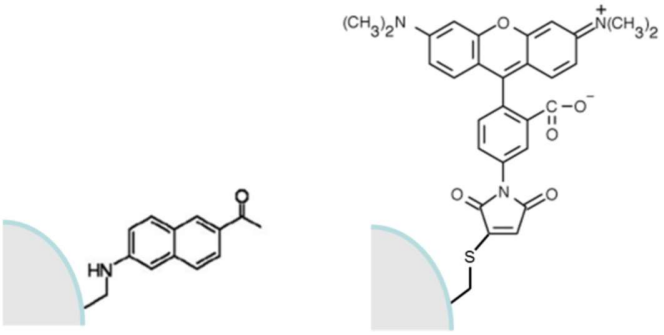

Figure 7.1 Anap and TMR-maleimide
The two fluorophores, Anap (left) and TMR-maleimide (right), are compared when attached to the protein backbone.

Next, two-color fluorometry with TMR at Ala359 and Anap at the bottom of S1 at Val234, showed that the fluorescence voltage dependency of the two signals were similar, but they differed kinetically. The Anap signal was two times faster than the TMR signal and TMR did not exhibit a delay compared to Anap which means they were prompted simultaneously. The overlapping FV curves suggest that the fluorophores probe the same transition. The kinetics suggest that the bottom of S1 reaches the final state before the upper S4, but it can also be due to TMR being a larger molecule than Anap thus moving slower. Regardless of the kinetics, the findings strongly suggest that the lower S1 helix and the upper S4 have at least one conformational change in common, and they do not undergo two completely distinct movements. This observation argues against a sequential model for the two components of the voltage sensor movement in which one rearrangement (vertical displacement) is followed by another (tilt/bend). Since both ends of

the voltage sensor rearrange simultaneously with the same voltage dependency, the two movements are likely initiated together.

Finally, we were also able to measure the movement of the S6 bundlecross. In accordance with the consensus model for pore opening, we found that pore opening occurs after voltage sensor activation. This finding adds to the already existing evidence that the main activation gate is located in the S6 terminal in Shaker-related K_V channels. However, we also found that opening occurred in two sequential transitions, one which happened before pore opening, and one during pore opening. These fluorescence observations led to the proposal of a mechanism by which the S6 bundlecross undergoes two sequential concerted transitions. Since the mutation which was used for the bundlecross gate (H486) exhibited an uncoupling gating behavior, the findings confirm that concerted movements develop in the pore, as opposed to originate from the voltage sensors.

The study contributes to a better understanding of K_V channel function by elucidating movements of electrically silent transitions and movements in regions which had not been characterized before. Since voltage sensor activation and pore opening are fundamental mechanisms in many ion channels, it is possible that these findings also apply to a wide range of other voltage gated ion channels which share functional features with the Shaker-related K_V group.

7.2 The S4-S5 linker movement during activation and inactivation in voltage-gated K^+ channels

In this study, dynamics of the S4-S5 linker are investigated to shed light on its role in electromechanical coupling. The linker and the S6 helix need to be compatible for efficient coupling, and specific interactions between the two regions have shown to be important for coupling and for stabilization of the open state [3, 4]. The findings point towards a model in which the linker plays an important role in transferring energy from the voltage sensors to the pore, but any dynamic information is lacking on the subject.

To describe the movement of the S4-S5 linker in detail, we incorporated Anap into 4 different positions, and two-color fluorometry allowed the comparison of linker movement and upper S5 helix movement.

First, the voltage dependency and kinetics of the fluorescence signals from the N-terminal part of the linker (Leu382) were similar for Anap and TMR, suggesting that the proximal part of the linker moves with the S4 helix during charge movement. This agrees with the findings of the previous project where we show that the intracellular part of the voltage sensor moves together with the upper part.

However, the corresponding signals from the more distal part of the linker (Arg387, Lys390, Ala391) exhibited a different behaviour, where Anap fluorescence developed at higher potentials than TMR, and Anap also exhibited different kinetics than TMR with a delay in the fluorescence time course. These findings suggest that the C-terminal part of the linker move after the N-terminal part, in a second and distinct rearrangement.

The observations support a model for activation in which the S4 helix and the interhelical hinge of the S4-S5 linker move together in response to early activation. We suggest that, due to flexibility within Leu382 and Arg387, energy is briefly stored in this region and is followed by a release of the S4-S5 linker in a second movement. Then, due to coupling between the linker and S6, energy release is followed by pore opening. These results are those expected according to the current notion of electromechanical coupling in voltage gated ion channels, and now we can add the findings of this technique to further confirm our current mechanistic understanding of the gating mechanism.

A highly conserved glycine at position 386 is a good candidate for allowing flexibility between Leu382 and Arg387 (figure 7.2) and has previously been suggested to play a key role as a flexible determinant in electromechanical coupling [5]. In fact, this hypothesis is supported by the finding that pore opening is disrupted in G386Anap channels (chapter 4, only gating currents were visible, data not shown). In agreement with this, Hull et al. [6] have shown that the corresponding glycine in hERG channels (Gly546) regulates critical flexibility during activation.

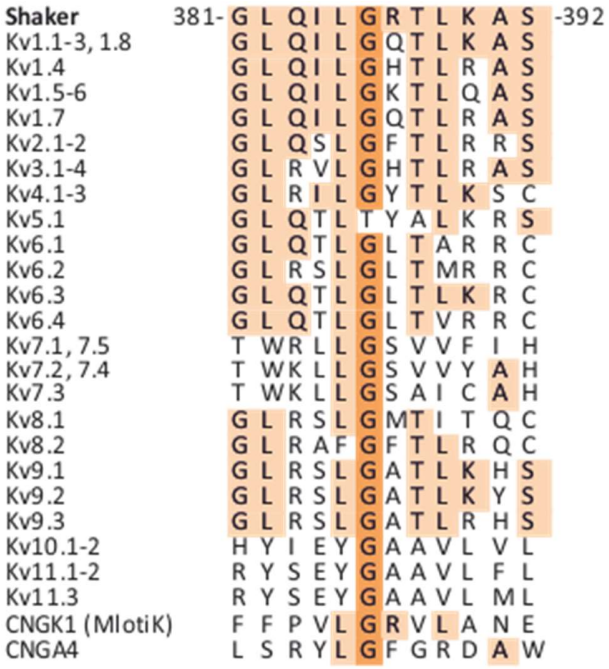

Figure 7.2 Sequence alignment of the S4-S5 linker.
Conserved residues in human K_V channels and in human and bacterial CNG channels with respect to Shaker are highlighted in orange with the glycine at position 386 in bold which is proposed to serve as a flexible hinge.

We also found that the gating mechanism was significantly altered in the presence of accelerated C-type inactivation (W434F), suggesting a mutual influence between the selectivity filter and the S4-S5 linker. The observation supports the notion that in the W434F mutant, the whole linker assumes the same voltage dependence as the S4, suggesting that an energetic coupling between the S4-S5 linker and pore disappears. The findings show that C-type inactivation and the state of the selectivity filter not only affects the ionic conductance but has a global mechanistic effect on the channel as a whole. In agreement with this, we found in this, and the previous paper, that C-type inactivation induces global conformational changes throughout the channel.

N-type inactivation is fast, and is thus the dominating mechanism for channel closure when present, e.g. in K_V1.4 or K_V1 channels assembling with β1 or β3 subunits. C-type inactivation on the other hand, is slower and as a result, does not affect the electrical activity when the channel opens in the presence of N-type inactivation, but it controls the rate of recovery from inactivation as the rate limiting step. C-type inactivation therefore plays a crucial role in the availability of the channel for the next action potential and thus determines crucial firing properties. The presence of an energetic coupling between the S4-S5 linker and the pore domain

is interesting because auxiliary subunits, present in vivo, which interact with the cytosolic domain, such as the β subunits, may influence the state of the S4-S5 linker, and thus C-type inactivation. For example, the S4-S5 linker was proposed by Holmgren et al. [7] to form part of the receptor site for the IP during N-type inactivation. It raises the possibility that N-type inactivation could influence the rate of recovery from C-type inactivation, by interacting with the S4-S5 linker.

7.3 Probing dynamics of the ball and chain in K_V channels during N-type inactivation

N-type inactivation is a key component of electrical activity in K_V channels. It is a dynamic process in which the long and flexible N-terminus of about 50 amino acids long, enters the side windows of the intracellular T1 domains and occludes the pore. Mutational, structural and electrophysiological studies have yielded most of what is known about the process, but any dynamic information is lacking. We therefore chose to insert Anap at various key positions to get a better understanding of the N-terminus inactivation particle (IP) pathway. To summarize our findings, we found that residues 3, 8, 19 and 35 experience rearrangements which correlate with a pre-inactivation step, while only the tip region (residue 3 and 8) experiences rearrangements which correlate with pore occlusion. With the direct physical measures of the IP dynamics, we can conclude that the IP rearrange at least twice, and that only the very first amino acids are involved in the final binding step. These findings confirm the current proposed model of N-type inactivation in Shaker, in which one transition involves the downstream IP region followed by another transition which involves binding of the tip region to the pore. The use of different techniques which yield findings that support the same molecular mode of action is without question the most powerful way forward in generating a consensus model of protein function in fundamental research. With our results confirming the dynamic implication of different regions of the IP, it is credible to say that a consensus model of N-type inactivation in Shaker is achieved.

Although recordings of Shaker channels expressed in Xenopus oocytes allow determination of kinetics with little contamination from other channels, it represent limitations when it comes to interpretation of K_V1 channel function in vivo, for two reasons. First, the IPs of K_V1 channels which undergo N-type inactivation have no homology with Shaker. Second, $K_V1.4$ is the only

channel of the group which is intrinsically inactivated, while the other members are only inactivated in presence of a β subunit which is likely to affect the positioning of the IP at rest and implies a longer distance which the IP travels to reach the T1 windows. It would therefore be interesting to perform a corresponding experiment with K_V1 channels in presence of β subunits to shed light on how much the IP pathway varies as a function of the IP identity.

There exist, to my knowledge, no disease which has been identified to be caused by mutations in the IP region of K_V channels or K_V β subunits. However, malfunction of N-type inactivation caused by mutations in other regions have been identified. For example, we showed that an episodic ataxia type 1 mutation in the S1 helix of the $K_V1.1$ voltage sensor affects the gating mechanism, C-type inactivation and also N-type inactivation in Shaker [8]. Malfunction of N-type inactivation would lead to longer action potentials in neurons. There exists no consistent pharmacological treatment for this disease, and to understand how a single amino acid substitution can have devastating physiological effects, it is necessary to obtain deep insight into K_V channel function.

7.4 Reinitiation at non-canonical start codons leads to leak expression when incorporating unnatural amino acids

The N-type inactivation project was temporarily interrupted due to relatively high leak expression in the absence of Anap, for which the cause was initially unclear to us. Up to 5-10 µA of leak currents were detected when the amber stop codon was situated in the N-terminus, so it was necessary to clarify the origin of these currents before we could make reliable interpretations of the findings in the N-type inactivation project.

There were three interesting features about the leak currents. First, there was no downstream start codon from which the channels could have been translated. Second, leak currents exhibited increasing inactivation the more downstream the stop codon was located. Third, the high amount of leak expression appeared to be specific for N-terminal stop codons.

These factors led us to consider the possibility that translation would initiate at noncanonical start codons. That way, N-terminal truncated channels would result from translation at noncanonical start codons and free cytosolic inactivation particles (IP) would result from translation at the first methionine canonical start codon. The free IPs would be responsible for

inactivating the truncated channels in the same way that Zagotta et al. [9] restored inactivation by adding a 20 amino acid long peptide of the Shaker N-terminus to non-inactivating Shaker channels. In agreement with our hypothesis, we found that removal of the non-canonical start codons also removed leak expression.

The paper recapitulates how two distinct biochemical and cellular features (non-canonical start codons and translation reinitiation) combines with the amber stop codon suppression technique to produce unreliable results when incorporating an UAA for the study of structural biology. With the clarification of leak expression, the project concerning N-type inactivation could precede in a reliable fashion by silently mutating the non-canonical start codons. The phenomenon principally relates to all studies where UAA incorporations are used in the N-terminus of any protein. With the increasing use of the amber stop codon suppression technique and the continuous development of new unnatural amino acids, these findings may contribute to an awareness of predictable leak expression and potentially more reliable results in the context of UAA incorporation in general.

7.5 VCF data interpretation

VCF is a powerful tool which has contributed a wealth of details on the workings of numerous membrane proteins. The simultaneous detection of current and fluorescence in real time in a living cell allows for reliable measures of dynamical structure-function relationship. The experimental procedure is relatively straightforward, and the data output is caused by well understood biophysical mechanisms. However, the data interpretation with respect to protein structure-function relationships is the challenging part. The ultimate goal in understanding how proteins work is discerning the sequence of events and the energies and forces which govern them. When VCF fluorescence experiments report on a movement with a similar kinetic and voltage-dependence as a functional event, it only suggests that the movement is associated to that event. One cannot necessarily conclude whether the movement is a cause or a result of the event, or whether they both are caused by the same event. An optimal VCF time resolution (fs) would indeed allow a better determination of the sequence of events, but the underlying energetic considerations would remain to be elucidated to fully understand protein structural dynamics.

An example of such limited interpretation of VCF data is presented by the S4-S5 linker project described in chapter 4, in which both independent and cooperative movements were detected. The results can generally be interpreted in two ways. Either the linker is a passive hinge which simply moves according to the covalently bound domains, or, the linker plays an active role in transmitting VS force to pore gating. Considering the required compatibility between the S4-S5 linker and S6 tail [3, 10], and the effect of S4-S5 linker mutations on electromechanical coupling [4, 11-13], it is unlikely that the measured movements are irrelevant with respect to force transmission. While the independent VS movement has been studied in a highly systematic manner, less information is available concerning the structural implications of the more complicated cooperative movement. We can therefore not be certain, yet, whether cooperative movements originate from the pore or are transmitted from the VS via the S4-S5 linker. One way to investigate this question is to use two-color UAA-VCF on adjacent subunits when a second fUAA becomes available for VCF. By labeling the S4-S5L with Anap in one subunit and the S6 intracellular gates with another fUAA (using the quadruplet codon technique [14]), one could perform mutational perturbation studies and observe the temporal relation between each movement.

Another limited feature of VCF data interpretation is that a fluorescence change only reports on a relative movement. This means that it is either the inserted fluorophore which moves, or it is nearby amino acids which are moving. In cases where Anap is inserted into compact protein regions, it can be challenging do determine the moving part which can be within a radius of a few Ångströms (effective quenching radius is within 10 Å). According to the K_V1.2 crystal structure [15], only one transmembrane residue used in this thesis for Anap incorporation is located in a completely buried region: the L382 position in the S4-S5 linker (figure 7.3A-B). L382 is situated in a hydrophobic pocket consisting of residues from S4 of the same subunit and from S5 of the neighboring subunit (figure 7.3C). It is therefore possible that the reported movement of L382Anap channels is that of the S4 or S5 helix, and that L382Anap is stationary. The similarity of fluorescence signals between V234Anap-A359C and L382Anap-A359C argues against the possibility that L382Anap probes S5 helix movements. Furthermore, LRET studies on K_VAP channels measured a 4 Å radial displacement of all the residues in the S4-S5 linker during

activation, including the corresponding L382 residue in Shaker [16]. It is therefore most likely an S4-S5 linker movement which is probed by L382Anap channels.

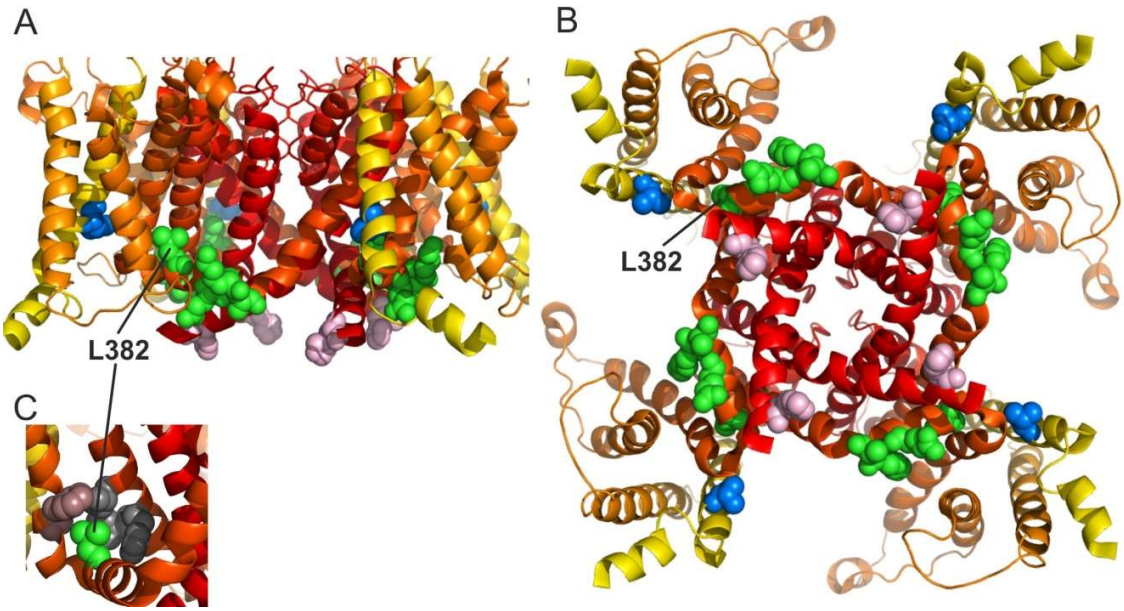

Figure 7.3 Overview of residues used for Anap incorporation
A) Side view and **B)** bottom view of the transmembrane segments of the K_V channel. Residues used in this thesis for Anap incorporation are shown as spheres: V234 (blue), H486 (light pink), S4-S5 linker sites (green) **C)** L382 is situated in a hydrophobic pocket of residues from the S4 helix (in brown F373, L375) and the neighboring S5 helix (in grey F401, F402, I405).

The fluorophore's sensitivity to the microenvironment comprises the fundamental strength of VCF. However, absence of a fluorescence signal cannot be interpreted as no movement, although that would be an intuitive conclusion. The fluorophore may remain in close contact with a quencher throughout a movement or not encounter a quencher at all, or alternatively, the fluorophore can move from one hydrophobic environment to another without causing a fluorescence change. For example, the absence of a 4-AP sensitive fluorescence component in the chain region of the IP during N-type inactivation (K19Anap and E35Anap, figure 5.3A-B), does therefore not exclude movement during the final binding step. An important aspect of VCF data interpretation is to focus on the detected fluorescence signals and to avoid conclusions based on the absence hereof.

7.6 Anap incorporation

Anap incorporation into Shaker channels was presented as being experimentally a straightforward procedure, but there exist nevertheless a number of factors which can affect the chance of obtaining successful results and which are reasonable to consider when designing a research project using Anap-VCF.

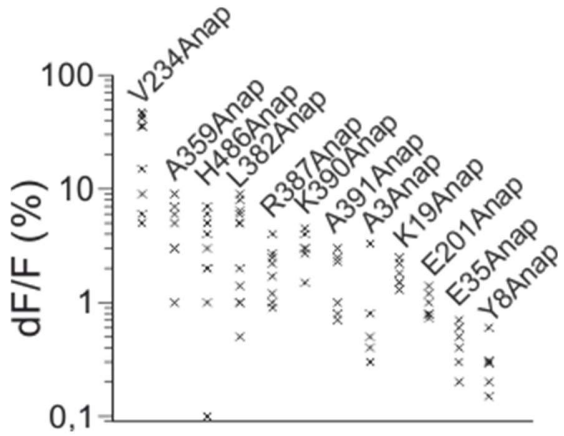

Figure 7.4 dF/F values for each Anap mutation used in the thesis
Fluorescence efficiency in VCF depends on the site of interest. Graph shows dF/F values of each mutation used in the thesis. Only oocytes of similar expression levels are plotted.

First, high expression levels (40-60 µA*) were usually required in order to detect Anap fluorescence changes, which is likely due to the limited brightness of Anap with QY = 48% and extinction coefficient (ε) = 17.500 $cm^{-1} \cdot M^{-1}$ [17]. For comparison, TMR exhibits a similar QY of 41% but with ε = 78.000 $cm^{-1} \cdot M^{-1}$ [18]. V234Anap was the only mutation which exhibited fluorescence changes above 10% dF/F (figure 7.4) and therefore also the only mutation from which fluorescence changes could be detected at low expression (5-20 µA*). Except for V234Anap, it was generally complicated to obtain high enough expression of the conducting mutants while keeping the oocytes healthy. The W434F mutation was a great advantage in that regard as it allows for high expression levels without affecting oocyte viability. Depending on the sensitivity of the site, the minimal protein density required for detection of 1% dF/F of Anap fluorescence in oocytes with VCF can be estimated to 30-400 channels per μm^2 ** (the lowest density being

* ionic currents elicited by a voltage jump from -90 mV to 50 mV
** calculated by using a single channel conductance of 20 pS and an oocyte spherical cap area of 0.17 mm^2 (clamped area in COVC)

V234Anap and the highest being Y8Anap). Anap-VCF would therefore not be suited for proteins which exhibit limited expression.

A second factor which may affect Anap-VCF experiments, is position-dependent leak expression. As described in chapter 6, N-terminal truncation via translation reinitiation may occur when the stop codon for UAA Anap insertion is located in the N-terminus. Additionally, if the stop codon is located in the C-terminal region, and the C-terminus is not required for channel expression, then C-terminal truncated proteins may express (e.g. IVS in the case of ion channels). Both truncation mechanisms depend on the availability of Anap-charged tRNAs during translation which can vary within the same batch of oocytes. Consequently, truncation represents a potential risk of a heterogenous population of channels when working with UAAs in general. Fortunately, both truncations in Shaker resulted in recognizable current profiles which allowed us to identify leak expression. In chapter 4, C-terminal truncation led to IVS channels which open at hyperpolarized potentials. In chapter 6, N-terminal truncation would result in abolishment of N-type inactivation which was not the case since leak expression was limited thanks to efficient Anap incorporation. On the other hand, if the profile of truncated proteins during UAA experiments would be indistinguishable from full length proteins and if UAA incorporation is limited, it is worthwhile to choose a site of interest within the range which does not lead to neither N-terminal nor C-terminal truncation. For Shaker, the region in which leak expression due to truncation would not occur is approximately between residue 100 and 382, which represents 43% of the channel. In experiments with proteins of similar lengths (or shorter) where truncation is to be avoided completely, this would represent a major restriction.

During my time working with Anap, I have encountered periods of insufficient or lack of expression with Anap incorporation. Successful expression can vary within the same batch of oocytes as well as among batches obtained from different frogs. Indeed, one of the few disadvantages of using *Xenopus* oocytes as expression system is variations in oocyte quality which can result in less or no heterologous expression. This factor of variance is multiplied greatly when using UAAs as more cellular mechanisms are required for channel expression (transcription of tRNAs, transcription and translation of synthetases, tRNA aminoacylation).

7.7 Perspectives

The relatively low brightness of Anap restricts the application of the Anap-VCF technique to robustly expressing proteins with sites exhibiting significant fluorescence sensitivity. One could try to optimize the detector to function with low brightness, but a second brighter fUAA would not only enhance the efficiency of VCF, but would also allow for internal two-color VCF, add new possibilities for LRET and FRET applications and potentially enable single channel fluorescence recordings. Unfortunately, brightness requires a highly conjugated system and thus comprises larger fluorophores, surpassing the size limitation for the synthetase binding pocket. A way to overcome this issue is to use click-chemistry in which UAAs bearing strained alkenes/alkynes (e.g. TCO and BCN) react with fluorophores containing azide/tetrazine groups [19, 20]. The advantage of this strategy is that it only requires one RS/tRNA pair to label with many different fluorophores. However, intracellular labeling using TCO or BCN has been described as a major limitation in mammalian cells [20] and have not been successful in Xenopus oocytes either (Kalstrup & Blunck, unpublished). The Anap-VCF technique therefore remains most compelling in that regard.

7.7.1 Other Anap studies

The establishment of the Anap-VCF technique in Xenopus oocytes has encouraged two other research groups to study cytosolic gating mechanisms with Anap.

The Ci-VSP (voltage sensing phosphatase) is a membrane protein consisting of a voltage sensor with an intracellular catalytic phosphatase domain instead of an ionic pore. The molecular mechanism of coupling between the voltage sensor movements and catalytic activity is not clear, so Sakata et al. [21] expressed Ci-VSP with Anap in the catalytic domain to assess the movements during activation using TEVC fluorometry. They found that the catalytic region moved on membrane depolarisation and they identified voltage-dependent states in the C2 region which were sensitive to substrate availability. They also used FRET analysis between Anap and the plasma membrane stained with dipicrylamine which showed that the catalytic domain remains close to the membrane, and thus the substrate (membrane bound phosphoinositides). These results show that voltage sensor movement regulates rearrangements throughout the catalytic domain and that the catalytic domains does not change the distance from the plasma membrane,

ruling out the possibility that rearrangements modulates the availability of the substrate to reach the active site by moving away from the membrane. The use of Anap-VCF here has shed light on the role with which VSPs use the membrane potential to confer their catalytic activity.

The Zagotta group has used transition metal ion FRET (tmFRET) between Anap (donor) and Co^{2+} (acceptor) to study intracellular distance changes in three different ion channels [22]. First, they measured distance changes between the pain-transducing ion channel TRPV1 and the plasma membrane in HEK cells, by incorporating Anap into various positions in the ankyrin repeat domain. Co^{2+} was bound to the intracellular surface of the membrane. The measured distances correlated with the cryoEM structure which show that tmFRET offers a trustworthy new approach to study structures and dynamics relative to the cell membrane. Activation of the channel by capsaicin did not induce changes between the ARD and the membrane, which also correlated with the comparison of the open and closed state of the TRPV1 structures. The method thus has the potential to offer new insights into a wide range of membrane proteins with intracellular domains conferring rearrangements relative to the cell membrane. Examples of interesting studies using tmFRET, range from questions concerning how the family of G protein-coupled receptors detect molecules outside the cell and transduces crucial intracellular signal pathways to which rearrangements in peripheral membrane proteins directly regulate membrane protein function. Knowledge about relative distance changes to the membrane using Anap and tmFRET would contribute to a better understanding of the underlying mechanisms of many membrane proteins with intracellular key regions.

Next, the Zagotta group used the same technique in Xenopus oocytes to investigate how transition metal binding potentiates activation of a cyclic nucleotide-gated channel (CNGA1) [23]. Using patch clamp fluorometry, quenching of Anap by Co^{2+} revealed a potential histidine binding site for the potentiators and suggest a mechanism for potentiation in which the distance between the membrane and the binding site decreases. CNGA1 channels are involved in phototransduction where they are responsible for the electrical signaling which is activated from the light captured by the eye and transmitted to the brain. Defects in the gene, among other genes in phototransduction, causes retinitis pigmentosa autosomal recessive disease which decreases the sight affecting 1 in 5000 people.

The last protein which the Zagotta group has studied using Anap with tmFRET is the ELK channel (K_V12) [24], which is abundantly expressed in the brain regulating excitability. The exact role of the ELK channel is unclear, but knock-out mice suffer from neuronal hyperexcitability and epilepsy, and the channel has also been shown to be overexpressed in cancer. The ELK channel, like most ion channels, has a large intracellular domain which governs electrical properties of the channel. By introducing a histidine pair at one site and incorporating Anap at another site and applying Co^{2+} to excised patches of Xenopus oocytes, they show that the two sites come in close contact which stabilizes the open pore, resulting in a mode shift mechanism which is characterized by a shift in activation to more hyperpolarized voltages in response to depolarization. The findings provide evidence for a key contribution of the intracellular domain to regulate ELK channel function.

These studies are solid examples showing that the Anap-VCF approach can be extrapolated to the study of other ion channels and of proteins which are electrically silent and whose action is not as easily captured as ion channels. The technique was shown to function in combination with FRET and patch clamp fluorometry, and in HEK cells, opening up many new and exciting paths of research possibilities. With the establishment of the Anap-VCF approach and the demonstration of the validity of if, this thesis has contributed to a technical advancement in the field of structural biology.

Due to the heterogeneity of subunit assembly in vivo, potassium channels represent the most complex class of voltage-gated ion channels from both a functional and structural view. The scientific findings of this thesis are obtained from homomeric tetramers in the absence of K_V beta subunits and can therefore not necessarily be directly extrapolated to the function of all K_V1 channels in neurons, cardiac myocytes and muscle, among many other cell types. It remains nevertheless essential to understand how individual subunits work to understand how different subunits perform their function when combined. Obviously, potassium channels have a central role in neurons, but the Xenopus oocyte has the proven ability to provide information about the fundamental features of ion channel function in a controlled setting and will continue to be a highly influential expression system in molecular physiology and neuroscience.

7.8 References

1. Cha, A. and F. Bezanilla, *Characterizing voltage-dependent conformational changes in the Shaker K+ channel with fluorescence.* Neuron, 1997. **19**(5): p. 1127-40.
2. Claydon, T.W., M. Vaid, S. Rezazadeh, S.J. Kehl, and D. Fedida, *4-aminopyridine prevents the conformational changes associated with p/c-type inactivation in shaker channels.* J Pharmacol Exp Ther, 2007. **320**(1): p. 162-72.
3. Lu, Z., A.M. Klem, and Y. Ramu, *Coupling between voltage sensors and activation gate in voltage-gated K+ channels.* J Gen Physiol, 2002. **120**(5): p. 663-76.
4. Batulan, Z., G.A. Haddad, and R. Blunck, *An intersubunit interaction between S4-S5 linker and S6 is responsible for the slow off-gating component in Shaker K+ channels.* J Biol Chem, 2010. **285**(18): p. 14005-19.
5. Balleza, D., E. Carrillo, and F. Gomez-Lagunas, *Conservation analysis of residues in the S4-S5 linker and the terminal part of the S5-P-S6 pore modulus in Kv and HCN channels: flexible determinants for the electromechanical coupling.* Pflugers Arch, 2015. **467**(10): p. 2069-79.
6. Hull, C.M., S. Sokolov, A.C. Van Slyke, and T.W. Claydon, *Regional flexibility in the S4-S5 linker regulates hERG channel closed-state stabilization.* Pflugers Arch, 2014. **466**(10): p. 1911-9.
7. Holmgren, M., M.E. Jurman, and G. Yellen, *N-type inactivation and the S4-S5 region of the Shaker K+ channel.* J Gen Physiol, 1996. **108**(3): p. 195-206.
8. Petitjean, D., T. Kalstrup, J. Zhao, and R. Blunck, *A Disease Mutation Causing Episodic Ataxia Type I in the S1 Links Directly to the Voltage Sensor and the Selectivity Filter in Kv Channels.* J Neurosci, 2015. **35**(35): p. 12198-206.
9. Zagotta, W.N., T. Hoshi, and R.W. Aldrich, *Restoration of inactivation in mutants of Shaker potassium channels by a peptide derived from ShB.* Science, 1990. **250**(4980): p. 568-71.
10. Lu, Z., A.M. Klem, and Y. Ramu, *Ion conduction pore is conserved among potassium channels.* Nature, 2001. **413**(6858): p. 809-13.
11. Haddad, G.A. and R. Blunck, *Mode shift of the voltage sensors in Shaker K+ channels is caused by energetic coupling to the pore domain.* J Gen Physiol, 2011. **137**(5): p. 455-72.
12. Ledwell, J.L. and R.W. Aldrich, *Mutations in the S4 region isolate the final voltage-dependent cooperative step in potassium channel activation.* J Gen Physiol, 1999. **113**(3): p. 389-414.
13. Chowdhury, S., B.M. Haehnel, and B. Chanda, *Interfacial gating triad is crucial for electromechanical transduction in voltage-activated potassium channels.* J Gen Physiol, 2014. **144**(5): p. 457-67.
14. Wang, K., W.H. Schmied, and J.W. Chin, *Reprogramming the genetic code: from triplet to quadruplet codes.* Angew Chem Int Ed Engl, 2012. **51**(10): p. 2288-97.
15. Long, S.B., X. Tao, E.B. Campbell, and R. MacKinnon, *Atomic structure of a voltage-dependent K+ channel in a lipid membrane-like environment.* Nature, 2007. **450**(7168): p. 376-82.
16. Faure, E., G. Starek, H. McGuire, S. Berneche, and R. Blunck, *A limited 4 A radial displacement of the S4-S5 linker is sufficient for internal gate closing in Kv channels.* J Biol Chem, 2012. **287**(47): p. 40091-8.
17. Lee, H.S., J. Guo, E.A. Lemke, R.D. Dimla, and P.G. Schultz, *Genetic incorporation of a small, environmentally sensitive, fluorescent probe into proteins in Saccharomyces cerevisiae.* J Am Chem Soc, 2009. **131**(36): p. 12921-3.
18. Grimm, J.B., et al., *A general method to improve fluorophores for live-cell and single-molecule microscopy.* Nat Methods, 2015. **12**(3): p. 244-50, 3 p following 250.

19. Lang, K., et al., *Genetic Encoding of bicyclononynes and trans-cyclooctenes for site-specific protein labeling in vitro and in live mammalian cells via rapid fluorogenic Diels-Alder reactions.* J Am Chem Soc, 2012. **134**(25): p. 10317-20.
20. Nikic, I., J.H. Kang, G.E. Girona, I.V. Aramburu, and E.A. Lemke, *Labeling proteins on live mammalian cells using click chemistry.* Nat Protoc, 2015. **10**(5): p. 780-91.
21. Sakata, S., Y. Jinno, A. Kawanabe, and Y. Okamura, *Voltage-dependent motion of the catalytic region of voltage-sensing phosphatase monitored by a fluorescent amino acid.* Proc Natl Acad Sci U S A, 2016. **113**(27): p. 7521-6.
22. Zagotta, W.N., M.T. Gordon, E.N. Senning, M.A. Munari, and S.E. Gordon, *Measuring distances between TRPV1 and the plasma membrane using a noncanonical amino acid and transition metal ion FRET.* J Gen Physiol, 2016. **147**(2): p. 201-16.
23. Aman, T.K., S.E. Gordon, and W.N. Zagotta, *Regulation of CNGA1 Channel Gating by Interactions with the Membrane.* J Biol Chem, 2016. **291**(19): p. 9939-47.
24. Dai, G. and W.N. Zagotta, *Molecular mechanism of voltage-dependent potentiation of KCNH potassium channels.* Elife, 2017. **6**.